Final Report 2000-25

Research

Effects of Pre-Release Cracks in High-Strength Prestressed Girders

Technical Report Documentation Page

1. Report No.	2.	3. Recipient's Accession No.
2000-25		

4. Title and Subtitle	5. Report Date
EFFECTS OF PRE-RELEASE CRACKS IN HIGH-STRENGTH PRESTRESSED GIRDERS	July 2000
	6.

7. Author(s)	8. Performing Organization Report No.
Tina Wyffels, Catherine French, Carol Shield	

9. Performing Organization Name and Address	10. Project/Task/Work Unit No.
Department of Civil Engineering University of Minnesota 500 Pillsbury Dr. S. E. Minneapolis, MN 55455-0220	11. Contract (C) or Grant (G) No.

12. Sponsoring Organization Name and Address	13. Type of Report and Period Covered
Minnesota Department of Transportation 395 John Ireland Boulevard Mail Stop 330 St. Paul, Minnesota 55155	Final Report
	14. Sponsoring Agency Code

15. Supplementary Notes

16. Abstract (Limit: 200 words)

Pre-release cracks have been observed during the fabrication process of some prestressed concrete girders. The pre-release cracks were observed to begin at the top flange and extend into the depth of the section, sometimes penetrating through the entire depth. The cracks close due to the effects of prestressing and girder self-weight when the prestressing strands are released. The objective of this report was to determine the effects these pre-release cracks have on girder camber, flexural cracking capacity, and steel stress ranges. The research included a parametric study investigating stress ranges in the prestressing strands in uncracked, cracked, and partially cracked girder sections to determine if steel fatigue was a concern. An analytical study was also performed which modeled several pre-release cracks, including models of two experimental girders that developed pre-release cracks, to determine the effect of various cracks on girder stress and camber.

It was found that steel fatigue in the prestressing strand is a concern in girders that become cracked in service. Fatigue of the steel strands has typically not been a concern in prestressed girders because the girders are designed so the section remains uncracked under service load. However, a loss of compressive stress is believed to occur in the bottom fiber of the girder due to pre-release cracks, which may result in the section cracking at a lower applied load. The loss of compressive stress in the bottom fiber of girders with pre-release cracks was determined using finite element modeling. Additional results of the analytical models were that pre-release cracks result in a loss of girder camber, the effects of the pre-release cracks remained local to the crack location, non-linear stress distributions occurred during the process of crack closure, and the magnitude of the pre-release crack effects was dependent on the number of cracks, the crack width, and the crack depth.

17. Document Analysis/Descriptors	18. Availability Statement
Pre-release cracks; prestressed concrete girders; flexural cracking; fatigue.	No restrictions. Document available from: National Technical Information Services, Springfield, Virginia 22161

19. Security Class (this report)	20. Security Class (this page)	21. No. of Pages	22. Price
Unclassified	Unclassified	169	

Effects of Pre-Release Cracks in High-Strength Prestressed Girders

Final Report

Prepared by

Tina Ann Wyffels
Catherine E. French
Carol K. Shield

Department of Civil Engineering
University of Minnesota

August 2000

Published by

Minnesota Department of Transportation
Office of Research Administration
200 Ford Building Mail Stop 330
117 University Avenue
St. Paul, Minnesota 55117

ACKNOWLEDGMENTS

The work on this project was conducted under the sponsorship of the Minnesota Department of Transportation (Mn/DOT). Appreciation is expressed to the members who served on the Mn/DOT Technical Advisory Panel for their input and assistance. Appreciation is also acknowledged to the Minnesota Supercomputer Institute for the use of the computer software ABAQUS.

TABLE OF CONTENTS

LIST OF TABLES

LIST OF FIGURES

EXECUTIVE SUMMARY

Pre-release cracks have been observed during the fabrication process of some prestressed concrete girders. The pre-release cracks were observed to begin at the top flange and extend into the depth of the section, sometimes penetrating through the entire depth. The cracks close due to the effects of prestressing and girder self-weight when the prestressing strands are released. The objective of this report was to determine the effects these pre-release cracks have on girder camber, flexural cracking capacity, and steel stress ranges. The research included a parametric study investigating stress ranges in the prestressing strands in uncracked, cracked, and partially cracked girder sections to determine if steel fatigue was a concern. An analytical study was also performed which modeled several pre-release cracks, including models of two experimental girders that developed pre-release cracks, to determine the effect of various cracks on girder stress and camber.

It was found that steel fatigue in the prestressing strand is a concern in girders that become cracked in service. Fatigue of the steel strands has typically not been a concern in prestressed girders because the girders are designed so the section remains uncracked under service load. However, a loss of compressive stress is believed to occur in the bottom fiber of the girder due to pre-release cracks, which may result in the section cracking at a lower applied load. The loss of compressive stress in the bottom fiber of girders with pre-release cracks was determined using finite element modeling. Additional results of the analytical models were that pre-release cracks result in a loss of girder camber, the effects of the pre-release cracks remained local to the crack location, non-linear stress distributions occurred during the process of crack closure, and the magnitude of the pre-release crack effects was dependent on the number of cracks, the crack width, and the crack depth.

CHAPTER ONE
INTRODUCTION

1.1 Background

Pre-release cracks have been observed to occur during the fabrication process of some prestressed concrete girders (Ahlborn, 1998; Green, 1984; Roller, 1993). The pre-release cracks have been observed to begin at the top flange and extend into the depth of the section, sometimes penetrating through the entire depth. These cracks are thought to be the result of restrained shrinkage and thermal effects, incurred while the prestressed girder sits in the precasting bed prior to release. When the prestressing strands are released, the cracks close due to the effects of prestressing and girder self-weight. Earlier reports suggest that pre-release cracks cause little or no effect on girder behavior because the cracks were believed to undergo autogenous healing (Green, 1984).

Experimental results from Ahlborn suggested that pre-release cracks do have an effect on girder behavior. The measured camber and flexural cracking load of a test girder that incurred pre-release cracks were less than predicted using measured material properties of the girder.

To conceptualize the phenomenon, it can be thought of as the girder pivoting about the crack tip to close the pre-release crack when the strands are released and the girder is subjected to compressive stresses at the top fiber due to prestress and self weight. In order to close the pre-release cracks, a lengthening of the girder fibers below the crack tip must occur. This causes a reduction in compressive stress below the crack tips. As a consequence of crack closure, the girder camber would be less than anticipated and it would take less load to flexurally crack the girders due to the reduced compressive stress in the vicinity of the pre-release cracks. A reduction in flexural cracking capacity may cause corrosion problems or lead to fatigue of the prestressing strands. The research detailed in this report was performed to investigate the effects of pre-release cracks on girder camber, flexural cracking capacity, and steel stress ranges.

1.1.1 Literature Review

The literature sources regarding pre-release cracks in prestressed girders were limited. A brief description of three reports stating an occurrence of pre-release cracks is included, as well as current recommended fatigue limits for stress ranges in prestressing strands.

Ahlborn (1998), Green (1984), and Roller (1993) all stated an occurrence of pre-release cracks in prestressed concrete girders tested. The results from Ahlborn prompted the current research study. Two prestressed girders were fabricated simultaneously on the same precasting bed, with each girder varying in concrete mix design, end strand patterns, and stirrup anchorage details. A more detailed description of the two girders is included in Chapter Four of this report. One of the girders did not develop any pre-release cracks during fabrication while fifteen pre-release cracks were observed to develop in the other. The pre-release cracks were concentrated within the middle 50% of the span length and extended various depths toward the bottom flange. All of the cracks closed after release, and testing indicated a reduction in camber and flexural cracking load in the girder that developed pre-release cracks, below what was predicted using measured properties of the girder.

Green (1984) details the results of five girders manufactured on the same line bed that were tested after three of the beams were rejected by the fabricator because of cracks that occurred prior to strand release. Flexure, shear, and permeability tests were performed on the girders. The flexure and shear results of the cracked beams were essentially the same as the results of uncracked beams. Permeability tests showed that each beam behaved similarly, except for one location at the top of a beam where the water traveled through the material faster in the cracked section. Green concluded that autogenous healing in the cracked sections caused the beams to recover their strength, and the one location where water traveled through the cracked section faster was most likely from incomplete autogenous healing of the section at that location because of the low compressive stresses at the location. Three conditions were present in the test specimens which helped the sections regain strength through autogenous healing. The cracks formed at an early age, large compressive stresses were imposed on the cracked sections from the prestressing, and the curing of the girders took place in a moist environment.

Three steam-cured girders tested by Roller (1993) were also observed to develop pre-release cracks. One of two girders with a deck slab and one without a deck slab were tested to evaluate flexure and shear strength. A second girder with a deck slab was used to determine behavior under full design dead load over an 18-month period. The authors indicated that the girders showed little or no effect from the pre-release cracks. A girder without pre-release cracks, similar to the cracked girders, was not tested so the conclusion made by Roller that pre-release cracks had little effect on the beams was made from comparing the measured results from

testing to the calculated predictions using the measured material properties of the girders.

Several studies have been published regarding investigation of the fatigue life of prestressing strand, but the majority of these studies did not involve testing of strands in cracked concrete sections. Strand stress ranges increase in cracked sections because of the local strain in the steel strands that occurs from crack opening. The increased steel stress ranges increase the fatigue concern in the strands. Previously there has been little concern regarding steel fatigue in prestressed girders because the strand stress ranges are small when sections remain uncracked in service, as has been the design practice. Cracked sections may occur however, from an overload, which would increase the strand stress ranges. During testing performed by Rabbat (1979), strand fractures were observed in cracked sections after three million cycles of load from a strand stress range of only 9 ksi. This fatigue failure occurred at a significantly lower stress range than is allowed in uncracked sections due to the local stress effect that occurs in the steel at a crack location.

ACI Committee 215 (1994) recommends a fatigue limit of $0.10f_{pu}$ for the stress ranges in prestressing strand in uncracked sections. This limit corresponds to a stress range of 27 ksi for Grade 270 ksi prestressing strand. A lower limit of 20 ksi was suggested by Paulson (1983) for cracked sections. ACI provided a suggested recommendation of $0.04f_{pu}$ for a fatigue limit for prestressing strand in cracked sections until further research was conducted (Hawkins, 1982). In 1994, the Committee recommended the stress range in the prestressing strands be limited to $0.06f_{pu}$ based on a cracked section analysis, despite the experimental results from Rabbat of fatigue failures at stress ranges lower than this limit. The $0.06f_{pu}$ limit corresponds to 16.2 ksi for Grade 270 ksi prestressing strands. The results of the fatigue testing by Rabbat had a 40% reduction in the fatigue limit recommended by ACI Committee 215.

1.1.2 Geometric Compatibility Theory

A geometric compatibility theory (GCT) was developed to predict the effects of pre-release cracks on girder camber and flexural cracking loads based on the geometry changes required to close the pre-release cracks in the girder (Shield, 1997). The equations required for the application of the GCT are repeated here. The GCT is based on the following three assumptions: the camber of the girder can be modeled as an arc of a circle, the pre-release cracks all extend to the same depth, and the pre-release cracks are spaced evenly throughout the length

of the beam. Figure 1.1 shows the expected cambered shape of a girder had it not had pre-release cracks. The figure includes the following notations: h is the girder depth, z_{na} is the depth of the neutral axis from the top of the girder, z_{crack} is the depth of the crack measured from the top of the girder, $s_{e\text{-}na}$ is the expected neutral axis length assumed to be the length of the girder on the bed prior to strand release, $s_{e\text{-}crack}$ is the expected arc length at the crack tips, $s_{e\text{-}top}$ is the expected arc length at the top of the girder (had it not developed pre-release cracks), and c_e is the expected girder camber.

The camber of a prestressed girder is very small relative to the overall girder length, so the modeling of the girder as an arc of a circle results in a very small central angle (χ_e). A transcendental equation was developed to determine the central angle based on the geometry of the beam. This equation was

$$c_e = \frac{s_{e4na}}{\chi_e}\left(1 - \cos\frac{\chi_e}{2}\right). \tag{1.1}$$

The radius of curvature was found after determining the central angle using the relationships from a segment of a circle. This equation was

$$r_{e4na} = \frac{s_{e4na}}{\chi_e}. \tag{1.2}$$

The expected arc length at the top of the girder and at the crack tip were found after determining the central angle and the radius of curvature. These equations were

$$s_{e4top} = r_{e4na} - z_{na}\chi_e, \tag{1.3}$$

and

$$s_{e4crack} = r_{e4na} - z_{na} - z_{crack}\chi_e. \tag{1.4}$$

The shape of the girder after crack closure was obtained as the superposition of the expected shape of the uncracked girder (camber from prestressing minus the deflection from girder self-weight) with the bending of the girder for crack closure. The shape after crack closure is shown in Figure 1.2. As shown in the figure, closure of the pre-release cracks resulted in a reduced camber and a shorter arc length at the top of the girder. The shortening at the top of the girder ($\div_{top}$) corresponded to the sum of the lengths of the crack openings. The bending of the girder about the crack tips for crack closure resulted in an arc length at the crack tips equal in both the expected and actual girder shape.

$$s_{e4crack} = s_{a4crack}. \tag{1.5}$$

Equations (1.1) through (1.3) were revised to describe the girder geometry in its actual shape. These equations were

$$c_a = \frac{s_{a4crack}}{\chi_a}\left(4\cos\frac{\chi_a}{2}\right), \tag{1.6}$$

$$r_{a4crack} = \frac{s_{a4crack}}{\chi_a}, \tag{1.7}$$

and

$$s_{a4top} = r_{a4crack}\,2\,z_{crack}(\chi_a. \tag{1.8}$$

The shortening of the top arc due to crack closure was the difference between the expected arc length and the actual arc length. This equation was

$$\div_{top} = s_{e4top}\,4\,s_{a4top}. \tag{1.9}$$

A simplified equation was developed for use in this report using the above equations (1.1 through 1.9) and the following approximation:

$$\cos\frac{\chi_e}{2} = 14\frac{1}{2}\left(\chi_e\right)^2. \tag{1.10}$$

This approximation eliminated the transcendental equations necessary in the GCT equations (1.1 and 1.6) to determine the central angle. The simplified equation used to predict the actual camber, using a known girder length (L, $s_{e\text{-}na}$ in GCT equations), expected camber (c_e), neutral axis depth (z_{na}), depth of cracks (z_{crack}), and total width of all cracks ($O_{Crwidths}$, $\div_{top}$ in GCT equations) is:

$$c_a = \frac{8c_e z_{crack}\,4\,LO_{Crwidths}(L^2\,2\,8c_e z_{na}\,4\,z_{crack}(}{8L^2 z_{crack}} \tag{1.11}$$

This equation was used for calculations in this report that investigated the validity of the GCT theory in predicting effects of pre-release cracks.

1.2 Objective and Scope

The objective of this research was to determine the effects of pre-release cracks on camber, flexural cracking loads, and steel fatigue, and to determine the validity of the geometric compatibility theory in predicting pre-release crack effects.

The effect of pre-release cracks on stress ranges in the prestressing strands due to a reduced flexural cracking capacity, and the possibility of fatigue failure of the strands, were determined using the computer programs SPAN (Leap Software, 1990) and RESPONSE (Collins, 1990). Effects on camber and flexural cracking loads were determined using the finite element program ABAQUS (HKS Inc., 1994). The results from ABAQUS were also used to determine the validity of the GCT for predicting crack effects. The final stage of the research included ABAQUS modeling of the two experimental girders tested by Ahlborn. The analytical results were compared to the limited experimental data to determine the accuracy of finite element modeling in predicting girder behavior. The ABAQUS results were also used to determine if the occurrence of the pre-release cracks in the test girder could account for the observed reduction in camber and flexural cracking load.

1.3 Organization of the Study

Chapter Two details a parametric study used to investigate the effect of variations in concrete strength, girder type, girder spacing, and strand size, on the steel strand stress ranges to determine if fatigue of the prestressing strand could become a concern as a result of early flexural cracking due to pre-release cracks. Chapter Three describes the ABAQUS finite element modeling of a 45 in. depth by 22 in. width (1140 mm by 560 mm) rectangular prestressed girder cross section and the results of single and multiple pre-release crack models. Chapter Four describes finite element modeling of the experimental girders tested by Ahlborn, and compares the results to the measured experimental data. Chapter Five concludes the report with a summary of the results of the study and includes recommendations for further research into the effects of pre-release cracks on prestressed girders.

CHAPTER TWO
INVESTIGATION INTO STEEL FATIGUE

2.1 Introduction to the Parametric Study

Pre-release cracks have been observed in high strength prestressed concrete girders (Ahlborn, 1998; Green, 1984; Roller, 1993). These cracks are believed to cause a reduction in the camber and flexural cracking capacity of the girders (Ahlborn, 1998). Reduction of the flexural cracking capacity may cause large localized stress ranges in the steel strands due to crack opening under service load conditions. A parametric study to investigate steel stress ranges was performed to determine if fatigue of the prestressing strands could become a concern as a result of early flexural cracking due to pre-release cracks.

Six girder designs that varied in concrete strength, girder type, girder spacing and strand size were developed to investigate steel stress ranges possible in current bridge designs. The purpose of the parametric study was to determine the largest steel stress range expected in design, and to determine the increase in the expected steel stress range if the girder became cracked (e.g. due to an overload). Data from two computer programs, SPAN (Leap Software, 1990) and RESPONSE (Collins, 1990), were used in determining the steel stress ranges in uncracked, cracked, and partially cracked girder sections.

2.1.1 Girder Designs

The six girder designs used to investigate steel stress ranges possible in current bridge designs are listed in Table 2.1. The parameters investigated were similar to those used in a parametric study by Ahlborn (1998) where the maximum span lengths for different girder designs were determined. Cases 1-4 used 7,000 psi (48 MPa) concrete and 0.5 in. (12.7 mm) diameter Grade 270 ksi (1860 MPa) low relaxation prestressing strands. The variables in Cases 1-4 were the type of cross section and the girder spacing. Minnesota Department of Transportation (Mn/DOT) 45M and 81I sections spaced at 4 and 12 ft (1.2 and 3.7 m) were investigated. Case 5 was used to examine the effect of concrete strength on steel stress range. A Mn/DOT 81I section spaced at 12 ft, similar to Case 1, was used but the concrete strength was increased to 10,000 psi (69 MPa). Case 6 was used to examine the effect of strand size on steel stress range. It used the same girder design as Case 1, but the strand size was increased to 0.6 in.

(15.2 mm) diameter Grade 270 ksi (1860 MPa) low relaxation prestressing strand. The span length used for each case was the maximum length possible for the design parameters. Intermediate girder spacings of 7 and 10 ft (2.1 and 3.0 m) and intermediate Mn/DOT section sizes of 54M, 64I, and 72I were not analyzed in the parametric study because these designs would have resulted in stress ranges bounded by those of the spacings and sections used.

Two computer programs were used to determine the change in stress in the bottom prestressing strand due to an applied live load. The first program, SPAN (Leap Software, 1990), was used to determine a strand pattern for prestressed concrete bridge girders based on AASHTO Specifications (1993). For a given girder spacing, girder type, strand size, concrete strength and applied load, the program determined the number and location of prestressing strands to satisfy the allowable stress limits throughout the girder at release and under service load. Additional information computed in SPAN that was used for the steel stress calculations included:

- Midspan moments prior to live load and with live load,
- uncracked moments of inertia using transformed sections,
- neutral axis locations of the composite sections as measured from the bottom of the section, and
- bottom fiber stresses due to the applied load.

This information is shown in Table 2.2. Discussion of how this data was used in the stress calculations is included with the sections pertaining to each girder condition: uncracked, cracked and partially cracked. The second computer program used to aid in the steel stress range calculations was the moment-curvature program RESPONSE (Collins, 1990). This program was used for the steel stress calculations involving partially cracked sections. These calculations are discussed in Section 2.4.

Additional design information necessary for the computer analyses included information such as the overall bridge width, material properties, sustained dead load and initial prestress force. A sample SPAN output file including the echo of the input file information is included in Appendix A. Appendix B includes the input file for a RESPONSE analysis. The assumptions used in the girder designs were similar to those used in Ahlborn (1998) and were as follows:

- 52 ft. (16 m) overall bridge width with a 48 ft. (15 m) road width,
- Grade 270 ksi (1860 MPa) prestressing strands with an elastic modulus of 28,500 ksi

(197 GPa),

- initial prestressing force equivalent to 75% of the ultimate strength,
- composite deck consisting of a 9 in. (230 mm) deck with a 1 in. (25 mm) haunch made from 4,000 psi concrete with a density of 150 lb/ft^3 (2400 kg/m^3),
- density of the girder concrete of 155 lb/ft^3 (2480 kg/m^3), and
- only interior girders analyzed.

The stress range in the steel was only calculated at the midspan because this was the location of the largest applied live load moment. No draping or debonding of the prestress was included because these details do not affect the midspan stress.

The prestressing force, girder self-weight and deck self-weight were automatically applied to the noncomposite section in the SPAN analyses. Additional loading applied in each design included a superimposed sustained dead load to the noncomposite section, a superimposed sustained dead load to the composite section, and a live load from the HS-25 standard truck and military load. The superimposed sustained dead loads applied to the composite and noncomposite sections for the six girder designs are listed in Table 2.3.

The superimposed sustained dead load applied to the noncomposite section included the weight of the diaphragms only. The weight of each diaphragm was calculated using the "Concrete Intermediate Diaphragms" detail from the *Mn/DOT Bridge Details Manual* (1991). Spans 90 ft. or greater had diaphragms placed at the third points and spans less than 90 ft. had a diaphragm placed at the midspan. The diaphragm weight was converted into an equivalent unit load that produced the same midspan moment.

The superimposed sustained dead load applied to the composite section included a J rail load, a two-inch wearing course and a future wearing course. The J rail load was determined using the "Type "J" Railing on Inplace Box Culverts" detail from the *Mn/DOT Bridge Details Manual* (1991). To remain consistent with the designs used in the parametric study by Ahlborn (1998), one-third of the J rail load was assumed to act on the first interior girder, the two-inch wearing course was assumed to be 25 lb/ft^2 (1.2 kPa) and the future wearing course was assumed to be 17 lb/ft^2 (0.8 kPa).

To calculate the steel stress range for each of the girder designs, the girders were loaded with the HS-25 standard truck and the military live loads. An analysis was also run for each girder design without any live load applied. Detailed descriptions of the calculations and the

results of the steel stress ranges are given in the following sections.

2.2 Uncracked Section

The change in stress in the bottom steel strand due to the live load was calculated for an uncracked section. First the change in concrete stress at the level of the bottom strand due to live load was calculated according to the following equation:

$$\div\omega_c \mid \frac{\div M \Delta y}{I}, \tag{2.1}$$

where $\div\omega_c$ is the change in concrete stress in the section at location y from the neutral axis, $\div M$ is the change in moment applied to the section, and I is the moment of inertia. To determine the change in concrete stress due to the live load, $\div\omega_{c,LL}$, the change in applied moment due to application of live load, $\div M_{LL}$, was used. The live load moments, composite gross moments of inertia, and neutral axis locations were all determined from SPAN and were included in the output files. The moments of inertia and neutral axis locations ($I_{g,c}$ and $y_{g,c}$) were listed in Table 2.2. The changes in applied moments due to the application of live load were calculated by subtracting the "Prior to Live Load" moments from the "With Live Load" moments listed in Table 2.2. The bottom steel strand was located 2 in. (50 mm) above the bottom of the section, so y in Equation (2.1) was 2 in. less than the neutral axis height. The stress resulting from Equation (2.1) was the change in concrete stress at the location of the bottom steel strand due to live load. Assuming perfect bond between the steel strand and the concrete, the change in strain in the steel and concrete due to live load application at this location were assumed to be equivalent. The change in steel stress due to live load ($\div\omega_{s,LL}$) was then calculated using relationships between stress and strain. The equation converting the change in concrete stress to a change in steel stress due to live load was:

$$\div\omega_{s,LL} \mid \div\omega_{c,LL} \Delta \frac{E_s}{E_c}, \tag{2.2}$$

where E represents the modulus of elasticity, and the subscripts s and c denote steel and concrete, respectively. The steel modulus of elasticity was assumed to be 28,500 ksi (197 GPa). The concrete modulus of elasticity was assumed to be 5,300 ksi (37 GPa) for 7,000 psi (48 MPa) concrete and 6,400 ksi (44 GPa) for 10,000 psi (69 MPa) concrete, calculated from the modulus of elasticity equation in ACI 318-95. This equation was:

$$E_c \mid w_c^{1.5} \Delta 33\sqrt{f'_c}, \qquad (2.3)$$

where w_c is the unit weight of concrete (lb/ft^3) and f'_c is the concrete compressive strength (psi).

The stress ranges for the uncracked sections are listed in Table 2.1 under the column heading Uncracked Stress Range. The steel stress range for the uncracked section ranged between 3.72 ksi and 6.77 ksi. The largest stress range occurred in Case 2 (the smaller girder section at the larger girder spacing) which was expected because the larger girder spacing yielded a higher moment and the value *y/I* of Equation (2.1) increases for smaller section sizes. The stress ranges determined from the SPAN results are what would be expected in design because the sections are not expected to be cracked under service load. Sections are designed to keep the tensile stresses below the tensile strength of the concrete. The uncracked section stress ranges were all well below the 20 ksi fatigue limit suggested by Paulson (1983) and the $0.10f_{pu}$ fatigue limit suggested by ACI Committee 215 (1994). Fatigue would not be a concern for these girders if the section did not crack under service load. However, a loss of compressive stress is expected in the bottom fiber of the girder due to pre-release crack closure. This loss of compressive stress may result in the section cracking at a lower applied load. A cracked section would have higher steel stress ranges and a lower fatigue limit. The steel stress ranges possible in fully cracked girder sections are detailed below.

2.3 Cracked Section

The steel stress ranges for cracked sections were determined using the fully cracked moments of inertia for each girder section. The cracked moments of inertia were calculated by assuming all of the concrete below the neutral axis in each section had cracked and did not provide any tensile resistance in the section. The steel tendons were the only part of the section balancing the compressive force from the concrete above the neutral axis. The cracked moments of inertia and neutral axis locations (I_{cr} and y_{cr}) for the six girder designs were listed in Table 2.2.

The stress range in the bottom steel strand was calculated by assuming the live load that brought the bottom fiber stress to zero acted on an uncracked section and the additional live load was applied to the cracked concrete section. This case simulated the stress condition for a section that had been precracked (possibly due to an overload), such that the concrete had zero

tensile resistance. The live load midspan moment and the bottom fiber stress in the section prior to live load were determined by SPAN. These values were tabulated in Table 2.2, where the live load midspan moment is equal to the difference between the two moments tabulated. The portion of the live load moment corresponding to the bottom fiber stress of zero, M_{LLZ}, was determined by solving Equation (2.1) for $\div M$, using $\div \omega_c$ equal to the change in stress required for the bottom fiber to reach zero stress from the stress state prior to the addition of live load, y equal to the neutral axis depth of the uncracked composite section measured from the bottom fiber, and I equal to the moment of inertia of the uncracked composite section.

For example, the change in stress required for the bottom fiber to reach zero in Case 1 was 632 psi (stress to overcome state of stress prior to live load), determined from the SPAN analysis and listed in Table 2.2. The calculated moment using Equation (2.1) corresponding to this change in stress using the uncracked composite section properties was 1383 k-ft. The remaining portion of the live load moment which was assumed to act on the section with a stiffness given by the cracked moment of inertia was 1094 k-ft. To determine the total change in steel stress due to the live load, first the change in concrete stress at the bottom steel strand location was calculated as follows:

$$\div \omega_{c,LL} = \frac{M_{LLZ}(y_g - y_{strand})}{I_g} - \frac{M_{LLR}(y_{cr} - y_{strand})}{I_{cr}}, \qquad (2.4)$$

where M_{LLZ} was the portion of the live load moment corresponding to zero stress in the bottom fiber, M_{LLR} was the remaining portion of the live load moment, above the amount required to bring the bottom fiber to zero stress, y_g and y_{cr} were the locations of the uncracked and cracked composite neutral axes from the bottom of the section, y_{strand} was the location of the bottom steel strand from the bottom of the section, assumed to be 2 in., and I_g and I_{cr} were the moments of inertia of the uncracked and cracked composite sections, respectively. Equation (2.2) was then applied to calculate the change in steel stress. Using Case 1 as an example, the change in concrete stress at the location of the bottom steel strand from M_{LLZ} was 0.6 ksi. The additional change in concrete stress from M_{LLR} was 4.9 ksi. The total change in concrete stress at the level of the bottom strand from the live load moment was 5.5 ksi, corresponding to a bottom steel strand stress change of 29.5 ksi.

The stress ranges for the cracked sections are listed in Table 2.1 under the column heading Cracked Stress Range. The stress range in the bottom steel strand for a cracked section

ranged between 21.2 ksi and 33.5 ksi. The largest stress range occurred in Case 2 (the smaller girder section placed at the larger girder spacing), as for the case of the uncracked section analysis. All of the stress ranges calculated using cracked section analysis exceeded the 20 ksi fatigue limit suggested by Paulson (1983), and half exceeded the $0.10f_{pu}$ fatigue limit of ACI Committee 215 (1994). However, these limits were only applicable to sections that did not crack. Cracked sections require a much lower fatigue limit. ACI Committee 215 (1994) recommends that a stress range not exceed $0.06f_{pu}$ for cracked sections. This limit corresponds to 16.2 ksi for Grade 270 ksi prestressing steel. All of the steel stress ranges for the cracked sections exceeded this recommended limit.

Many of the neutral axis locations used in calculating the cracked moments of inertia were located in the concrete deck. This was because the composite deck raised the neutral axis due to the large amount of concrete at the top of the composite section. A comparison of the neutral axis locations of the cracked (y_{cr}) and uncracked (y_g) sections is shown in Table 2.2. In determining the neutral axis location, all of the concrete below the neutral axis was assumed to have cracked, thus it did not supply any tensile resistance for the section. Because the neutral axes were very high in the section, it was not expected that the entire section below this location would crack under overloads. The stress ranges determined for the cracked sections were thought to be larger than would be expected in the field. To establish a more accurate representation of the girder behavior with a portion of the section cracking in flexure, the stress range in the steel was determined using an effective moment of inertia. This procedure was completed using the computer program RESPONSE and is detailed below.

2.4 Partially Cracked Section

The moment-c

the differences in section geometry and material properties. The tensile strength of the concrete (f_{cr}) was set to zero to simulate a precracked section. A smaller portion of the section "opened" in these analyses than for the fully cracked section because the live load moment was not large enough to fully crack the section.

Two different

MPa). The second model was a more complex model used for relating stress to strain for higher concrete strengths. This model was used for the 10,000 psi (69 MPa) concrete. The high-strength concrete model is described in Collins and Mitchell (1991) and follows the equation:

$$\frac{f_c}{f'_c} = \frac{n\left(\frac{\varepsilon_c}{\varepsilon_c'}\right) - \left(\frac{\varepsilon_c}{\varepsilon_c'}\right)^k}{1 + (n-2)\left(\frac{\varepsilon_c}{\varepsilon_c'}\right)}$$

where f_c is the concre
equal to f'_c/ε'_c, and k is a decay factor.

Additional input was required for the RESPONSE analyses to account for the prestressing force and the composite deck. An initial strain was applied to the steel layers to model the prestressing force. This strain was caused by the steel stress at the steel center of gravity after all losses. The steel stress after losses was calculated in SPAN and the strain applied to the steel in RESPONSE is shown in Table 2.4. In addition to the initial strain applied to the steel strands, an initial strain distribution was imposed on each girder to account for the strain discontinuity at the interface of the prestressed girder and the composite deck that existed because the composite deck was added to the section at a later construction phase. This strain distribution was due to the stress in the girders from the prestressing force accounting for all losses, the girder self-weight, the weight of the diaphragms, and the deck weight. These loads acted on the noncomposite section so strains were not induced in the concrete deck. The strains at the top and bottom fiber of the noncomposite section that were imposed on each girder are listed in Table 2.4 under the column "Initial Strains for RESPONSE". The concrete strain distribution in the section was linear between the two strains. The strain at each change in section width and at the steel locations were also necessary for the RESPONSE input file. The initial concrete strain distribution, as specified in the input file, is shown in the strain distribution of Figure 2.1 for Case 1. The top fiber strain in the girder was -0.303×10^{-3} and the bottom fiber strain was -0.229×10^{-3}. The initial strain in the deck was zero. This simulated a stress

free deck added to a girder that had already been loaded with a prestressing force, its self-weight, the weight of the diaphragms, and the weight of the concrete deck. Appendix B includes a copy of the RESPONSE input file for Case 1.

The stress range in the steel for a partially cracked section was determined using the moment-curvature relationship for that section. RESPONSE calculated the curvature and top and bottom fiber strain of the composite section for a given moment. The curvature and strain output for RESPONSE analyses that involved initial strains was not the total curvature and strain in the section, but rather the change in curvature and strain that occurred after the section became composite. For example, the curvature and strain output for a moment input of 10 k-ft more than the moment corresponding to the initial strain input data (initial strain moment + 10 k-ft) would be the curvature and strains for a moment of 10 k-ft, not the initial strain moment + 10 k-ft. The total applied moment corresponded to the change in strain and curvature from the time the section became composite. The total strain could be determined by superimposing the initial strain distribution of the noncomposite section and the additional linear strain distribution of the composite section given by RESPONSE, as shown in Figure 2.2. However, only the change in strain due to live load was necessary for computing the steel stress ranges, so the total strains were not computed.

The curvature and top and bottom fiber strains of the composite section were determined using RESPONSE for both the midspan moment prior to the application of any live load and with live load. These moments were determined in SPAN and were shown in Table 2.2. The change in strain at the location of the bottom steel strands was determined using the linear strain distributions from RESPONSE. The steel stress range for the partially cracked section was calculated by multiplying the change in strain in the bottom steel strands by the steel modulus of elasticity.

The total moment prior to the application of the live load calculated in SPAN for Case 1 was 3885 k-ft (Table 2.2). The curvature corresponding to this moment as 1.65×10^{-6} rad/in. according to RESPONSE. The corresponding top and bottom fiber strains were -0.024×10^{-3} and 0.126×10^{-3} (Table 2.4), respectively. These were the changes in curvature and strain from the time the section became composite, not the total curvature and strain for the section due to the output characteristic of the RESPONSE program for sections involving initial strains. Using a linear strain distribution between the top and bottom strain output from RESPONSE, the strain

at the location of the bottom strand of steel for the moment prior to the application of live load was 0.123×10^{-3}.

The total moment with live load calculated in SPAN for Case 1 was 6362 k-ft (Table 2.2). The curvature calculated from RESPONSE for this moment was 7.71×10^{-6} rad/in. and the top and bottom fiber strains were -0.139×10^{-3} and 0.563×10^{-3} (Table 2.4), respectively. Using a linear strain distribution between the top and bottom strain output from RESPONSE, the strain in the concrete at the location of the bottom steel strand for the moment with the live load 0.548×10^{-3}.

The stress range in the bottom steel strand for the partially cracked section of Case 1 was determined by multiplying the change in strain due to live load at the level of the bottom steel strands by the steel modulus of elasticity. This calculation assumed perfect bond between the concrete and the steel. The change in strain for Case 1 was 0.425×10^{-3} (0.548×10^{-3} - 0.123×10^{-3}) which corresponded to a steel stress range of 12.11 ksi. The same procedure was used to determine the stress range in the bottom steel strand for the other five girder designs. The moments used for the designs were determined in SPAN and are listed in Table 2.2. The extreme fiber strains calculated in RESPONSE for these moments are listed in Table 2.4.

The stress ranges for the partially cracked sections are listed in Table 2.1 under the column heading Partially Cracked Stress Range. The steel stress ranges for partially cracked sections ranged between 7.24 ksi and 13.25 ksi. The largest stress range occurred in Case 2 (the smaller girder section at the larger girder spacing). The results using the partially cracked section analyses represent girder performance in an average sense because the effects of cracks are distributed over a larger length. The stress range at a specific crack location may be closer to the results from the cracked section analysis. The stress in the steel at a crack location is increased due to the local strain in the steel from the crack opening. The partially cracked section results provide a lower bound for the steel stress range in a cracked girder, and the cracked section results provide an upper bound for the steel stress range at a crack location because the stress range in the steel is dependent on the bond between the strands and the concrete. The stress ranges determined using the cracked sections exceed the recommended fatigue limit by ACI Committee 215 (1994). The stress ranges determined using the partially cracked sections approached but did not exceed the recommended limit from ACI. The partially cracked section stress ranges did exceed the experimental fatigue failure of 9 ksi recorded by

Rabbat (1979), indicating fatigue should be a concern in cracked girder sections, especially until more research has been completed and a more definite fatigue limit for steel in cracked sections has been determined.

2.5 Moment of Inertia Comparison

To compare the three cases used in determining strand stress ranges, the composite girder stiffnesses for the three cases of uncracked (I_g), partially cracked (I_{eff}), and cracked (I_{cr}) were computed. The composite moments of inertia for the three cases were included in Table 2.2. The uncracked moment of inertia was determined in SPAN, the cracked moment of inertia was calculated assuming all of the concrete below the neutral axis in each section had cracked and did not provide any tensile resistance in the section, and the partially cracked moment of inertia was calculated using the moment curvature relationship from RESPONSE. The stiffness of the partially cracked sections were calculated using the formula

$$EI_{eff} \mid \frac{M_{LL} 4 M_{NLL}}{\lambda_{LL} 4 \lambda_{NLL}}, \tag{2.6}$$

where *LL* represents the results of the analysis including live load and *NLL* represents the results of the analysis prior to the application of live load. This equation represents the slope of the line between the two data points on the moment-curvature plot. The slope divided by the modulus of elasticity yields the effective moment of inertia, representative of a partially cracked section. As expected, the stress range in the bottom strand of steel increased with the decrease in moment of inertia.

2.6 Summary

The results from the parametric study show that a fatigue concern may exist for girders that develop pre-release cracks. Pre-release cracks cause a reduction in the bottom fiber compressive stress of the girder, resulting in a reduced flexural cracking capacity. The stress ranges in the bottom steel strand for sections that have cracked in flexure can exceed the recommended fatigue limit from ACI Committee 215 of $0.06f_{pu}$ (1994), especially in the steel strand near a flexural crack location.

CHAPTER THREE
INVESTIGATION INTO CAMBER AND STRESS STATE

3.1 Introduction

This chapter describes the finite element modeling of pre-release cracks using ABAQUS (HKS Inc., 1994) software. Pre-release cracks begin at the top flange and extend into the depth of the section. When the girder is removed from the precasting bed, the cracks close due to the prestress and girder self-weight. The purpose of the analytical models was to determine the effects the pre-release cracks had on girder stresses and camber. Several different crack widths and depths were modeled. Closure of pre-release cracks was expected to cause a decrease in girder camber and bottom fiber compressive stress. It was also expected that the stress changes would be local, occurring only near the pre-release crack locations. This chapter first describes the effects of a single pre-release crack at midspan. Using ABAQUS models, changes in camber and stress throughout the section were determined for changes in crack width and crack depth. The results from models involving three cracks were then compared with the ABAQUS results from the single crack models. The chapter concludes with the application of the geometric compatibility theory described in Section 1.1.2. The predicted camber using this theory was compared with the camber results from ABAQUS.

3.2 ABAQUS Single Crack Models

Nine different models of a single pre-release crack at midspan were created. Each model varied in the pre-release crack size. All combinations of three different crack depths and widths were modeled. The crack depths were 12, 24 and 33 in. (305, 610 and 838 mm). Crack widths were 1/100, 1/32 and 1/16 in. (0.25, 0.8 and 1.6 mm). Additional crack depths between 30 and 36 in. were modeled when investigating the crack depth effect. This is discussed in Section 3.2.4. The camber loss and stress state were determined for each crack size.

3.2.1 ABAQUS Model Description

The ABAQUS model consisted of a simply supported 45 in. by 22 in. (1140 mm by 560 mm) rectangular section spanning 135 ft (41 m). Prestressing was modeled using truss elements with the nominal area of steel equivalent to 46 - 0.6 in. (15.3 mm) diameter strands. The model

used properties similar to the full-scale experimental girder tested at the University of Minnesota (Ahlborn, 1998) that developed pre-release cracks. A rectangular cross section was used rather than an I-section to simplify the model. The 22 in. width was selected so that the moment of inertia of the gross concrete section (167,063 in^4) was similar to the gross moment of inertia of a noncomposite Mn/DOT 45M section (167,048 in^4). A composite deck was not added to the model. The modulus of elasticity used for the concrete and the steel were 4,800 ksi and 28,500 ksi (33.1 MPa and 200 MPa), respectively.

The concrete girder was modeled using two-dimensional solid elements of type CPS8R. The two dimensions modeled the length and depth of the girder. The width was specified to be 22 in. (560 mm) for all of the CPS8R elements. CPS8R elements are plane stress elements with 8 nodes that incorporate reduced integration in the analysis. Thirty layers of 1.5 in. (40 mm) height elements were used to model the 45 in. (1140 mm) depth of the girder section. The elements near the midspan, between 59 and 76 ft (18 and 23 m), were 4 in. (100 mm) in length and 1.5 in. (40 mm) in height. Element A in Figure 3.1 represents a CPS8R element 4 in. (100 mm) long and 1.5 in. (40 mm) high, similar to the elements at midspan in the ABAQUS models. The nodes in Figure 3.1 are represented by circles and the lines form the boundaries for the elements. Each element had eight nodes to define its location, labeled 1-8 on Element A in Figure 3.1.

The element length was increased to 12 in. (305 mm), while keeping the height at 1.5 in. (40 mm), at the two ends of the span. The longer elements modeled the span between 0-59 ft (0-18 m) and 76-135 ft (23-41 m). The longer element length increased the aspect ratio (length/height) of the elements to 8 at the girder ends. This was a larger aspect ratio than is generally acceptable, but the stresses at the midspan and the overall girder camber were not affected by the larger element size at the two ends of the girder. Larger elements were used after determining that the stress effects from pre-release cracks were local to the crack area. The elements in the region of the pre-release crack were only 4 in. (100 m) in length, giving an aspect ratio less than three where stresses were of interest. The larger elements at each end of the girder reduced the degrees of freedom in the models, improving the efficiency of the ABAQUS analyses.

The prestressing strands were modeled using T2D2 elements. T2D2 elements are two-dimensional linear truss elements containing two nodes. The truss elements were placed 9 in.

(230 mm) up from the bottom of the girder. This location was higher than the center of gravity of the prestressing strands in the experimental girder. The higher steel location was used so the pre-release cracks would close completely in more of the models. As the crack depth decreased and/or the crack width increased, the girder was more resistant to crack closure.

The cross-sectional area of the steel was specified as 9.89 in^2 (6380 mm^2). The steel location is shown as a dark dashed line in Figure 3.1. Elements D, E, F, G, H and I are T2D2 elements. All of the truss elements were 2 in. (50 mm) in length in the midspan region. The elements lengthened to 6 in. (150 mm) at the two ends of the girder where the CPS8R elements were 12 in. (305 mm) in length. Element D connected nodes 9 and 10, Element E connected nodes 10 and 11, and so on along the span length. Prestressing was added to the steel by assigning an initial stress to the truss elements. A sample ABAQUS input file is included in Appendix C. The ABAQUS code for adding the initial stress to the truss elements is *INITIAL CONDITION, TYPE=STRESS. A stress of 303,300 psi (2,090 MPa) was applied to the truss elements. This stress corresponded to an initial prestressing force of 3,000 kips (13,350 kN). This force was greater than 75% of ultimate strength, but the larger force was necessary to have the cracks close in many of the models involving larger crack widths or smaller crack depths.

The girder was modeled as simply supported by restraining the girder in the x and y degrees of freedom at the left end of the span and in the y degree of freedom at the right end of the span. These restraints were placed on the single node on each girder end that was located at the prestressing steel height, 9 in. (230 mm) up from the bottom of the section.

A pre-release crack was placed at the midspan location of 67.5 ft (20.5 m). The crack was modeled as an inverted triangle with its base representing the crack width at the top of the girder. The height of the triangle represented the crack depth that extended into the girder depth. Figure 3.1 shows a pre-release crack width and depth dimensioning. The crack width for this crack was the distance between Nodes 16 and 17 and the crack tip is shown located at Node 18.

The pre-release crack at midspan was located such that it split the 4 in. (100 mm) long elements at midspan, that were within the depth of the crack, into two elements each. This required new nodes to be specified along the crack boundary so the elements could be separated to model an open crack. The elements directly beneath the crack did not change in size due to the pre-release crack. The elements that were split became two 2-in. (50 mm) long elements. Elements B and C in Figure 3.1 are two elements that were created from a 4-in. long element that

was split by the pre-release crack. The new 2-in. long elements were still CPS8R elements.

The nodes along the crack boundary were assigned nodal positions to model an open crack. If the crack width in the model was 0.01 in. (0.25 mm), the location of Node 16 in Figure 3.1 was 0.005 in. (0.125 mm) less than the midspan location and Node 17 was located a distance 0.005 in. (0.125 mm) greater than the midspan location. This created an opening between Nodes 16 and 17 equal to the crack width of 0.01 in. (0.25 mm). Each nodal location along the crack boundary was calculated in this same manner based on the width of the crack at the height in the section.

Gap elements of type GAPUNI were added to the models to connect the two nodes spanning the crack opening. Gap elements are one-dimensional contact elements that allowed stress to be transferred across the crack when the crack closed. Dashed lines represent the gap elements across the crack opening in Figure 3.1. Elements J, K and L are GAPUNI elements. Each of the gap elements had an initial length assigned to it that represented the width of the crack opening at the gap location. Gap element J had an initial length of 0.01 in. (0.25 mm) for the models with 1/100 in. crack widths.

Additional nodes were also added for the 2-in. (50 mm) long elements along the sides of the pre-release crack. Nodes at the midspan of the top and bottom element boundaries were necessary to define these CPS8R elements. Nodes 19 and 20 were the two nodes that were added for Element B in Figure 3.1.

The self-weight applied to the girders in the ABAQUS models was based on the area of the Mn/DOT 45M section that was used in the experimental girder and an approximate cubic weight of 160 lb/ft^3 (25 kN/m^2). The cross-sectional area of the 45M section was 624 in^2 (4030 cm^2). This area corresponded to a lineal weight of 694 lb/ft (10.2 kN/m) applied in the ABAQUS analyses. Effectively this lineal load corresponded to a cubic weight of 100 lb/ft^3 (16 kN/m^3) for the 45 in. by 22 in. (990 in^2 [6,390 cm^2]) rectangular section. To apply the self-weight loading on the girders, point loads were assigned to all of the nodes along the top of the girder. The nodes were grouped into node sets based on their tributary length. The node sets were then loaded with the appropriate force using the lineal weight of 694 lb/ft (10.2 kN/m) for that tributary length. If the tributary length for a node set was 3 in. (75 mm), the nodes in the set were loaded with one-quarter (3 in./12 in.) of the self-weight load per lineal foot (173.5 lb/ft [2.5 kN/m]).

Several different loads were applied in the ABAQUS models. The first load consisted only of the self-weight loading described above. The other load cases had an additional load applied with the self-weight load. The additional load varied from 100 lb/ft to 800 lb/ft (1.46 to 11.7 kN/m), using 100 lb/ft increments. The additional load was added to close the pre-release crack in many of the models. The additional load applied also provided insight toward the stress behavior of the section during crack closure.

An ABAQUS model that did not have any pre-release cracks was loaded with the same prestressing force and lineal load as the cracked models. The results from this model were used as a reference in determining the camber and stress changes resulting from a pre-release crack.

3.2.2 Affected Area

The elements in the models that changed in stress due to the presence of a pre-release crack were local to the pre-release crack location. Figure 3.2 shows the region of the girder that experienced stress change due to a single crack placed at midspan. Elements for which stress magnitude (compressive) increased are shown darker than elements for which stress magnitude (compressive) decreased. The change in stress decreased to zero as the element's horizontal distance from the crack location increased. The greatest change in stress occurred in the elements directly below the crack.

The elements at the bottom of the section had a decrease in magnitude of compressive stress relative to the uncracked model. These elements lost compression due to the pivoting of the girder about the crack tip to close the pre-release crack. The pivoting action to close the crack opening at the top of the girder caused the bottom fiber of the girder to lengthen. This lengthening of the bottom fiber caused a reduction in the compressive stress in the bottom elements of the section. The elements near the crack tip location increased in compressive stress due to the pivoting action about the crack tip. These elements compressed to close the crack. The elements at the top of the girder section had a reduction in compressive stress relative to the uncracked girder because the pre-release crack was initially open when the prestressing force was applied. The stress at the crack location was zero if the nodes along the crack boundary were not in contact with one another. Compressive stress at the top of the girder in the cracked models resulted only after the crack had closed. The compressive stress due to the prestressing that was seen at the top of the girder in the uncracked model was not present in the cracked

model because the crack was initially open.

The length over which there was a difference in the stress state between the uncracked girder model and the precracked girder model was limited to the depth of the girder (d = 45 in. [1140 mm]) on each side of the pre-release crack location. This region included all of the elements that had at least a one percent change in stress magnitude from the uncracked model. The change in stress was calculated using the following formula:

$$\frac{\omega_{ucr} - \omega_{cr}}{\omega_{ucr}} \Delta 100 \qquad (3.1)$$

where the subscript *ucr* refers to the stress in the uncracked model and *cr* refers to the stress in the cracked model. Figure 3.2 shows that the affected stress area spans a distance of 88 in. (2235 mm). This length is nearly equal to 90 in. (2285 mm), which is a depth of the girder (45 in. [1140 mm]) on each side of the crack.

The affected stress areas for all of the models with pre-release cracks are listed in Table 3.1. Three different criteria were established and tabulated for determining the affected stress area. The first criteria included the length over which elements had at least a 1% change in stress from the uncracked model. The second criteria included the length over which elements had at least a 4% change in stress from the uncracked model. The final criteria listed was "(max. change)/4". The affected area for this criterion consisted of the elements that had a change in stress equivalent to at least one-quarter of the maximum bottom element stress change from the pre-release crack. The maximum stress change occurred directly beneath the pre-release crack location. The percent change equivalent to "(max. change)/4" for each of the models was listed next to the affected area in Table 3.1. All of the results are from models loaded with an 800 lb/ft (11.7 kN/m) load in addition to the self-weight load (self-weight + 800 lb/ft). This load was used because it closed the pre-release crack in the greatest number of models.

The 4% change provides the best results of the three criteria listed in Table 3.1. A 4% stress change establishes an area around the crack that could reasonably be considered to be affected by the pre-release crack in a fabricated girder and not from other causes. Material properties alone could cause a stress change between two fabricated girders of more than 1%. The 1% criteria does not define the area where a legitimate concern regarding the change in stress is deemed because a 1% change would more likely be attributed to the non-homogenous nature of concrete and the ambiguity in prestress losses rather than due to the occurrence of a

pre-release crack.

The "(max. change)/4" criteria could be useful for the larger crack width models, but for the models using 1/100 in. (0.25 mm) width cracks, the "(max. change)/4" percentage was lower than 4%. For the model using a 1/32 in. (0.8 mm) crack width by 33 in. (840 mm) deep, the maximum stress change was 42%. The "(max. change)/4" percentage for this model was 10%, resulting in an affected stress area of 32 in. (815 mm) The maximum change in stress was 12% for the model with the 1/100 in. (0.25 mm) crack width by 33 in. (840 mm) deep. The "(max. change)/4" percentage for this model was 3% which resulted in an affected stress area of 40 in. (1015 mm) The 1-3% stress change area encompassed half of the affected area for this model. When the limiting percentage was below 4%, which it was using the "(max. change)/4" criteria, the affected area appeared to increase. This did not accurately represent girder behavior for all of the cracked models so the second criteria (4% change) was used in analyzing the stress changes.

The stress change decreased rapidly near the crack and then remained at a 1-3% change for a distance greater than $d/4$ at the edges of the affected area. The rapid decrease in stress change is shown in Figure 3.3. The change in stress in the bottom element for two of the 33 in. (840 mm) depth crack models is shown.

All future references in this report regarding affected stress area will use the stress results from the second criteria (4% change). The affected area increased as the crack width increased and decreased as the crack depth increased. Table 3.1 shows that for a 33 in. (840 mm) depth crack, the affected area of the three crack widths increased from 32 to 48 to 56 in. (815 to 1220 to 1420 mm) as the crack width increased. The affected area for a 1/100 in. (0.25 mm) width crack decreased from 40 to 32 in. (1015 to 815 mm) with an increase in crack depth from 24 to 33 in. (610 to 840 mm). Deeper cracks also resulted in a greater compressive stress loss in the bottom fiber of the element. This is discussed in Section 3.2.4. These two characteristics combined resulted in a large compressive stress loss in a concentrated region for deep cracks.

3.2.3 Stress Distributions as Crack Closed

The stress behavior in the section at the crack location was investigated to determine if the stress distributions remained linear. The distribution as the crack was closing and after it had closed were both analyzed. A nonlinear stress distribution occurred during crack closure, with

linear stress distribution increments occurring for additional loading after the crack was fully closed.

Figures 3.4 through 3.12 show the stress distribution at the crack location for the nine different pre-release crack models. The stress values plotted are the ABAQUS stresses at the center of each element at the crack location. The stress was directly beneath the crack location for the elements below the crack tip because the centers of the elements were directly beneath the crack tip. The elements within the depth of the crack were split into two elements, shown in Figure 3.1, so the stresses plotted for these elements were 1 in. to the side of the crack location. Figures 3.4 though 3.6 show the stress distributions for crack widths of 1/100 in. (0.25 mm), Figures 3.7 through 3.9 show the stress distributions for crack widths of 1/32 in. (0.80 mm) and Figures 3.10 through 3.12 show the stress distributions for crack widths of 1/16 in. (1.6 mm). The load when the crack was completely closed is noted in all of the figures. The crack depth is shown as a horizontal dashed line. Also shown in the figures is the stress distributions for the uncracked model loaded with self-weight and self-weight + 800 lb/ft. The height where the two uncracked model results are equal is the neutral axis location of the rectangular section. This height was 21.7 in. (550 mm). The stress distribution for the uncracked section varied linearly through the cross section for any load.

The stress behavior in the girders resulting from the load application varied depending on whether the crack was open (BCC - before crack closure) or closed (ACC - after crack closure). The following generalizations can be made from the analyses regardless of the crack width or depth:

- Before crack closure (BCC), the stress distributions were nonlinear through the cross section, and the changes in stress with load changes were nonlinear.
- After crack closure (ACC), the stress distributions were not linear because a non-linearity was created from the crack initially being open, but the changes in stress with load changes were linear. The change in stress was proportional to the change in load and the distance of the element from the neutral axis ($\div\omega\mid \frac{\div M\,\Delta y}{I_{g,t}}$). As an example, ACC the change in stress in the bottom element with a load change of 100 lb/ft was 324 psi, and the change in stress in the top element with a load change of 100 lb/ft was 347 psi. These stress changes were the same as in the uncracked section.

- BCC, the elements at the top of the section (above where the crack was open) had zero stress. These elements were unloaded because the crack remained open.
- BCC, the position of the neutral axis changed with the load application because the effective depth of the section changed as the crack closed. The neutral axis rose as more of the crack became closed.
- ACC, the neutral axis did not change. The neutral axis was the same as the neutral axis for the uncracked transformed section (21.7 in. [550 mm]).

A comparison between the cracked and uncracked stress distributions shows that a loss of compressive stress resulted at the top and bottom elements in the section, and an increase in compressive stress resulted near the crack tip.

Additional generalizations were made regarding effects of crack size. Deeper cracks closed at smaller loads because there was a smaller portion of the section remaining below the crack to resist crack closure. Wider cracks closed at larger loads because the larger crack width required more pivoting action of the girder about the crack tip to close. Wider cracks also had a greater loss of compressive stress in the top and bottom elements and a greater increase in compressive stress at the crack tip. Table 3.2 shows the change in stress from the uncracked model at the top, bottom, and crack tip location in each model. The closure load is also tabulated. The changes in compressive stress relative to the uncracked model increased between the self-weight load and the self-weight + 800 lb/ft load in all of the cases where the crack remained open with only the self-weight load applied.

Figures 3.13 through 3.21 show the stress distributions for the girder section located two feet away from the pre-release crack location. Figures 3.13 through 3.15 show the stress distributions for the 1/100 in. (0.25 mm) crack width models, Figures 3.16 through 3.18 show the stress distributions for the 1/32 in. (0.8 mm) crack width models and Figures 3.19 through 3.21 show the stress distributions for the 1/16 in. (1.6 mm) crack width models. All of the figures show that the stress distribution was not linear two feet (0.6 m) away from the pre-release crack location, although the distributions were nearly linear in Figures 3.13, 3.14, 3.15, and 3.18. Minor changes in stress can be seen by comparing the cracked stress distribution to the uncracked stress distribution in any of the figures. The non-linearity is easily seen in the results from the models with 1/16 in. (1.6 mm) crack widths (Figures 3.19-21). The non-linearity is consistent with the affected stress area results because the elements are located less than the

distance equal to the depth of the girder (d = 45 in. [1140 mm]) away from the crack.

Figures 3.22 through 3.30 show the stress distributions for the girder section located four feet (1.2 m) away from the pre-release crack location. Figures 3.22 through 3.24 show the stress distributions for the 1/100 in. (0.25 mm) crack width models, Figures 3.25 through 3.27 show the stress distributions for the 1/32 in. (0.8 mm) crack width models and Figures 3.28 through 3.30 show the stress distributions for the 1/16 in. (1.6 mm) crack width models. The stress distributions in these figures are linear. The stresses in the girders at this location are not affected by the pre-release crack. The stresses in the cracked and uncracked models are identical in these figures. The data representing the uncracked models is included in the figures but is not visible because it is covered up by the identical data from the cracked models. This is consistent with the affected stress area results. The affected stress area is limited to the depth of the girder on each side of the pre-release crack location. The depth of the girder (45 in. [1140 mm]) is less than the four foot (1.2 m) distance used in the stress distributions of Figures 3.22 through 3.30.

3.2.4 Crack Depth

Several models were analyzed to determine the effect crack depth had on bottom fiber stress beneath the pre-release crack location. The crack depth was varied between 12 in. and 36 in. (305 and 915 mm) while the crack width remained constant at 1/100 in. (0.25 mm). Five crack depths were modeled between 30 in. and 36 in. (760 and 915 mm) to determine the crack depth that resulted in the greatest loss of compressive stress in the bottom element. A model of each crack depth was also analyzed with the crack width increased to 1/32 in. (0.8 mm).

Figure 3.31 shows the percent change in bottom element compressive stress for each model. The stress change was the difference in stress between the bottom element located directly beneath the pre-release crack in the cracked and uncracked models using Equation (3.1). Three different loads were applied to each of the models. The loss of compressive stress for all of the models increased with an increase in crack depth for depths less than 31.5 in. (800 mm). Regardless of the load applied or the crack width, the deeper crack depth caused a larger compressive stress loss in the bottom element. Crack depths greater than 31.5 in. did not continue to have a loss of compression. The stress change began to decrease for crack depths greater than 31.5 in. indicating the bottom element was regaining some compressive stress because of equilibrium and crack closure.

As the crack depth increased, the amount of concrete beneath the crack tip resisting crack closure decreased. Less resistance resulted in less compression required near the crack tip for closure. For equilibrium of the section, the loss of compression in the bottom of the section would be reduced because less compression was needed at the crack tip to close the crack. In addition, as the crack depth increased, the elements near the crack tip that increased in compressive stress began to overlap with the elements beneath the crack that lengthened due to the pivoting action of the girder. The compressive stress in the bottom element began to increase because it was compressing to close the crack in addition to lengthening from the pivoting action of the girder. Figure 3.32 shows that about half of the elements beneath the crack tip increased in compressive stress and the other half lost compressive stress. There were ten elements beneath the crack tip that lost compressive stress in the 12 in. (305 mm) depth model and twelve that increased in compressive stress. The 24 in. (610 mm) crack depth model had seven elements with a compressive stress loss and six with a compressive stress gain, and the 33 in. (840 mm) crack depth model had five elements with a compressive stress loss and three with a compressive stress gain. The elements beneath the crack tip in the deeper crack models were both near the crack tip and near the bottom of the section. The increase in compression near the crack tip from crack closure and loss of compression at the bottom of the section from pivoting action combined to result in an overall compressive stress loss smaller than for shallower depth cracks.

Figure 3.32 shows the changes in stress relative to an uncracked model for the entire affected stress area of three models with a 1/32 in. (0.8 mm) crack width located at midspan (67.5 ft [20.6 m]) and loaded with self-weight + 800 lb/ft. The crack depths were 12 in., 24 in. and 33in. (305 mm, 610 mm, and 840 mm), respectively, in the three models. As the crack depth increased from 12 in. to 24 in. to 33 in., the loss in compressive stress at the bottom fiber increased from 28% to 40% to 42%. The increase in compressive stress near the crack tips had the opposite effect. The stress near the crack tip in the deeper crack depth model had the smallest stress change. The compressive stress increased from 29% to 49% to 78% as the crack depth decreased from 33 in. to 24 in. to 12 in. As the crack depth deepened, there was less concrete beneath the crack tip that was resisting crack closure for a given crack width. The smaller resistance resulted in less compression necessary near the crack tip to close the crack in the section with the deeper crack. Compressive stress loss at the top of the section also increased

as the crack depth decreased. The greatest loss of compressive stress occurred for the 12 in. (305 mm) crack because this crack was most resistant to crack closure. The loads required for crack closure in the three models were listed in Table 3.2. Because the 12 in. crack did not close until the self-weight + 800 lb/ft load, very little stress had developed at the top of the girder for the stresses shown in Figure 3.32. This resulted in a large stress difference between the cracked and uncracked models.

The bottom element compressive stress loss for all of the crack sizes are listed in Table 3.3. Several of the models had pre-release cracks that did not close. The results from these models are italicized. These percentages are a lower bound for the percent loss that would be expected. To close the crack opening that remained in the models, the girder would have had to pivot further about the crack tip. The pivoting would result in a lengthening at the bottom of the girder, which would further decrease the compressive stress. This would result in a greater loss of compression in the bottom element.

3.2.5 Crack Width

Several models were analyzed to determine the effect crack width had on bottom fiber stress beneath the pre-release crack location. Three crack widths were modeled at three crack depths. The bottom element compressive stress loss for the three crack widths were listed in Table 3.3. The results showed a linear decrease in bottom element compressive stress for all three crack depths for an increase in crack width, regardless of the applied load. Figure 3.33 shows the linear change in bottom element stress for the self-weight + 800 lb/ft load. The results from the 24 in. (610 mm) and 33 in. (840 mm) crack depth models show a linear increase in compressive stress loss for increasing crack widths. The results from the 12 in. (305 mm) crack depth model did not remain linear between the 1/32 in. (0.8 mm) crack width and the 1/16 in. (1.6 mm) crack width. The non-linearity occurred because the 12 in. depth crack of 1/16 in. width did not close. If the crack had closed completely, a 55% loss of compression could be expected for this crack size. This is the percent change for a 1/16 in. crack width that would have kept the compressive stress loss linear for the 12 in. depth crack.

Figure 3.34 shows the change in stress for cracked models relative to the uncracked case for the entire affected stress area for the 33 in. (840 mm) crack depth at three different crack widths. The crack widths were 1/100 in., 1/32 in. and 1/16 in. (0.25 mm, 0.8 mm, and 1.6 mm).

As the crack width decreased between the three crack widths, the loss of bottom element compressive stress, relative to the uncracked case, decreased from 83% to 42% to 13%. These values were tabulated in the bottom row of Table 3.3. The compressive stress increase in the elements near the crack tip also decreased with a decrease in crack width. The maximum increase in compressive stress went from 62% to 29% to 10% as the crack width decreased. The loss of compressive stress in the top element also decreased with a decrease in crack width. The top element in the 1/16 in. (1.6 mm) crack width model had a 15% loss of compressive stress while the same element in the 1/100 in. (0.25 mm) crack width model had a 2% loss of compressive stress. The smaller crack width required less compression near the crack tip for crack closure, which resulted in smaller stress changes throughout the girder depth.

3.2.6 Camber Loss

Pre-release crack closure caused a reduction in the girder camber relative to the uncracked case. The reduction in camber for the nine crack sizes was determined using ABAQUS. Each model was loaded with self-weight.

The deflected shape of the bottom row of nodes in the ABAQUS models is shown in Figures 3.35 through 3.37. Each figure shows the deflected shape of four models: the uncracked model, the 12 in. (305 mm) crack depth model, the 24 in. (610 mm) crack depth model and the 33 in. (840 mm) crack depth model. Several models did not have a large enough applied load to close the pre-release crack. Cracks that did not close are noted in each of the figures. The midspan camber for each crack model is listed in the figures. The deflected shapes of the 1/100 in. (0.25 mm) crack width models plotted in Figure 3.35 were very similar, but the midspan cambers listed indicate slight differences in camber loss. The greatest camber loss shown in this figure was only 1.2%. A larger variance in camber loss occurred in the larger crack width models because more pivoting action was required to close the crack.

The midspan camber is also listed in Table 3.4 for all of the crack models, at three different loads. As the crack depth or crack width increased, the loss in camber also increased. For example, as the crack depth increased from 12 in. to 33 in. (305 mm to 840 mm), the midspan camber for a 1/100 in. (0.25 mm) crack width loaded with self-weight + 400 lb/ft decreased from 5.03 in. to 4.98 in. (128 mm to 126 mm). As the crack width increased from 1/100 in. to 1/16 in. (0.25 mm to 1.6 mm), the midspan camber for the 33 in. (840 mm) crack

depth loaded with self-weight + 400 lb/ft decreased from 4.98 in. to 4.45 in. (126 mm to 113 mm). The midspan camber is italicized in Table 3.3 if the pre-release crack did not close.

3.3 ABAQUS Multiple Crack Models

ABAQUS models involving three pre-release cracks were created to ensure that the camber and stress effects determined from the single crack models remained the same for multiple crack models. The three pre-release cracks were initially spaced 136 in. (3.45 m) apart so the affected stress area of one crack did not extend into the affected stress area of another crack. Later models investigated the stress changes resulting from closely spaced cracks. Crack widths were 1/100 in. (0.25 mm) for all of the cracks in the multiple crack models.

3.3.1 ABAQUS Model Description

The modeling of the multiple crack files began with the model used for the single pre-release crack at midspan. The only change necessary to the model was the addition of two pre-release cracks. A new crack was placed on each side of the already existing crack at midspan. Additional nodes were required at the new crack boundaries and additional gap elements were required to model the two additional open cracks. To model the additional pre-release cracks, the same procedure was used as described in Section 3.2.1 to model the single crack at midspan. The crack width was kept at 1/100 in. (0.25 mm) so that all three cracks would close upon loading.

Seven models involving multiple pre-release cracks were created. Four of the models had cracks located at 674 in., 810 in., and 946 in. (17.1 m, 20.6 m, and 24.0 m). These cracks were spaced greater than 90 in. (2285 mm) apart so their affected stress areas (d = 45 in. [1140 mm] on each side of the crack) did not extend into the affected stress area from an adjacent crack. The first had three 12 in. (305 mm) depth cracks, the second had three 24 in. (610 mm) depth cracks and the third had three 33 in. (840 mm) depth cracks. The fourth had 33 in. (840 mm) depth cracks at 674 in. and 946 in. (17.1 m and 24.0 m) with a 24 in. (610 mm) depth crack at the midspan (810 in. [20.6 m]).

Three additional models were created that placed the cracks such that the affected stress areas extended into one another. All three crack depths remained at 24 in. (610 mm) for these three models. The first model placed the cracks at 742 in., 810 in. and 878 in. (18.8 m, 20.6 m,

and 22.3 m) (68 in. spacing [1725 mm]), the second model placed the cracks at 770 in., 810 in. and 850 in. (19.6 m, 20.6 m, and 21.6 m) (40 in. spacing [1015 mm]), and the final model placed the cracks at 794 in., 810 in., and 826 in. (20.2 m, 20.6 m, and 21.0 m) (16 in. spacing [405 mm]). The amount of the affected stress area that extended into the adjacent stress area increased for each of these models. The first model involved the overlapping of only a few elements, the second model involved overlapping about half of the elements, and the final model had the cracks spaced such that each crack affected the stress in the elements at all three of the crack locations.

3.3.2 Results from Multiple Crack Models

The changes in stress in the multiple crack models with the cracks spaced greater than the distance 2*d* apart had stress changes relative to the uncracked case identical to those considering the cracks occurring independently. Each of the three cracks had a separate affected stress area so the effects from one crack did not affect the others. This followed the behavior that was shown in the stress distributions in Section 3.2.3. Elements four feet away from the pre-release crack location were identical to the distribution of the uncracked model. The effects of each crack remained local to the crack area.

When the cracks were spaced such that their affected stress areas overlapped, the resulting stress effect was the superposition of the stress change from each of the separate cracks. The superposition of stresses for the multiple crack models with closely spaced cracks is shown in Figure 3.38. This figure shows a plot of the bottom element stress change relative to the uncracked case. The bottom element change in stress is also shown for a single crack at the midspan. The pre-release cracks were all 24 in. (610 mm) deep and 1/100 in. (0.25 mm) wide. The change in bottom element compressive stress for the single crack model is shown with data markers on a solid line. The change in bottom element compressive stress for this crack was identical to the change in bottom element compressive stress at the center crack in the model with cracks located at 742 in., 810 in. and 878 in. (18.8 m, 20.6 m, and 22.3 m) (68 in. spacing [1725 mm]). The only difference was that the stress change reduced to zero at 774 in. and 846 in. (19.7 m and 21.5 m) for the single crack model. The multiple crack model kept a 1% stress change at these locations because the stress was mildly affected by the cracks located at 742 in. and 878 in. (18.8 m and 22.3 m). The elements at the edge of the affected stress areas were the

only elements that had the superposition of stress change resulting from two cracks for this model because the cracks were spaced 68 in. (1725 mm) apart. The maximum stress change from the multiple crack files was in the model with cracks located at 794 in., 810 in. and 826 in. (20.2 m, 20.6 m, and 21.0 m) (16 in. spacing [405 mm]). The bottom element compressive stress loss increased to 11% because the stress in the bottom element at 810 in. (20.6 m) was affected by all three pre-release cracks in the model.

The camber loss in the multiple crack models remained consistent with the behavior determined from the single crack models in Section 3.2.6. As the crack depth increased, the loss in camber also increased. The additional cracks also caused an increase in the camber loss. This was expected because the total crack opening at the top of the girder had increased. The pivoting action to close the larger cumulative crack opening reduced the midspan camber.

Figure 3.39 shows a comparison of the midspan camber of several models including the uncracked girder. The models of the 12 in. (305 mm) depth crack and the 24 in. (610 mm) depth crack did not close completely and this is noted in the figure. The crack locations and depths are listed in the figure. All of the cracks had a 1/100 in. (0.25 mm) width and the models were loaded with self-weight. A loss of camber resulted from the presence of the pre-release cracks, regardless of the number or size of cracks. The uncracked model had a midspan camber of 8.61 in. (220 mm), which was the largest camber shown in the figure. The models involving a single pre-release crack had larger midspan cambers than any of the models involving multiple cracks because the crack opening in the single crack models was one-third the opening in the multiple crack models. The camber for the single crack models decreased as the crack depth decreased. The same trend occurred for the multiple crack models involving three of the same depth cracks spaced a distance greater than 2*d* apart.

3.4 Comparison of ABAQUS Results to Geometric Compatibility Theory

The midspan cambers for several of the crack sizes modeled in ABAQUS loaded with the self-weight load were predicted using the geometric compatibility theory (GCT) developed by Shield (1997) (Section 1.1.2). A simplified equation was developed using the equations from the GCT with the cosine approximation shown in Equation (1.10). The simplified equation (Equation (1.11)) is:

$$c_a \approx \frac{(8c_e z_{crack} - LO_{Crwidths}(L^2 - 8c_e(z_{na} - z_{crack})))}{8L^2 z_{crack}}. \qquad (3.2)$$

Camber predictions using the simplified equation were compared to the midspan camber from the ABAQUS models. In order to predict the camber of a girder involving a pre-release crack using Equation (3.2), the *expected* camber (c_e) of an uncracked girder was necessary. The midspan camber of the uncracked model in ABAQUS was used for this value (8.61 in. [220 mm]). The change in arc length along the top fiber ($O_{Crwidths}$) was equal to the crack width modeled. The length of the beam (L) and the neutral axis depth (z_{na}) were 135 ft (41 m) and 21.7 in. (550 mm), respectively, consistent with the ABAQUS models.

Table 3.5 shows the predicted camber from ABAQUS and from the geometric compatibility theory. The difference in camber between the two predictions was also calculated using the following formula:

$$\frac{c_{ABAQUS} - c_{GCT}}{c_{ABAQUS}} \Delta 100 \qquad (3.3)$$

where the subscript *ABAQUS* represents the camber prediction from the ABAQUS model and the subscript *GCT* represents the camber prediction using the geometric compatibility theory equations. Only two of the models involved cracks that closed completely in ABAQUS. These were the models of a 33 in. (840 mm) depth crack with crack widths of 1/100 in. and 1/32 in. (0.25 mm and 0.8 mm). The results of the other models where the crack did not close were italicized in Table 3.5.

Error was expected between the GCT predictions and the ABAQUS predictions for the models with cracks that did not close because the GCT assumed the cracks closed completely. However, additional error between the ABAQUS and GCT predictions existed in the camber loss for increasing crack depths. Both of the camber predictions had a decrease in camber for an increase in crack width. However, the GCT predicted an increase in midspan camber as the crack depth increased, which was opposite the prediction from ABAQUS. The ABAQUS results predicted a decrease in midspan camber as the crack depth increased. This resulted in the GCT predicting a larger camber than the ABAQUS predictions for the 33 in. (840 mm) depth cracks (negative % difference), and a smaller camber than the ABAQUS predictions for the 12 in. (305 mm) depth cracks (positive % difference). The difference in the camber predictions indicates

that an assumption used in developing the GCT equations is not consistent with the ABAQUS analyses. An assumptions used in the development of the GCT equations was that plane sections remained plane when the cracks closed. This assumption is not consistent with the results shown in the stress distributions in Section 3.2.3, resulting in error between the camber predictions of the GCT equations and the ABAQUS analyses.

3.5 Conclusions Regarding Stress State and Camber of Girders with Pre-release Cracks

ABAQUS models were used to determine the effects pre-release cracks had on girder stresses and camber relative to the uncracked girders. The following effects were determined:

- Pre-release crack effects remain local to the pre-release crack location (within the distance *d* on either side of the crack).
- Non-linear stress distributions occur during the process of crack closure and are "locked in" to the cross section.
- Linear stress changes occur for all elements after crack closure and are equal to the stress changes for an uncracked model.
- Deeper crack depths and smaller crack widths cause the crack to close at a smaller load.
- Larger stress changes occur for deeper and wider cracks up to a crack depth of 31.5 in. Stress changes began to decrease for crack depths greater than 31.5 in. because of equilibrium and crack closure.
- The compressive stress increases near the crack tip location, and decreases at the top and bottom of the section relative to an uncracked model.
- Greater camber losses occur with deeper and wider cracks.
- Stress effects from multiple pre-release cracks can be superimposed upon one another if the cracks are spaced such that their affected stress areas overlap.

It is important to note that the results obtained from the ABAQUS models described in this chapter pertain only to the 45 in. by 22 in. (1140 mm by 560 mm) section shape. The conclusions mentioned above would remain relevant, but the exact values and percent changes stated would change with a change in section size or shape.

CHAPTER FOUR
COMPARISON BETWEEN ANALYTICAL AND EXPERIMENTAL RESULTS OF GIRDERS I AND II

4.1 Introduction

Models were made of two full size high-strength concrete prestressed girders (Girders I and II) that were tested at the University of Minnesota to compare analytical results using ABAQUS (HKS Inc., 1994) to the limited available experimental data regarding pre-release cracks. A complete description of the testing and results of the two full-size girders can be found in a report by Ahlborn (1998). The initial deflection and the flexural cracking load were the two parameters compared in the current study.

Girder I did not develop pre-release cracks during fabrication while fifteen pre-release cracks were observed to develop in Girder II. These pre-release cracks were concentrated within the middle 50% of the span length. They began at the top of the girder and extended various depths toward the bottom flange. After release, the only visible signs of the pre-release cracks were the lines that had been drawn on Girder II adjacent to the cracks.

The predicted initial camber and flexural cracking load for Girders I and II were determined using the measured material properties of the girders. The predicted flexural cracking load using the measured properties for Girder II was larger than that for Girder I, however Girder II cracked at a lower load than Girder I. Using a calibrated response that assumed the relationship between the predicted and measured response of Girder I was representative of girder behavior without pre-release cracks, an expected camber and flexural cracking load of Girder II were determined. The measured camber and flexural cracking load of Girder II were both lower than the expected response using the calibrated prediction. A primary difference between the two girders that was not taken into account using the calibrated prediction was the presence of the pre-release cracks in Girder II.

Three ABAQUS models, designated *Girder I*, *Girder II without pre-release cracks*, and *Girder II with pre-release cracks*, were used to investigate the girder behavior. The Girder II with pre-release cracks model was intended to simulate the expected response of Girder II had the pre-release cracks not occurred. Comparisons of the finite element results to the experimental results were made to determine if the models accurately represented girder

behavior and if the occurrence of the pre-release cracks could account for the reduction in camber and flexural cracking load.

4.1.1 Description of Girders I and II

Two high-strength prestressed bridge girders were tested at the University of Minnesota. The girders were Mn/DOT 45M sections that spanned 132 ft. 9 in. (40.5 m). Each girder had 46 prestressing strands of 0.6 in. (15.3 mm) diameter. The strands were Grade 270 ksi (1860 MPa) low-relaxation strands with a measured initial strand stress of 71.3% f_{pu} (191.6 ksi [1320 MPa]). Figure 4.1 shows the dimensions of the Mn/DOT 45M section with the strand pattern at midspan. Composite concrete decks were cast on the girders at 200 days.

Girders I and II had different mix designs, end strand patterns, and stirrup anchorage details. Girder I used a limestone aggregate concrete mix, which had a measured 28-day compressive strength of 12,100 psi (83.4 MPa). The concrete used for Girder II was a glacial gravel with microsilica mix, which had a measured 28-day compressive strength of 11,100 psi (76.5 MPa). Variances in the end strand patterns and stirrup anchorages were not incorporated into the ABAQUS models. These details were local to the girder ends and were assumed not to affect midspan flexural behavior.

The depths and locations of the pre-release cracks that developed in Girder II are listed in Table 4.1. These cracks began at the top flange of the section and extended vertically into the girder depth. Some of these cracks extended into the bottom flange of the section. The widths of the cracks at the top of the girder flange were not measured, but were estimated visually to be on the order of 0.01 in. (2.5 mm).

4.1.2 ABAQUS Model Description

Three ABAQUS models were created to compare the analytical results to the experimental data of Girders I and II. Each model was 132 ft. 9 in. (40.5 m) long and included 46 - 0.6 in. (15.3 mm) diameter prestressing strands placed as shown in Figure 4.1. The models were designed to simulate the geometry and material properties of the experimental girders.

In the ABAQUS models, two-dimensional type CPS4R plane stress elements were used to model the concrete and type T2D2 linear truss elements were used to model the strand. Each CPS4R plane stress element had four nodes and incorporated reduced integration in the analysis.

Two-inch long elements were used along the length of the beam. Additionally, a one-inch long element was placed at the right end of the girder to account for the entire 132 ft. 9 in. (40.5 m) span length of the experimental girders.

The I-shape of the Mn/DOT 45M section was modified slightly for ease of input into ABAQUS. The modified section shape is shown in Figure 4.2. The triangular areas in the Mn/DOT 45M section between the flanges and the web were replaced by rectangular areas in the ABAQUS models. The rectangular areas were necessary because the two-dimensional models would only allow a constant width for each element layer. The section height was divided into 25 element layers. Most of the aspect ratios (height/length) for the elements were one, and no aspect ratio was greater than four. The height of each layer was chosen based on the section geometry and the locations of each of the prestressing strand layers. Element boundaries were required at each of the strand locations as well as at changes in section width. The height of each element layer is shown with the corresponding section width in Figure 4.2.

The modified section shape used in the ABAQUS models was the same as the section used in the *Pbeam* analyses by Ahlborn (1998). This section was configured to have similar moments of inertia as the Mn/DOT 45M section. The moments of inertia and centers of gravity for Girders I and II at release and at flexural crack testing are tabulated with the section in Figures 4.1 and 4.2. The moments of inertia and centers of gravity were calculated using the corresponding initial or flexural crack testing measured material properties of Girders I and II. These properties are listed in Table 4.2 and were also the material properties used in the ABAQUS analyses. Girders I and II had different transformed inertia values (Figures 4.1 and 4.2) because the concrete modulus of elasticity of each girder was different (Table 4.2).

The 46 prestressing steel strands used in the experimental girders were modeled in ABAQUS with seven layers of the T2D2 linear truss elements. Each element was bounded by two nodes. The elements were two inches in length with a single one-inch element at the right end of the girder. A total of 797 elements were connected to produce each strand layer. The bottom strand layer was two inches (50 mm) from the bottom of the section, and the top strand layer was 14 inches (355 mm) from the bottom of the section. The remaining layers were at two-inch increments between the two. The total area of steel for each layer was specified separately. The layers at 2 in. (50 mm), 4 in. (100 mm), and 6 in. (150 mm) from the bottom of the section consisted of 12 strands each so the area of steel in these layers was 2.7 in^2 (1765 mm^2). The

layer at 8 in. (205 mm) from the bottom of the section had the equivalent area of steel of four strands (0.9 in^2 [590 mm^2]) and the remaining three layers had an area of steel representing two strands (0.45 in^2 [294 mm^2]). An initial stress was defined for all of the truss elements to model the prestressing by using the *INITIAL CONDITIONS, TYPE=STRESS parameter in ABAQUS. The stress at release was specified to be equivalent to the 71.3% f_{pu} measured initial strand stress by Ahlborn (1998) (191.6 ksi [1320 MPa]). Draping and debonding of the prestressing strands that existed in the experimental girders was not modeled in ABAQUS. These details do not affect the stress conditions at midspan, which was the area of concern for the pre-release cracks.

The required material properties for the ABAQUS input file were the elastic modulus of the steel, the elastic modulus of the concrete girder and the concrete deck, and the area of steel per strand. Only elastic properties of the materials were incorporated into the ABAQUS analyses. The applied loads on the girders were not large enough to require modeling of inelastic behavior.

Pre-release cracks were added to the model Girder II with pre-release cracks by separating two adjacent elements at each crack location. The crack modeling for Girder II is shown in Figure 4.3. The cracks were placed between two elements. This crack placement was different from the modeling used in Chapter 3. The cracks in the earlier models were placed at the center of a column of elements so each element within the crack depth in the column of elements was split into two elements, each being half of the original length. The crack modeling used for the experimental girders did not reduce the length of the elements because the elements were being separated, not split into two parts. A new column of nodes was necessary to separate the elements at the crack location because each element needed its own set of four nodes in order to separate the two elements with a crack opening. The original and new nodes along the crack boundary were assigned new positions to model an open crack.

The cracks were triangular in shape with the crack opening being 0.01 in. (0.25 mm) at the top of the section. This was the estimated width of the cracks in the experimental girder; the exact width of the cracks was not measured. Any differences in the assumed crack widths of 0.01 in. (0.25 mm) and the actual crack widths could lead to some differences between the analytical and experimental results of Girder II. The results in Chapter 3 regarding the effect of crack width showed that an increased crack width caused an increase in the camber and bottom

element compressive stress loss. If the observed cracks in Girder II had a smaller crack width than 0.01 in. (0.25 mm), the analytical model using this assumed crack width would predict a smaller camber and flexural cracking load than the measured experimental results. Similarly, if the cracks in Girder II were larger than 0.01 in. (0.25 mm), the analytical model would predict a larger camber and flexural cracking load. Any variance between the modeled crack widths and the actual crack widths would cause the analytical models to over or under predict the camber and flexural cracking capacity, depending on the relationship of the modeled crack width to the actual width.

One-dimensional contact elements, gap elements of type GAPUNI, connected the two nodes across the crack boundary in each row of nodes. An initial gap distance was assigned to each gap element that was equal to the width of the crack opening at the location of the gap element, assuming a triangular shaped crack. The gap elements allowed stress to be transferred across the crack when the crack closed.

The crack locations and depths assumed in the ABAQUS models are recorded in Table 4.3. The positions of the pre-release cracks in the model closely corresponded to the eleven deepest pre-release cracks observed in Girder II. The crack locations were moved to the closest element boundary in the model so the pre-release cracks always separated two adjacent elements. The measured crack depths were modeled whenever possible, however the modeled crack depths were limited to 31 in. (785 mm). This depth corresponded to the location of the top layer of prestressing strands. The crack depth limit resulted from insufficient data to calibrate the ABAQUS models for modeling crack depths that penetrated the steel strands. Only two of the pre-release cracks modeled, both 27 in. (685 mm) in depth, were not affected by this 31 in. (785 mm) limit.

Crack depths that penetrated the steel were difficult to model accurately in ABAQUS because the crack opening effect on the steel at the crack location was not known. The steel strands would have lengthened an amount equal to the crack opening at the steel height, but the length of strand over which this elongation occurred was not known. An infinite number of solutions were possible because the affected strand length could have ranged anywhere between zero, resulting in infinite strain, and the span length. Due to the ambiguity of the affected length of steel spanning the pre-release crack opening, crack depths were not modeled deeper than the steel depth, 31 in. (785 cm) from the top of the section.

Two sets of analyses were run for each of the three ABAQUS models. The first set of analyses modeled the experimental girders with the material properties at release. The camber results of these models were compared to the measured initial camber of the experimental girders. The second set of analyses modeled the girders with the material properties at flexural crack testing. Concrete decks were added to the models for the second set of analyses to represent the composite section during crack testing. A detailed description of the procedure to model the composite deck is given in Section 4.3. The initial flexural cracking loads of the ABAQUS models were compared to the experimental loads using this set of analyses.

4.2 Initial Condition

The three girder models were assigned material properties consistent with the measured values for the initial condition listed in Table 4.2. Figure 4.4 shows the initial boundary conditions used in the ABAQUS models. The models were restrained in the *x* and *y* degrees of freedom at the bottom left end of the beam and in the *y* degree of freedom at the bottom right end of the beam. Each girder was loaded with a uniform load equivalent to its measured experimental self-weight. Girder I had a self-weight of 710 plf (10.4 kN/m) and the models of Girder II with and without pre-release cracks had a self-weight of 716 plf (10.4 kN/m). The initial stress condition specified in the steel layers was 191.6 ksi (1320 MPa). This corresponded to the measured initial strand stress in the experimental girders at seating. The prestressing combined with the self-weight load on the models produced an upward deflection (positive) in the girders referred to as camber. The loading combination of prestress plus self-weight closed the eleven pre-release cracks in the model of Girder II with pre-release cracks, as was observed in the field. The initial camber at transfer for all three ABAQUS models was compared to the experimental results.

4.2.1 Initial Camber Comparison

Camber was measured several times after strand release for the experimental girders. Girder camber is a time dependent measurement that is directly affected by the amount of stress in the prestressing strands. The prestressing in the steel changes over time due to steel relaxation, concrete creep and shrinkage, and temperature changes. A loss in the prestressing force results in a lower camber measurement. The first camber measurement was taken with the

girders still lying on the precasting bed (on-bed). Measurements were taken again the following morning while the girders remained on the precasting bed. A final measurement was taken after the girders were lifted and immediately set back down (lift/set). The stress in the prestressing strands would have been different for all of these measurements because time had elapsed between the readings. The true initial camber was expected to be a value between the on-bed camber and the lift/set camber because friction forces acted on the girder from the precasting bed. Friction resisted the upward deflection for the on-bed measurement and the downward deflection after lift/set. A reasonable approximation for the camber was taken as the average of the on-bed and lift/set camber measurements. The averaged camber values were 5.12 in. (130 mm) for Girder I and 3.96 in. (101 mm) for Girder II. Table 4.4 lists the measured cambers at release for Girders I and II along with the ABAQUS results for the initial cambers at midspan.

The initial deflections of the three ABAQUS models are shown in Figure 4.5 (curves) with the averaged measured centerline cambers for the experimental girders (symbols). The initial midspan camber predicted from ABAQUS for Girder I was 6.13 in. (156 mm). The initial ABAQUS camber prediction for Girder II with pre-release cracks was 4.96 in. (126 mm). Both of these camber predictions were about an inch larger than their corresponding averaged experimental results. The large difference between the corresponding analytical and experimental camber results is due to the difference between the analytical and experimental prestress loss in the strands. The ABAQUS models only considered prestress losses from elastic shortening of the girder. The analyses did not include any effects on prestress from time or temperature dependent properties of the materials. Prior to the time when the concrete bonds to the steel strands, the steel is heated due to the heat of hydration from the concrete curing. The change in temperature causes the strands to elongate which results in less prestressing force transferred to the concrete at release. A reduction in the prestressing force results in a reduced initial camber. This is consistent with the ABAQUS results having a larger initial deflection than the measured camber because the ABAQUS analyses did not account for this initial loss in prestress. The ABAQUS analyses also did not account for any prestressing change due to steel relaxation or creep and shrinkage of concrete that would have occurred prior to the lift/set measurement of the experimental girders.

A reasonable comparison can be made between the analytical and the experimental camber results by comparing the camber difference between Girders I and II. This comparison

partially neutralizes the time and temperature effects not accounted for in the ABAQUS analyses. Both of the experimental girders were expected to have undergone similar changes due to temperature and time because they were fabricated at the same location at the same time. However, the prestress losses in the two girders would have been different due to the different mix designs used, which each had a different modulus of elasticity. The initial camber is directly related to the amount of prestress in the strands, so there would still be some error in this comparison due to the effects of time and temperature on the stress in the prestressing strands. The experimental difference in camber between Girders I and II was 1.16 in. (29 mm) and the analytical difference between the model of Girder I and the model of Girder II with pre-release cracks was 1.18 in. (30 mm). These values differed by only 1.4%.

The ABAQUS models only approximated the crack widths for the eleven pre-release cracks because the actual crack widths in the experimental girders were not measured. The width of each crack was modeled as 0.01 in. (0.25 mm). If the experimental crack widths were larger than this, the measured camber loss would have been larger than the camber loss predicted by the ABAQUS analyses. This correlation was evident from the results in Chapter 3. Accordingly, if the crack widths in the experimental girder were smaller than 0.01 in. (0.25 mm), the measured camber loss would have been smaller than the camber loss predicted by the ABAQUS analyses. This parameter in the ABAQUS models could have caused minor differences in the camber loss for Girder II with pre-release cracks. The ABAQUS models also did not model the exact crack depths measured in the experimental girders because the crack depths in the models were limited to the steel depth. The results discussed in Chapter 3 indicate larger camber losses for deeper crack depths. Limiting the crack depths to the steel depth would cause the ABAQUS camber loss to be less than if the cracks would have been modeled accurately at their measured depths. These two modeling changes are additional sources of error that could have contributed to the difference between the analytical and experimental change in camber between Girder I and Girder II with pre-release cracks.

Figure 4.5 also shows the initial deflection using finite element modeling for Girder II without pre-release cracks. The deflection of Girder II without pre-release cracks was not the same as that of Girder I because the initial modulus of elasticity (E_c initial, Table 4.2) of the two girders was different. The analytical initial midspan camber for Girder II without pre-release cracks was 5.74 in. (146 mm). Comparing this result to the initial midspan camber of Girder II

with pre-release cracks indicates a 14% camber loss (0.78 in. [20 mm]) resulted from the eleven pre-release cracks modeled in Girder II. These results indicate that the presence of pre-release cracks could account for the lower than expected measured camber in Girder II.

The effect of the initial modulus of elasticity and pre-release cracks on the analytical elastic shortening prestress loss along the span length for Girders I and II is shown in Figure 4.6. The difference between the losses for Girder I and Girder II is due to the elastic moduli being different for the two girders. The analytical results for Girder II with pre-release cracks shows a local decrease in prestress loss at each of the pre-release crack locations. As the pre-release cracks close, the girder fibers below the cracks stretch to accommodate the crack closure. This causes a local increase in tensile stress in the prestressing strands (and concrete) below the pre-release cracks.

4.2.2 Geometric Compatibility Theory

The simplified geometric compatibility theory described in Chapter 1 that was developed to predict the effects on camber and cracking loads due to pre-release crack closure was used to compare the predicted camber for Girder II to that of the ABAQUS model. The *expected* camber (c_e) assumed for the geometric compatibility theory was taken from the ABAQUS model Girder II without pre-release cracks. This camber was 5.74 in. (146 mm). The total crack opening ($\div_{top}$) was taken as 0.11 in. (2.79 mm) due to eleven cracks of 0.01 in. (0.25 mm). Crack depths (z_{crack}) for all eleven pre-release cracks were taken to be 31 in. (785 mm) even though two of the cracks were only 27 in. deep (685 mm). The neutral axis location (z_{na}) was taken as 21.2 in. (542 mm). This was the centroid of the modified Mn/DOT 45M section for the transformed, non-composite section using the initial measured material properties.

The calculated camber for Girder II with pre-release cracks using the equations from the geometric compatibility theory was 5.04 in. (128 mm). This was a 1.6% difference from the 4.96 in. (126 mm) camber prediction from using the ABAQUS model of Girder II with pre-release cracks. A small error would have resulted in using 31 in. (785 mm) for all eleven pre-release cracks when the ABAQUS model had two of the eleven cracks modeled at 27 in. (685 mm). An additional error would have resulted from an inaccurate assumption used to develop the geometric compatibility equations that was not consistent with the ABAQUS analyses. This was discussed in Section 3.4. The geometric compatibility theory predicted an increase in

midspan camber as the crack depth increased, which was opposite to the ABAQUS prediction.

4.3 Condition at Cracking

Flexural crack testing was performed on Girders I and II to determine the initial cracking load and the load required to reopen the cracks. Several changes had occurred in the girders since the time of release. The concrete strength of the girders had increased, additional prestress losses had occurred, and concrete decks had been added to create a composite section. The ABAQUS models used for the analyses at crack testing needed to account for all of these changes.

A superimposed sustained dead load (sdl) and two hydraulic actuators were used for flexural crack testing of the girders. The load setup is shown in Figure 4.7. The girders were simply supported at 7.5 in. (191 mm) in from each girder end. The superimposed sustained dead load consisted of concrete masses and was necessary because the 35 kip (240 kN) actuators did not have enough capacity to crack the section. The superimposed sustained dead load applied a force of 35.0 kips (156 kN), half at each of the sdl locations shown in Figure 4.7. An additional load was applied at the actuator locations. At any given time, each actuator applied approximately the same load. The actuator loads each ranged from 0 to 33.4 kips (149 kN) in 2 kip (9 kN) increments.

Crack initiation and reopening was determined using acoustic emission (AE) monitoring equipment and LVDTs, respectively. Four AE transducers were placed on the underside of each girder to record the load and approximate location of the initial flexural crack. Prior to reloading the girders to determine the crack reopening loads, two LVDTs were placed on each girder. One LVDT was placed directly *over* a flexural crack on the bottom flange of the girder in the longitudinal direction of the beam. A second gage was placed *near* the crack, approximately 2 in. (50 mm) below the neutral axis and 2 in. (50 mm) toward the supported end in the longitudinal direction of the beam. The LVDTs were located at 74.4 ft. (22.7 m) and 74.9 ft. (22.8 m) from the left ends of Girders I and II, respectively. When the crack monitored by the LVDTs opened, the load-displacement characteristics of the two LVDTs diverged.

AE sensors recorded crack opening in Girder I when 21 kips of load had been applied at each actuator location in addition to the superimposed sustained dead load (21k+sdl). Crack opening was recorded for Girder II by the AE sensors when each actuator applied 14 kips with

the superimposed sustained dead load (14k+sdl). Cracks were not seen visually in either girder until more load was applied. Visual cracks were observed at loads of 28k+sdl and 18k+sdl in Girders I and II, respectively.

Crack reopening was determined using the LVDTs in both girders. Girder I recorded crack reopening with actuator loads of 6.4 kips plus the superimposed sustained dead load (6.4k+sdl). The monitored crack in Girder II remained open with only the superimposed sustained dead load applied, so the reopening load was taken as 0k+sdl.

It is important to note the LVDTs only monitored the displacements at the locations they were placed. In the testing of Girder II, the crack monitored by the LVDTs was not one of the first cracks to open. Because of this, the reopening load determined using the LVDTs was larger than the load required to reopen the first crack.

Three ABAQUS models were created to represent the two experimental girders during flexural crack testing. The girder models were loaded with the cracking and reopening loads determined from the AE and LVDT instrumentation in the experimental girders. The purpose of the analytical models was to determine if the models accurately represented girder behavior and if the occurrence of the pre-release cracks in Girder II could have resulted in the reduced flexural cracking load observed.

4.3.1 ABAQUS Models for Flexural Crack Testing

Modifications to the initial finite element models were necessary to compare the flexural cracking load with the experimental results from Girders I and II. Changes in the girders from the initial models included: a slight change in support conditions, an increase in the concrete strength, the addition of a concrete deck, and a loss of prestress in the steel strands. In the experimental tests, the supports for the girders were moved in on each end when relocating the girders for testing, and four foot wide concrete decks were added to each girder at an age of 200 days.

The supports for the ABAQUS models were placed at the bottom of the sections at 8 in. (203 mm) from the left end of the girders and 7 in. (178 mm) from the right end of the girders as shown in Figure 4.8. The experimental girders had the supports at 7.5 in. (191 mm) from each end. The difference in the ABAQUS models was necessary because the support needed to be located at a nodal location and the nodes were spaced at two-inch increments beginning at the

left end of the beam. The left support was restrained in both the *x* and *y* degrees of freedom, and the right support was only restrained in the *y* degree of freedom.

The locations of the point loads for the superimposed sustained dead load (sdl) and the actuator loads in the experimental tests are shown in Figure 4.7. The locations of the point loads in the ABAQUS models were moved 0.5 in. (13 mm) relative to the experimental locations because the loads needed to be applied at a node. The changes in location were chosen so that the midspan moment was identical to that of the experimental tests.

Concrete strength varies with time so the material properties used in the ABAQUS models for flexural crack testing were changed to the measured material properties of the experimental girders at crack testing. These properties were listed in Table 4.2.

A 10 in. (254 mm) thick concrete deck was added to each of the ABAQUS models by using seven rows of two-inch wide plane stress elements of varying heights. These elements were shaded in Figure 4.2 because they were only added to the models for flexural crack testing. The two-inch width was chosen so the deck elements were the same width as the elements modeling the girder. The first row of elements (adjacent to the top row of elements in the girder) was one inch (25 mm) in height while the remaining six rows were 1.5 in. (38 mm) high. Each row consisted of 747 elements similar to the element rows representing the girder. The element heights with their corresponding section widths are shown in Figure 4.2.

The procedure for modeling the concrete deck in ABAQUS was complex due to the strain discontinuity that occurs at the girder/deck interface from the deck being added to the section after release. At the time the deck has cured and the girder becomes composite, stresses exist in the girder from the prestressing force, the girder self-weight, and the deck self-weight, while the stress in the deck is zero. To model this in ABAQUS, the deck elements had to be removed prior to the application of any loads. Figure 4.9 illustrates the analysis procedure for modeling the concrete deck and a sample ABAQUS input file showing the analysis steps is included in Appendix C. The deck elements were removed in the first step of the analysis by using the *MODEL CHANGE, REMOVE parameter in ABAQUS. Steps two and three applied the three loads that acted on the non-composite section: the prestressing force, the girder self-weight, and the deck self-weight. The deck elements were reintroduced in the fourth step of the analysis by using the *MODEL CHANGE, INCLUDE parameter in ABAQUS. The procedure used to add the deck in a strain-free state to the deflected shape of the girder is described in the

next paragraph. Additional loading, which included the superimposed sustained dead load and the actuator loads, acted on the composite section and were applied in additional steps in the analysis.

ABAQUS calculates element stresses from the displacements of the nodes comprising each element. This characteristic of ABAQUS caused the complexity in adding the deck elements to the deflected shape of the girder. The nodal locations of the bottom row of nodes in the deck needed to be equal to the top row of nodes in the girder when the deck was reintroduced into the model. However, the displacements of the bottom row of nodes in the deck had to be manipulated to be zero so that the stress calculated for the deck elements was zero. To do this, three sets of nodes were defined. The first node set was named II and comprised all of the nodes along the top row of the girder. The second node set was named JJ and comprised all of the nodes along the bottom row of the deck. The third set of nodes was named KK and was a fictitious set of nodes that were used in the manipulation of the deck displacements. Each of the node sets had an identical number of nodes at the same location at the beginning of the analyses. Equations were implemented using the *EQUATION parameter in ABAQUS to relate the displacements of these three lines of nodes. Two equations were included, one relating the x displacements and one relating the y displacements. The first equation set the sum of the x displacements of JJ and KK equal to the x displacement of II. The second equation set the sum of the y displacements of JJ and KK equal to the y displacement of II. In the first three steps of the analyses when the deck elements were removed from the model, the displacement of node set JJ was zero so the displacement of the fictitious node set KK mimicked the displacement of II. When the deck was reintroduced in the model, the x and y displacement of each node in KK was fixed as the displacement of the corresponding node in II at that time. This was done using the *BOUNDARY, FIXED parameter in ABAQUS. The displacement of JJ for loading after this step was equal to the change in displacement of II because the sum of the JJ and KK displacements equaled the displacement of II, and node set KK was fixed. The stresses calculated by ABAQUS for the deck elements were only due to the change in displacement from the time the deck was reintroduced in the model because no displacement in the deck was recognized by ABAQUS from loading prior to the section becoming composite. The equations implemented in ABAQUS were only used for the bottom row of nodes in the deck. The

additional deck nodes did not move from their original location until loading was applied to the composite section.

Prestress losses at the time of flexural crack testing due to time dependent properties of the concrete and prestressing strand were included in the ABAQUS analyses. Two different analyses were run to determine the prestress losses. The first set of analyses used the traditional method for predicting prestress loss. This method assumed zero stress in the concrete at the time of release. Ahlborn (1998) determined the losses according to this assumption by using data collected from vibrating wire strain gages. The prestress losses were 26.6% for Girder I and 25.8% for Girder II. The analytical results from the ABAQUS models using these prestress losses are included in Appendix D. These losses were considered to be a lower bound for the experimental girders and did not correlate well with the experimental girder behavior. The steel strands would have had a larger loss of prestress than this prediction due to thermal effects prior to the concrete bonding to the strands. This was discussed during the initial camber comparison in Section 4.2.1.

The second set of analyses calibrated the prestress loss in the steel strands of the ABAQUS models to the strand loss in the experimental girders by using the known crack reopening loads for each girder. The stress at the bottom fiber of the girder at a flexural crack location is known to be zero when the crack reopens. There is no tensile capacity in the concrete because the section is already cracked. To calibrate the ABAQUS models to the experimental girders, the amount of prestress in the ABAQUS models was varied until zero stress occurred in the bottom element at the LVDT location with the crack reopening load applied. Crack reopening loads were 6.4k+sdl for Girder I and 0k+sdl for Girder II. The strand stress at crack reopening corresponded to prestress losses of 36.3% for Girder I and 38.0% for Girder II with pre-release cracks. Calibration of the models using the crack reopening load was more accurate than if the models were calibrated to the modulus of rupture stress at the bottom fiber with the initial flexural cracking load applied because the exact tensile strength of the concrete at the time of crack testing was not measured. Only the 28-day strength of the concrete used in each girder was known and concrete strength varies with time.

For lack of better information, the calibrated prestress loss determined for Girder II with pre-release cracks was also used for the model of Girder II without pre-release cracks. Comparisons made between the results of the two Girder II models illustrates the effects due to

pre-release cracks for a given strand stress, but it does not accurately represent what the experimental girder behavior would have been if Girder II had not developed pre-release cracks. The closure of the pre-release cracks caused local stress changes in the vicinity of the cracks, which caused an increase in the prestressing force at those locations. The local changes in the prestressing force were shown in Figure 4.6 for the girder modeled at release. A comparison of prestress losses in the two models of Girder II at the time of crack testing would be similar to the comparison shown at release. The increase in prestressing force decreased the prestress loss that would have occurred if the girder did not have initial cracks to close.

The amount of prestress that acted on the experimental girders at the time of crack testing was determined using the following equation:

$$\omega_b \mid 4\frac{P}{A_{net,nc}} 4\frac{Pe_{net,nc}c_{net,nc}}{I_{net,nc}} 2\frac{M_{sw}c_{net,nc}}{I_{net,nc}} 2\frac{M_{deck}c_{tr,nc}}{I_{tr,nc}} 2\frac{M_{sdl}c_{tr,c}}{I_{tr,c}} 2\frac{M_{ll}c_{tr,c}}{I_{tr,c}}, \quad (4.1)$$

where ω_b = concrete stress, P = total force of the prestressing strands, including losses at time of testing, A = area of concrete, e = eccentricity of the prestressing strand centroid from the neutral axis of the section, c = distance from the neutral axis of the section to the bottom fiber, I = moment of inertia of the cross section, and M = applied moment. The subscript *net* refers to the net section properties, *tr* refers to the transformed section properties, *nc* refers to the non-composite section, *c* refers to the composite section, *sw* refers to the self-weight of the concrete girder (710 plf for Girder I and 716 plf for Girder II), *deck* refers to the self-weight of the concrete deck (479 plf for both girders), *sdl* refers to the 35 kip (156 kN) superimposed sustained dead load, and *ll* refers to the actuator load (6.4 kips for Girder I and 0 kips for Girder II). The prestressing force, P, was calculated by setting M_{ll} equal to the moment from the reopening load and setting the bottom fiber concrete stress (ω_b) to zero. The moments in Equation (4.1) needed to be consistent with the location of zero stress, so the moment from the applied loads and self-weights were taken as the moments at the LVDT location. The prestress losses calculated for the experimental girders using this procedure were 34.3% and 37.8%. The calibrated analytical losses were 36.3% and 38.0% for Girders I and II, respectively. The slight differences in the loss between the experimental and analytical girders were attributed to the modified section shape used in the ABAQUS models (Figure 4.2) which had slightly different moments of inertia and neutral axis locations than the Mn/DOT 45M sections (Figure 4.1).

4.3.2 Cracking Load

Modulus of rupture tests were performed on the concrete used in Girders I and II at 28 days to determine the tensile strength of the concrete. These measured strengths were 950 psi (6.6 MPa) for Girder I and 750 psi (5.2 MPa) for Girder II. Because concrete strength varies with time, the tensile strength of the concrete in Girders I and II at the time of crack testing (593 days for Girder I and 725 days for Girder II) would have changed from their measured values at 28 days, however the strengths at the time of crack testing were not measured. The ABAQUS results for the models at crack testing were compared to a concrete tensile strength equal to the measured 28-day modulus of rupture because a more accurate strength was not available.

The experimental flexural cracking load for both girders was determined using acoustic emission (AE) monitoring equipment. Cracking began to occur on the bottom flange of Girder I at a load of 21 kips (93 kN) at each actuator location in combination with the 35 kip (156 kN) superimposed sustained dead load (21k+sdl). Girder II required the superimposed sustained dead load plus 14 kips (62 kN) of load at each actuator location (14k+sdl) for flexural cracking to occur. Locations of the first cracks are listed in Table 4.5 for Girder I and Table 4.6 for Girder II. The ABAQUS stress at each of the first crack locations for both the cracking and reopening loads are also listed. In addition, the maximum stresses predicted from the ABAQUS results and their locations are included.

Figure 4.10 shows a plot of the bottom element stress along the span at crack testing for Girder I. The analytical stress results from two different applied loads are shown. These loads correspond to the experimental initial flexural cracking load (21k+sdl) and the experimental crack reopening load (6.4k+sdl). The maximum stress determined by ABAQUS for the Girder I initial flexural cracking load (21k + sdl) occurred near midspan (801 in. [20.3 m]) and was +812.4 psi (5.6 MPa). Positive values of stress indicate a tensile stress. The first experimental cracks occurred to the right of midspan, at 858, 874 and 893 in. (21.8, 22.2 and 22.7 m) from the left end of the girder. These locations are indicated in the figure with data points. In addition, the location of the LVDTs is included at 893 in. (22.7 m) with a data point. The stress was zero for the crack reopening load of 6.4k+sdl at the LVDT location because this was the load and location used to calibrate the prestress in the model. Because cracking did not occur at the location of maximum stress, variances in the strength along the length of the girder were most likely present in the experimental girders. Additionally, the maximum bottom element stress in

the model did not attain the 28-day modulus of rupture, +950 psi (6.6 MPa) indicating that local defects were most likely present in the girder.

Figure 4.11 shows a plot of the bottom element stress along the span at crack testing for Girder II. The stresses resulting from the initial flexural cracking (14k+sdl) and crack reopening (0k+sdl) load are shown. The bottom element stresses are given for the models with and without pre-release cracks. The bottom element stresses along the span for the model with pre-release cracks illustrates the local losses in compressive stress near the pre-release crack locations. The pre-release crack locations are shown with dashed lines. An increase in the tensile stress in the bottom element is found to correspond to each of the eleven crack locations. Data points are included to identify the locations of the first six bottom flange cracks observed during crack testing and at the LVDT location at one of the bottom flange cracks. The first cracks occurred at 700, 718, 731, 746, 766 and 816 in. (17.8, 18.2, 18.6, 19.0, 19.4 and 20.7 m) from the left end of the girder. The LVDTs were placed at 899 in. (22.8 m). The stress was zero for the model of Girder II with pre-release cracks at the LVDT location with the crack reopening load applied because this was the load and location used to calibrate the prestress in the model. The LVDT was not placed over one of the first cracks to open so the stress exceeded zero at other locations in the girder with the reopening load applied. The maximum tensile stress determined by ABAQUS for the initial flexural cracking load (14k+sdl) occurred at 785 in. (19.9 m) and was +838.2 psi (5.8 MPa). The stress in the model of Girder II without pre-release cracks was 200 psi (1.4 MPa) more compressive at this location. An accurate model of Girder II without pre-release cracks was not able to be created because this girder never existed and a crack reopening load was not known. However, assuming the same prestressing at the onset of flexural crack testing for Girder II without pre-release cracks as the model of Girder II with pre-release cracks, an approximate loss in the bottom fiber stress due to the pre-release cracks could be determined. The comparison is only used to emphasize the effect pre-release cracks have on stress in a girder. The stresses at all of the crack locations and at midspan from the model of Girder II without pre-release cracks were included in brackets beside the Girder II with pre-release cracks stresses in Table 4.6. The maximum analytical stress predicted for Girder II with pre-release cracks exceeded the 28-day modulus of rupture (+750 psi [5.2 MPa]) indicating that the concrete tensile strength did not change significantly from its 28-day strength.

Figure 4.12 shows the percent difference in the stresses between the models of Girder II with and without pre-release cracks at the initial flexural cracking load using the following equation:

$$\frac{\omega_{cr} - \omega_{ucr}}{\omega_{ucr}} \Delta 100, \qquad (4.2)$$

where the subscript *cr* denotes the stress from the model of Girder II with pre-release cracks and the subscript *ucr* denoted the stress from the model of Girder II without pre-release cracks. The change in stress along the entire depth at each of the crack locations was calculated. The shaded regions in the figure show the areas where there were lower compressive stresses in the model with pre-release cracks than in the model without pre-release cracks. An increase in compressive stress was seen in the location of the crack tips. The stress increased in compression because the crack was pivoting about the crack tip to close. The pre-release cracks caused a reduction in the compressive stress for the bottom elements beneath all of the crack locations.

4.4 Summary

The analytical results from the models of Girders I and II clearly show that the reduction in camber and flexural cracking load that was observed in Girder II could have been caused by the pre-release cracks that developed during fabrication. ABAQUS results showed a 14% loss in the initial camber between the models of Girder II with and without pre-release cracks, and local stress changes at the pre-release crack locations were also present. Increased confidence can be placed on the pre-release crack effects that were discussed in Chapter 3 because the ABAQUS models replicating two experimental girders compared well with the measured girder behavior.

CHAPTER FIVE
CONCLUSIONS AND RECOMMENDATIONS

5.1 Summary

Pre-release cracks have been observed during the fabrication process of some prestressed concrete girders (Ahlborn, 1998; Green, 1984; Roller, 1993), but their effects were often assumed to be negligible because autogenous healing was assumed to restore the strength of the girders. Experimental results obtained by Ahlborn, however, indicated a reduced initial camber and flexural cracking load in a girder that had developed pre-release cracks. The effects of pre-release cracks on girder camber, stress state, and fatigue of prestressing strands were investigated to determine if pre-release crack effects are negligible, or what effects the cracks might have on steel fatigue due to early flexural cracking if the effects are not negligible.

The study began with an investigation regarding the fatigue of prestressing strands to determine expected stress ranges in the prestressing strands of cracked girder sections. The results of this portion of the study indicated that steel fatigue may be a problem in cracked sections. The next stage of the study included an investigation of the camber and stress state of a section resulting from several different pre-release crack sizes and locations. Finite element models were created to determine if a loss of compressive stress was apparent at the bottom of the girder due to pre-release crack closure. The loss in bottom element compressive stress indicated a reduced flexural cracking capacity of a section with pre-release cracks. The final stage of the study involved finite element analysis of the two experimental girders tested by Ahlborn. The results of the finite element models were compared to the limited available experimental data to determine if the models accurately represented girder behavior and if the occurrence of pre-release cracks could account for the reduction in camber and flexural cracking load observed by Ahlborn.

5.2 Conclusions Regarding Steel Fatigue

Fatigue of prestressing strand becomes a design concern when steel stress ranges exceed 20 ksi in uncracked girder sections (Paulson, 1983). This fatigue limit is reduced when the section becomes cracked. ACI Committee 215 (1994) suggests a limit of $0.06f_{pu}$ for cracked sections.

Cracked sections might occur when pre-release cracks develop, due to a reduced compressive stress in the bottom fiber of the girder that results from crack closure. As an example for the 45 in. deep, 135 ft. long rectangular beam investigated in Chapter 3, calculated reductions in bottom fiber compressive stress were on the order of 7% for the case of the 0.01 in. (0.254 mm) pre-release crack. As observed in Figure 3.31, reductions in compressive stress increased with crack depth, crack width, and level of applied loading. Cracked sections also might occur from an overload on the girder. As an example, a 10% increase in design load would result in flexural cracking of the 100 ft. long Mn/DOT 81I beam described in Appendix A, assuming flexural cracking occurs when the bottom fiber tensile stress reaches the concrete modulus of rupture ($7.5 \cdot f'_c$, psi; $0.7 \cdot f'_c$, MPa). In both of these instances, once the girder has cracked, the crack may reopen under normal service load conditions because the tensile capacity is lost at a crack location. Crack reopening increases the stress range in the steel strands which creates a fatigue concern.

A parametric study was performed to determine what stress ranges were expected in the steel strands of girder sections that have cracked. The parametric study looked at six girder designs which varied in concrete strength, girder type, girder spacing and strand size. Span lengths were maximized to attain the largest steel stress range for the girder design. The computer program SPAN (Leap Software, 1990) was used to determine a strand pattern based on AASHTO Specifications for each of the girder designs. Each girder design was analyzed as an uncracked section, a cracked section, and a partially cracked section to predict three different strand stress ranges. The strand stress range was calculated as the change in stress in the bottom steel strand due to an HS-25 live load.

The steel stres

what would be expected in design because sections are designed to keep the tensile stresses below the tensile strength of the concrete under service loads.

The steel stress ranges in cracked sections varied between 21.2 ksi and 33.5 ksi. These stress ranges exceeded the recommended $0.06f_{pu}$ fatigue limit for cracked sections from ACI Committee 215 (1994). This limit corresponds to 16.2 ksi for Grade 270 ksi prestressing steel which was used in this study. These stress ranges were very large due to the neutral axis location being very near or in the composite deck. Due to the high neutral axis location with respect to the girder bottom flange, it was not believed that all of the concrete below the neutral axis would crack under overloads. The stress ranges determined for the cracked sections were

thought to be larger than would be expected in the field. To establish a more accurate representation of the girder behavior with a portion of the section cracking in flexure, a third steel stress range was determined using an effective moment of inertia. The effective moment of inertia was determined using the moment-curvature program RESPONSE (Collins, 1990), and was assumed to be representative of a partially cracked girder.

The largest steel stress range using partially cracked sections was 13.25 ksi. This did not exceed the ACI Committee 215 recommended fatigue limit for cracked sections, but it did exceed the experimental evidence found by Rabbat (1979) of fatigue failure in cracked section with stress ranges of 9 ksi. Because the stress ranges for partially cracked sections approach the ACI recommended fatigue limit and because the amount of fatigue testing of the prestressing strands in cracked sections is limited, the stress range results from partially cracked sections indicate there is a concern regarding steel fatigue for a girder section that becomes cracked. The stress ranges from the partially cracked sections represent girder performance in an average sense because the effects of the crack are distributed over the length of the girder. The stress range at a specific crack location would be closer to the results from the cracked section analyses because the stress in the steel at the crack location is increased due to the local strain in the steel from the crack opening. The partially cracked section results provide a lower bound for the steel stress range in a cracked girder, and the cracked section results provide an upper bound for the steel stress range at a crack location because the stress range in the steel is dependent on the bond between the strands and the concrete. The results of the parametric study show that fatigue of prestressing strand is a concern for girders that develop flexural cracks that reopen under future load.

5.3 Conclusions from ABAQUS Models

Pre-release cracks were modeled using the finite element program ABAQUS (HKS Inc., 1994) to determine the effects pre-release cracks had on girder stresses and camber. Models were made with a single crack located at the midspan and with multiple cracks centered about the midspan. The crack widths varied between 1/100, 1/32, and 1/16 in. (0.25, 0.8, and 1.6 mm) and the crack depths varied between 12, 24, and 36 in. (305, 610, and 840 mm). After the effects from pre-release crack closure were determined, additional ABAQUS models were made to replicate the two experimental girders tested by Ahlborn (1998) in which one of the girders

developed pre-release cracks. The analytical results were compared to the limited available experimental data to determine if the ABAQUS models accurately represented girder behavior.

Closure of pre-release cracks was expected to cause a decrease in girder camber and bottom fiber compressive stress. It was also expected that the stress changes would be local, occurring only near the pre-release crack location. The results from the ABAQUS models verified that these expectations were true.

Stress changes from pre-release cracks occurred throughout the depth of the girders at the location of the pre-release crack. The span length where the stress state changed due to the pre-release crack was limited to the depth of the girder (d = 45in. [1140 mm]) on each side of the pre-release crack location. A 4% stress change criteria was applied to the results to establish an area around the crack that could reasonably be considered to be affected by the pre-release crack in a fabricated girder and not from other causes like material inconsistencies. The affected stress area increased as the crack width increased and decreased as the crack depth increased.

The stress behavior in the section at the crack location was investigated to determine if the stress distributions remained linear. The distribution before crack closure (BCC) and after crack closure (ACC) were both analyzed. A non-linear stress distribution occurred during crack closure, with linear stress distribution increments occurring for additional loading after the crack was fully closed. The linear stress increments ACC were equal to the stress increments in the uncracked model. The bottom elements in each section decreased in magnitude of compressive stress from the uncracked model due to the pivoting of the girder to close the pre-release crack. The areas near the crack tip locations increased in compressive stress due to the pivoting action about the crack tip. The elements at the top of the section had a reduction in compressive stress because that portion of the girder was initially open.

Several of the models involved cracks that did not close. The closure load was dependent on the size of the crack modeled. Deeper crack depths and smaller crack widths caused the cracks to close at smaller loads.

The size of the crack modeled also affected the amount of stress change in the girder from the uncracked model. Larger stress changes occurred for deeper and wider cracks. The deeper and wider cracks also caused greater midspan camber losses.

The ABAQUS models involving multiple cracks behaved similarly to the models involving a single crack. If the cracks were spaced such that their affected stress areas did not

overlap, the stress at each crack location was identical to that of an individual crack. When cracks were spaced so their affected stress areas overlapped, the stress effects were the superposition of the stress change from each of the separate cracks.

The results from the ABAQUS models replicating the two experimental girders clearly showed that the reduction in camber and flexural cracking load observed in the girder that developed pre-release cracks could have been caused by the pre-release cracks. A 14% loss in the initial camber and local stress changes at the pre-release crack locations were apparent. The results from the models compared well with the measured girder behavior, which indicated the computer analyses could be used to predict girder behavior due to pre-release cracks.

5.3.1 Conclusions Regarding the Geometric Compatibility Theory

The geometric compatibility theory (GCT) that was developed by Shield (1997) to predict the effects on camber and cracking loads due to pre-release crack closure was used to compare the predicted camber of several of the ABAQUS models. Error resulted in several of the calculations because the crack in the ABAQUS model did not close under the girder self-weight. The GCT equations assumed the crack was completely closed. Additional error existed in the predictions of the GCT camber and the ABAQUS camber for increasing crack depths. Both of the camber predictions had an increase in camber loss for increasing crack widths. However, the GCT predicted decrease in camber loss as the crack depth increased, where ABAQUS predicted an increase in camber loss as the crack depth increased. The difference in these predictions indicated that an assumption used in developing the GCT equations was not consistent with the ABAQUS analyses. One assumption used in the development of the GCT equations that was inconsistent with the ABAQUS results was that plane sections remained plane during crack closure.

5.4 Recommendations

The ABAQUS analyses investigating pre-release crack effects indicate that pre-release cracks do cause a reduction in the bottom element compressive stress, which would lead to a reduced flexural cracking capacity of the section. The reduced flexural cracking capacity of girders that develop pre-release cracks make them more likely to experience fatigue failure of the prestressing strands. The results from the parametric study investigating steel stress ranges

indicate a concern for fatigue failure in cracked sections due to the local strain in the steel that occurs from crack opening. These conclusions and the degree of concern necessary for girders that develop pre-release cracks should be correlated with experimental girders to ensure the results of the computer analyses are an accurate representation of girder behavior. Instrumentation on the experimental girders should include strain gages throughout the depth of the section to determine the stress distribution before and after crack closure, an additional strain gage at the top of the crack to determine crack closure, and gages along the prestressing strand to determine the effects the crack has on the steel strands. Changes in section shape and size from the girders used in the ABAQUS analyses of this report would result in different magnitudes of stress change from the reported data, but the general behavior of the experimental models should remain consistent with the conclusions of this report.

Additional data regarding the fatigue life of prestressing strand in cracked girder sections would also be beneficial because most fatigue data currently available is pertinent to uncracked sections only.

REFERENCES

Ahlborn, T. (1998). "High Strength Prestressed Concrete Bridge Girders." Thesis, Doctor of Philosophy, Department of Civil Engineering, University of Minnesota.

American Association of State Highway Transportation Officials (AASHTO). Standard Specifications for Highway Bridges, 15th Edition. Washington D. C., 1993.

ACI Committee 215 (1994). ACI 215-74/94 "Consideration for Design of Concrete Structures Subjected to Fatigue Loading." ACI Manual of Concrete Practice (1994).

ACI Committee 318 (1995). "Building Code Requirements for Structural Concrete and Commentary." ACI 318-95. American Concrete Institute (ACI), Detroit, Michigan.

Collins, Michael P., et al. RESPONSE. Computer software. Prentice-Hall, Inc., 1990.

Collins, Michael P., and Denis Mitchell. Prestressed Concrete Structures. Englewood Cliffs: Prentice-Hall, 1991.

Green, J. K., P. J. Cookson, and K. A. L. Johnson (1984). "Performance of Pretensioned Concrete Beams that have Cracked before Transfer of Prestress." The Structural Engineer. December.

Hawkins, N. M., and S. P. Shah (1982). "American Concrete Institute Considerations for Fatigue." Fatigue of Steel and Concrete Structures. International Association of Bridge and Structural Engineers.

Hibbitt, Karlsson & Sorensen, Inc. (1994). ABAQUS. Version 5.4, Pawtucket, Rhode Island.

Leap Software (1990). SPAN, Simple-Span Pretensioned Concrete Bridge Girder Design. Version 5.0, LEAP Software Inc., Tampa, Florida.

Minnesota Department of Transportation. Bridge Details Manual. St. Paul, MN, 1991 Update.

Paulson, Conrad Jr., and Karl H. Frank. "A Fatigue Study of Prestressing Strand." Materials and Member Behavior: Proceedings of the Sessions at Structures Congress '87. New York: ASCE, 1987.

Paulson, Conrad Jr., Karl H. Frank, and John E. Breen. A Fatigue Study of Prestressing Strand. Research Report 300-1, Center for Transportation Research, University of Texas at Austin, 1983.

Rabbat, B. G., Kaar, P. H., Russell, H. G., Bruce, R. N., (1979). "Fatigue Test of Pretensioned Girders with Blanketed and Draped Strands." PCI Journal, Vol. 24, No. 4, August, pp. 88-115.
Roller, J. J., Martin, B. T., Russell, H. G., Bruce, R. N., (1993). "Performance of Prestressed High Strength Concrete Bridge Girders." PCI Journal, Vol. 39, No. 3, May-June, pp. 34-45.

Shield, C. K., C. W. French and T. M. Ahlborn. "Effect of Pre-Release Cracks on High Strength Prestressed Girders." Submitted for publication in *ASCE Journal of Structural Engineering*, 1997.

Table 2.1 Steel Stress Range

Case	Concrete Strength	Girder Type	Span Length	Girder Spacing	Strand Diameter	Uncracked Stress Range	Partially Cracked Stress Range	Cracked Stress Range
1	7,000 psi	81I	100 ft.	12 ft.	0.5 in.	5.87 ksi	12.11 ksi	29.5 ksi
2	7,000 psi	45M	60 ft.	12 ft.	0.5 in.	6.77 ksi	13.25 ksi	33.5 ksi
3	7,000 psi	81I	160 ft.	4 ft.	0.5 in.	3.72 ksi	7.24 ksi	21.2 ksi
4	7,000 psi	45M	105 ft.	4 ft.	0.5 in.	5.08 ksi	8.18 ksi	23.9 ksi
5	10,000 psi	81I	114 ft.	12 ft.	0.5 in.	5.95 ksi	11.32 ksi	26.2 ksi
6	7,000 psi	81I	100 ft.	12 ft.	0.6 in.	5.87 ksi	12.14 ksi	29.3 ksi

Table 2.2 SPAN Results and Geometric Section Properties

Case	Midspan Moment Prior to Live Load [1] (k-ft)	Midspan Moment with Live Load (k-ft)	Bottom Fiber Stress Prior to Live Load (psi)	Neutral Axis $y_{g,c}$ (in)	$I_{g,c}$ (in^4)	Neutral Axis y_{cr} (in)	I_{cr} (in^4)	I_{eff} (in^4)
1	3885	6362	-632	64.2	1,684,500	83.7	220,200	1,128,400
2	1301	2605	-816	39.0	465,400	50.4	52,500	324,200
3	5514	6926	-237	53.1	1,246,100	78.0	235,400	911,000
4	2038	2912	-495	32.0	337,700	46.4	60,100	286,400
5	5012	7900	-773	62.1	1,602,900	82.7	232,700	1,168,700
6	3885	6362	-632	64.2	1,684,500	83.7	220,500	1,124,700

[1] Part of moment acts on noncomposite section and part acts on composite section. See Table 2.3 for loads.

Table 2.3 SPAN Superimposed Sustained Dead Load

Case	Superimposed Sustained Dead Load[1] (on noncomposite section) (plf)	Superimposed Sustained Dead Load (on composite section) (plf)
1	183.3	639.0
2	199.4	639.0
3	34.6	303.0
4	22.6	303.0
5	160.8	639.0
6	183.3	639.0

[1] Superimposed sustained dead load on the noncomposite section consisted only of the diaphragm weight.

Prestress, girder self-weight, and deck self-weight were automatically applied to the noncomposite

section in SPAN.

Table 2.4 RESPONSE Strain Results

	Initial Strains for RESPONSE			Strains Prior to Live Load		Strains with Live Load	
Case	**Steel (σκ)**	**Bottom Fiber (σκ)**	**Top Fiber[1] (σκ)**	**Bottom Fiber (σκ)**	**Top Fiber (σκ)**	**Bottom Fiber (σκ)**	**Top Fiber (σκ)**
1	5.561	-0.229	-0.303	+0.126	-0.024	+0.563	-0.139
2	5.597	-0.254	-0.250	+0.106	-0.022	+0.584	-0.155
3	5.762	-0.169	-0.496	+0.142	-0.052	+0.404	-0.181
4	5.508	-0.223	-0.463	+0.151	-0.056	+0.450	-0.221
5	5.289	-0.245	-0.371	+0.113	-0.042	+0.522	-0.173
6	5.547	-0.229	-0.293	+0.126	-0.024	+0.564	-0.139

[1] Top fiber of the noncomposite section.

Table 3.1 Affected Stress Area

	crack width		
	1/100"	**1/32"**	**1/16"**
12" depth crack			
1% change	72"	88"	96"
4% change	40"	56"	72"
(max. change)/4	56" [2%][1]	48" [7%]	48" [12%]
24" depth crack			
1% change	72"	88"	96"
4% change	40"	56"	72"
(max. change)/4	48" [3%]	40" [10%]	40" [19%]
33" depth crack			
1% change	64"	80"	88"
4% change	32"	48"	56"
(max. change)/4	40" [3%]	32" [10%]	32" [20%]

Self-weight + 800 lb/ft results.

[1] Bracketed terms equal the "(max.change)/4" percentage.

Table 3.2 Change in Stress Distribution Relative to Uncracked Model

			self-weight	self-weight + 800 lb/ft
Crack Depth	**Crack Width**	**Closure Load**	$\div\omega_{top}$ $\div\omega_{bottom}$ $\div\omega_{crack\ tip}$ (psi)	$\div\omega_{top}$ $\div\omega_{bottom}$ $\div\omega_{crack\ tip}$ (psi)
12"	1/100"	self-weight + 200 lb/ft	+445 +206 -723	+914 +224 -738
12"	1/32"	self-weight + 800 lb/ft	+442 +394 -1857	+2811 +700 -2347
12"	1/16"	open	+440 +461 -2649	+3254 +1251 -4546
24"	1/100"	self-weight + 100 lb/ft	+258 +322 -464	+262 +322 -464
24"	1/32"	self-weight + 200 lb/ft	+441 +987 -1396	+816 +1008 -1398
24"	1/16"	self-weight + 500 lb/ft	+435 +1836 -2756	+1764 +2016 -2787
33"	1/100"	self-weight	+83 +339 -239	+79 +342 -238
33"	1/32"	self-weight	+264 +1054 -796	+264 +1057 -795
33"	1/16"	self-weight + 100 lb/ft	+429 +2102 -1547	+489 +2105 -1546

$\div\omega$ = stress difference between cracked and uncracked ABAQUS models.

$= \omega_{cracked} - \omega_{uncracked}$.

Table 3.3 Bottom Element Compressive Stress Loss Relative to Uncracked Model

	crack width		
	1/100"	**1/32"**	**1/16"**
12" depth crack			
self-weight	*206 psi (4.0%)* [1]	*394 psi (7.7%)*	*461 psi (9.0%)*
self-weight + 400 lb/ft	224 psi (5.8%)	*659 psi (17.2%)*	*960 psi (25.0%)*
self-weight + 800 lb/ft	224 psi (8.8%)	700 psi (27.5%)	*1251 psi (49.2%)*
24" depth crack			
self-weight	*322 psi (6.3%)*	*987 psi (19.2%)*	*1836 psi (35.8%)*
self-weight + 400 lb/ft	322 psi (8.4%)	1008 psi (26.3%)	2016 psi (52.5%)
self-weight + 800 lb/ft	322 psi (12.7%)	1008 psi (39.6%)	2016 psi (79.3%)
33" depth crack			
self-weight	339 psi (6.6%)	1054 psi (20.5%)	*2102 psi (41.0%)*
self-weight + 400 lb/ft	341 psi (8.9%)	1055 psi (27.5%)	2104 psi (54.8%)
self-weight + 800 lb/ft	342 psi (13.4%)	1057 psi (41.6%)	2105 psi (82.8%)

Percentages were calculated using Equation (3.1).

[1] Italicized values denote a crack that did not close completely.

Table 3.4 Midspan Camber

		crack width		
	uncracked	**1/100"**	**1/32"**	**1/16"**
12" depth crack				
self-weight	8.61"	*8.56"* [1]	*8.51"*	*8.49"*
self-weight + 400 lb/ft	5.09"	5.03"	*4.92"*	*4.84"*
self-weight + 800 lb/ft	1.57"	1.51"	1.39"	1.25"
24" depth crack				

self-weight	8.61"	*8.52″*	*8.33″*	*8.08″*
self-weight + 400 lb/ft	5.09"	5.00"	4.80"	4.52"
self-weight + 800 lb/ft	1.57"	1.48"	1.29"	1.00"
33" depth crack				
self-weight	8.61"	8.50"	8.29"	*7.97″*
self-weight + 400 lb/ft	5.09"	4.98"	4.76"	4.45"
self-weight + 800 lb/ft	1.57"	1.46"	1.24"	0.93"

[1] Italicized values denote a crack that did not close completely.

Table 3.5 Camber Prediction Using Geometric Compatibility Theory Equations

	ABAQUS Camber	Geometric Compatibility Theory Camber	% Difference
SINGLE CRACK			
12" depth			
1/100" width[1]	*8.555"*	*8.443"*	*1.3%*
1/32" width	*8.505"*	*8.084"*	*5.0%*
1/16" width	*8.486"*	*7.557"*	*10.9%*
24" depth			
1/100" width	*8.518"*	*8.524"*	*-0.1%*
1/32" width	*8.328"*	*8.345"*	*-0.2%*
1/16" width	*8.082"*	*8.082"*	*0.0%*
33" depth			
1/100" width	8.502"	8.545"	-0.5%
1/32" width	8.287"	8.415"	-1.5%
1/16" width	*7.971"*	*8.223"*	*-3.2%*
MULTIPLE CRACKS			
3 - 12" x 1/100"	8.469"	8.105"	4.3%
3 - 24" x 1/100"	8.365"	8.356"	0.1%
3 - 33" x 1/100"	8.338"	8.423"	-1.0%

[1] Italicized text denote a crack that did not close completely.
All results are from self-weight load.
Midspan camber for uncracked model = 8.609 in.

Table 4.1 Measured Pre-release Crack Locations and Depths

Position in Span[1] (ft. [m])	Crack Depth from Top Flange (in. [mm])
32.8 [10.0]	37.0 [940]
34.0 [10.4]	6.75 [170]
34.2 [10.5]	36.5 [925]
39.5 [12.0]	37.5 [955]
41.0 [12.5]	4.0 [100]
54.3 [16.6]	34.5 [875]
58.7 [17.9]	4.0 [100]
59.7 [18.2]	31.0 [785]
63.0 [19.2]	28.0 [710]
65.5 [20.0]	37.0 [940]
66.0 [20.3]	3.38 [85]
69.5 [21.1]	34.8 [885]
76.3 [23.2]	40.3 [1020]
87.3 [26.6]	31.0 [785]
95.0 [28.9]	28.0 [710]

[1] Measured from left end of girder.

Table 4.2 Material Properties of Girders I and II

	Girder I	Girder II
E_s (ksi [GPa])	28,800 [198.6]	28,800 [198.6]
E_c - initial (ksi [GPa])	4,380 [30.2]	4,750 [32.8]
E_c - crack testing (ksi [GPa])	4,680 [32.3]	4,800 [33.1]
E_c - deck (ksi [GPa])	4,000 [27.6]	4,000 [27.6]
$A_{s/0.6\ in.\ strand}$ (in^2 [mm^2])	0.228 in^2 [147 mm^2]	0.228 in^2 [147 mm^2]

Table 4.3 ABAQUS Pre-release Crack Locations and Depths

Position in Span (ft. [m])	Crack Depth from Top Flange (in. [mm])
32.8 [10.0]	31.0 [785]
34.3 [10.5]	31.0 [785]
39.5 [12.0]	31.0 [785]
54.3 [16.6]	31.0 [785]
59.7 [18.2]	31.0 [785]
63.0 [19.2]	27.0 [690]
65.5 [20.0]	31.0 [785]
69.2 [21.1]	31.0 [785]
76.3 [23.3]	31.0 [785]
87.5 [26.7]	31.0 [785]
95.0 [28.9]	27.0 [685]

Table 4.4 Initial Cambers for Girders I and II

	Girder I (in. [mm])	Girder II (in. [mm])	Girder II - uncracked
Measured Results			
On-bed	4.76 [121]	3.86 [98]	
On-bed, next morning	4.84 [122]	3.74 [95]	
Lift/set	5.47 [139]	4.06 [103]	
Approximate Initial Camber [1]	*5.12 [130]*	*3.96 [101]*	
ABAQUS Results			
Midspan deflection	6.13 [156]	4.96 [126]	5.74 [146]

[1] Average value of on-bed and lift/set cambers to account for friction forces from the precasting bed

Table 4.5 Girder I - Bottom Element Stresses at the First Crack Locations and at the Location of Maximum Stress

Crack Location from Left Girder End (in.)	ABAQUS Stress (psi) Cracking Load - (21k+sdl)	ABAQUS Stress (psi) Reopening Load (6.4k+sdl)
893	+715.3	0.0[1]
874	+754.6	+44.0
858	+786.9	+72.3
max. ABAQUS stress[2]	*+812.4*	*+98.1*

[1] Location of LVDTs.
[2] Maximum bottom fiber stress at midspan [803 in.].

Table 4.6 Girder II - Bottom Element Stresses at the First Crack Locations and at the Location of Maximum Stress

Crack Location (in.)	ABAQUS Stress (psi) Cracking Load - (14k+sdl)	ABAQUS Stress (psi) Reopening Load - (0k+sdl)
700	+614.4 [+558.1][1]	-78.5 [-134.9]
718	+783.8 [+593.6]	+91.3 [-98.8]
731	+743.9 [+610.0]	+51.6 [-82.4]
746	+770.7 [+620.9]	+78.3 [-71.5]
766	+803.4 [+628.5]	+111.2 [-63.8]
816	+746.2 [+633.0]	+54.0 [-59.2]
max. ABAQUS stress[2]	*+838.2 [+633.6]*	*+145.9 [-58.6]*

[1] Bracketed terms are the stresses in the Girder II model without pre-release cracks.
[2] Maximum stress which occurred at the pre-release crack location of 785 in. in the model with pre-release cracks and at midspan [803 in.] in the model without pre-release cracks.

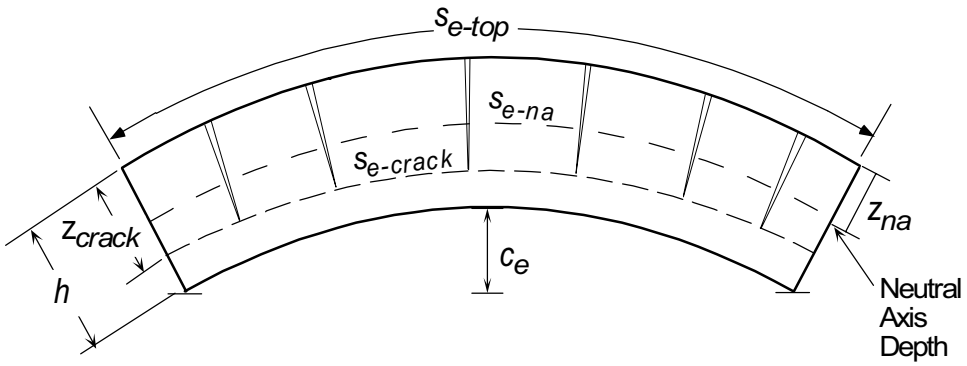

Figure 1.1 Expected Girder Shape

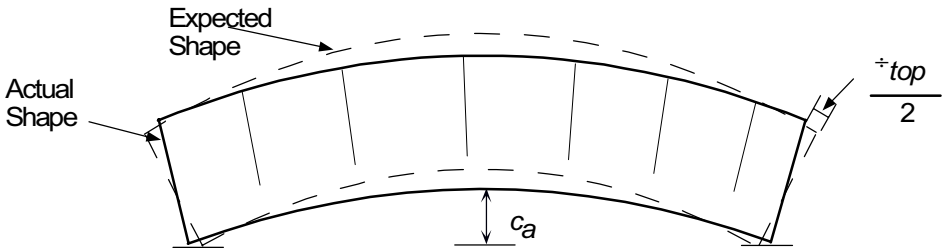

Figure 1.2 Girder Shape After Crack Closure

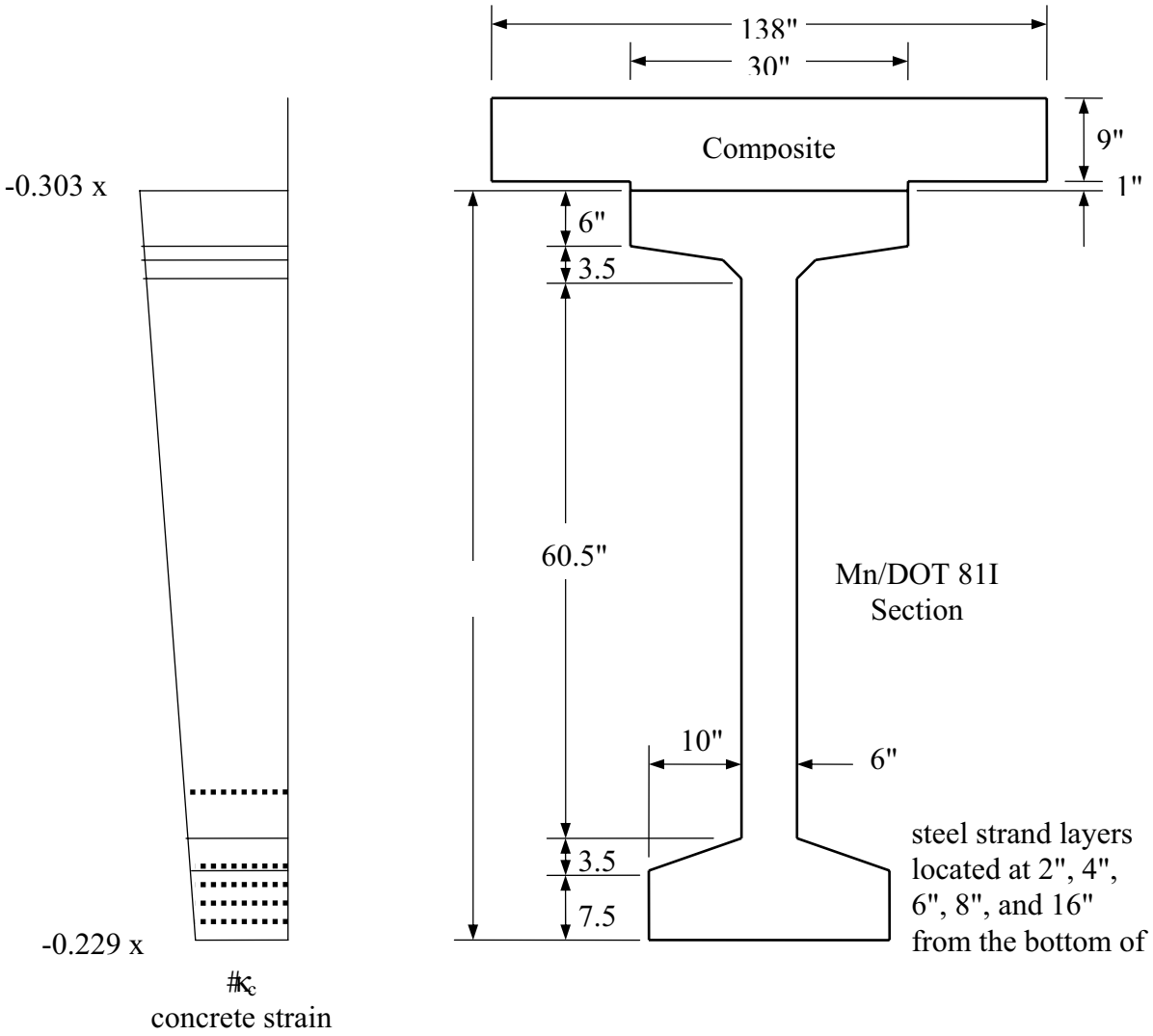

Figure 2.1 Initial Strain Distribution for RESPONSE Case 1

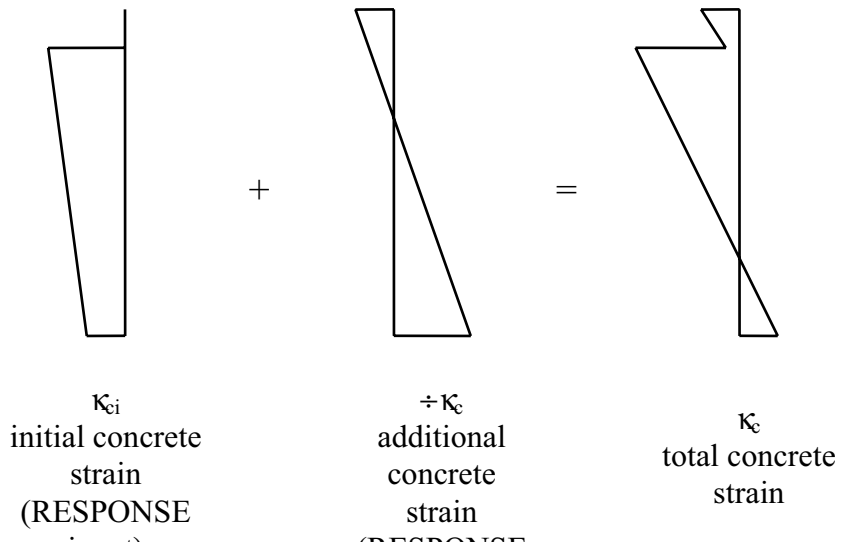

Figure 2.2 Concrete Strain Distribution using RESPONSE

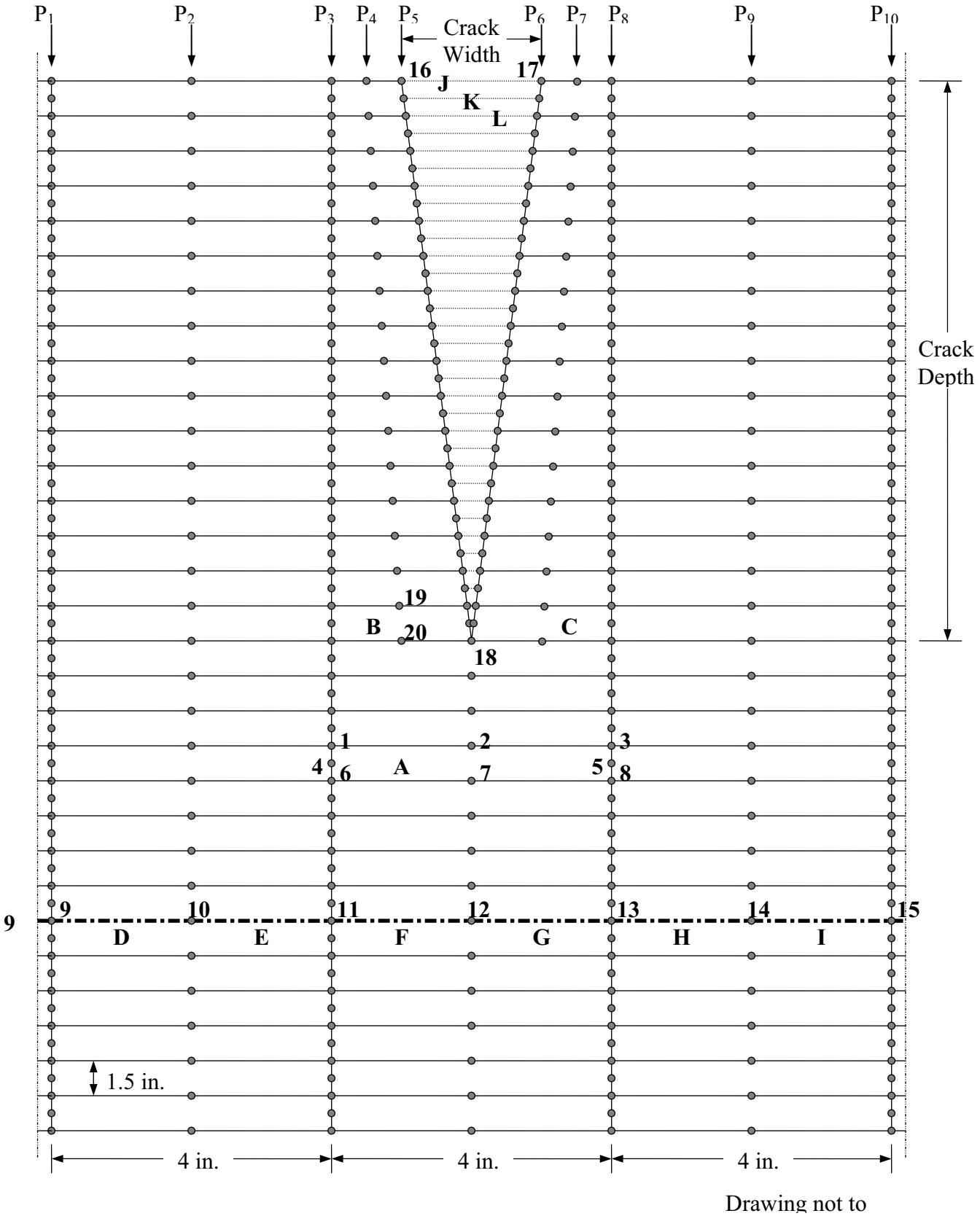

Figure 3.1 Element and Node Definitions for ABAQUS Models

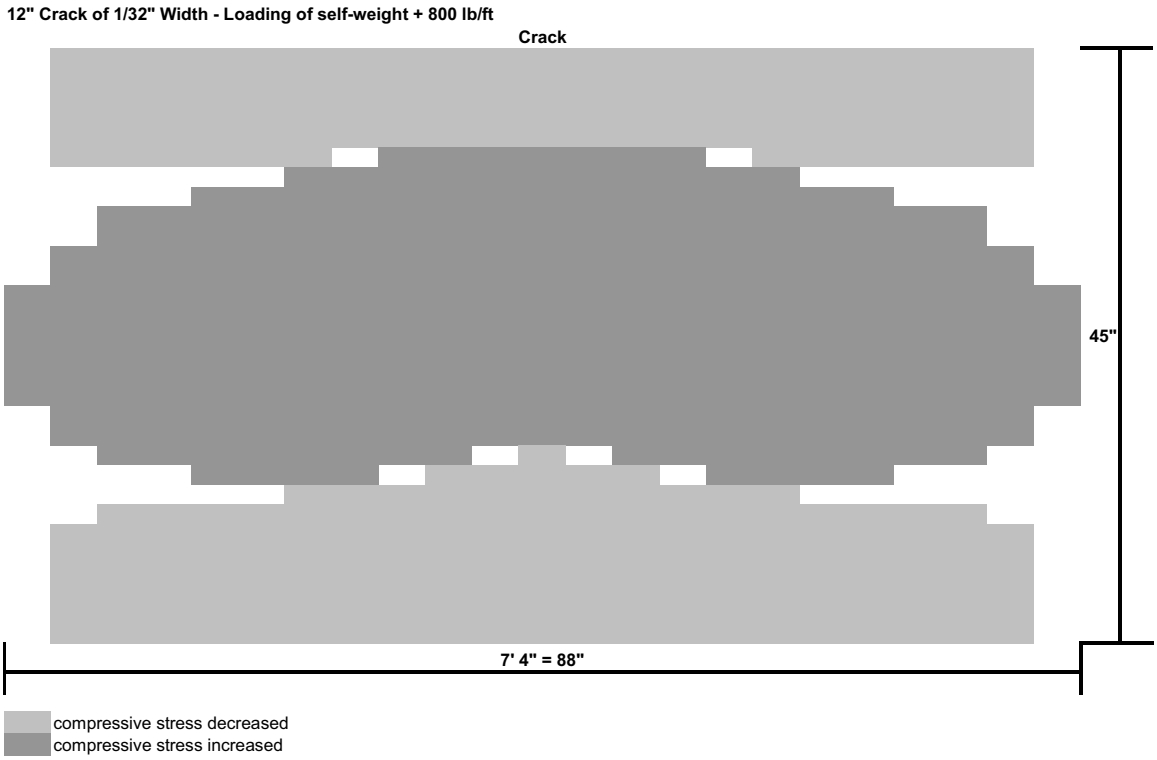

Figure 3.2 Affected Stress Area for a 12" Depth Crack of 1/32" Width

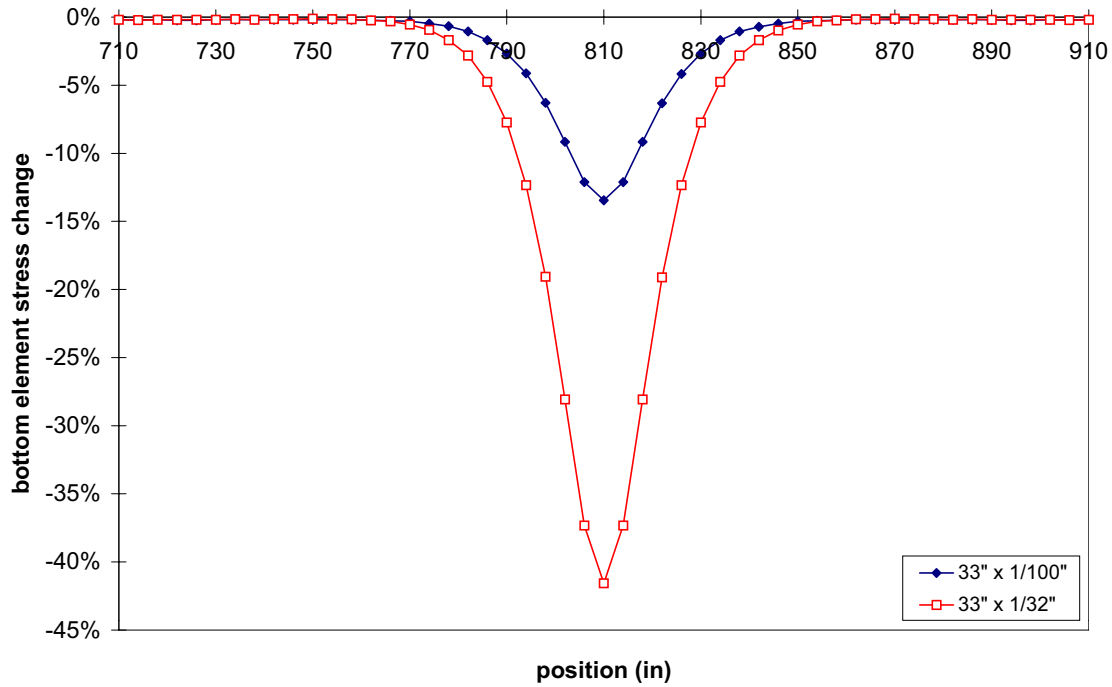

Figure 3.3 Bottom Element Stress Change Relative to Uncracked Case for 33" Depth Crack

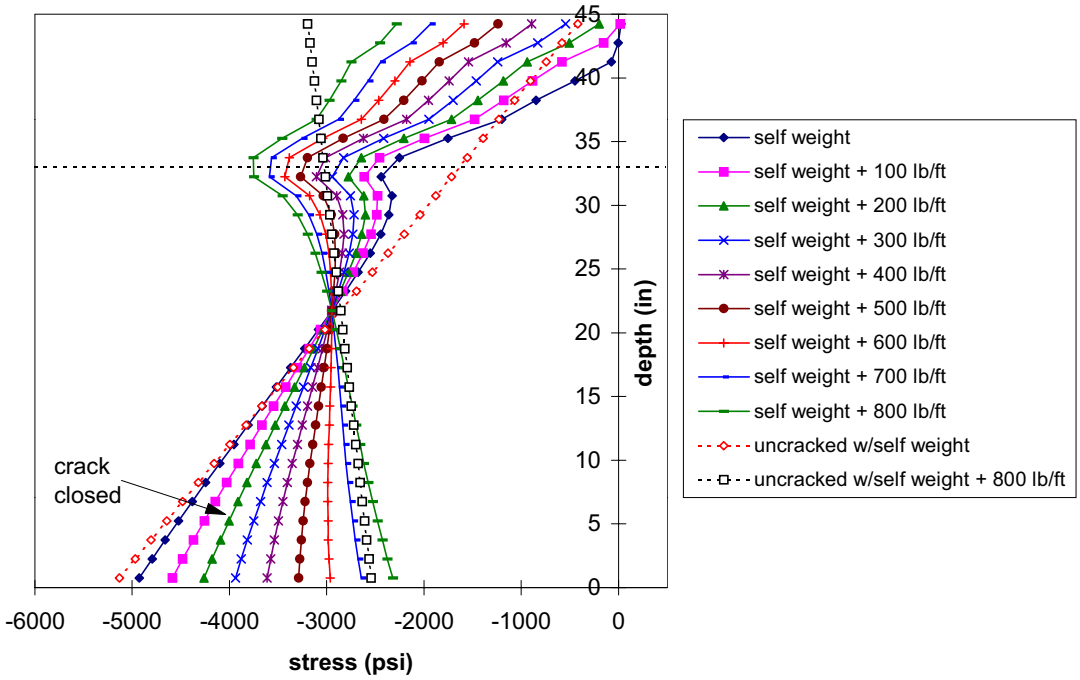

Figure 3.4 Stress Distribution at Midspan, Crack of 1/100" Width, 12" Depth

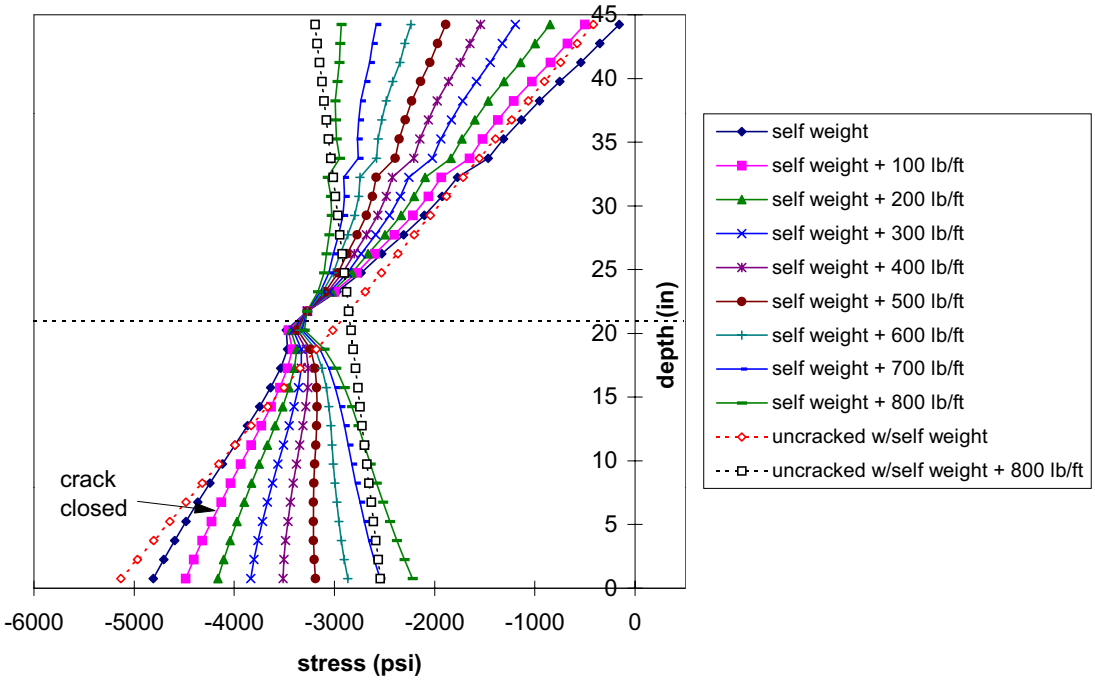

Figure 3.5 Stress Distribution at Midspan, Crack of 1/100" Width, 24" Depth

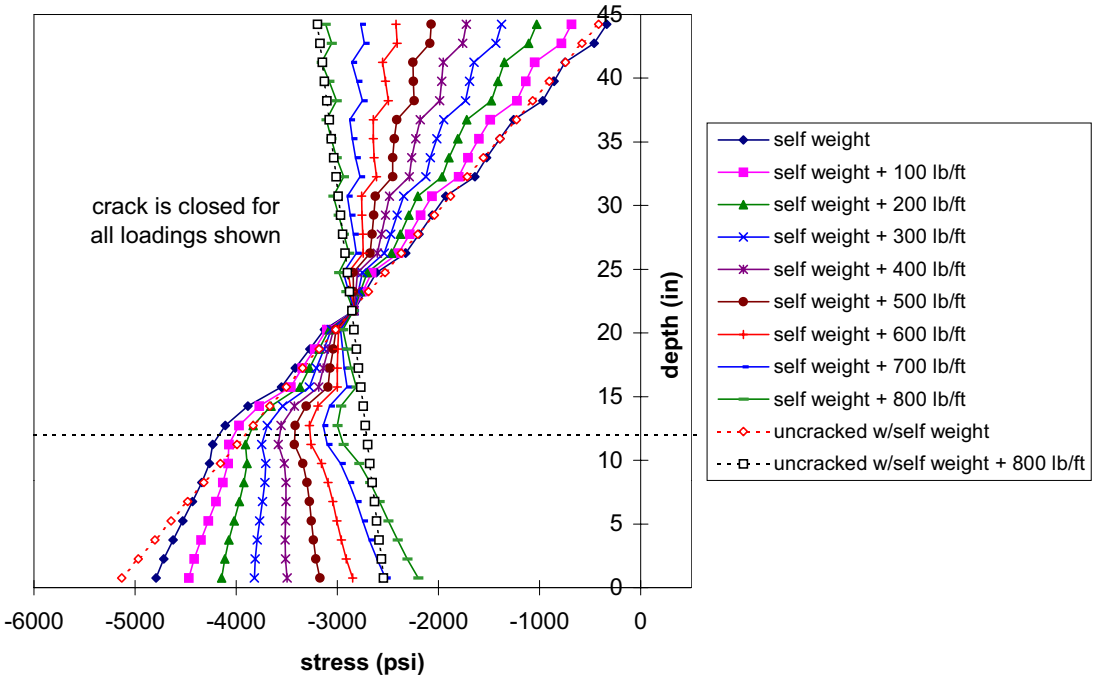

Figure 3.6 Stress Distribution at Midspan, Crack of 1/100" Width, 33" Depth

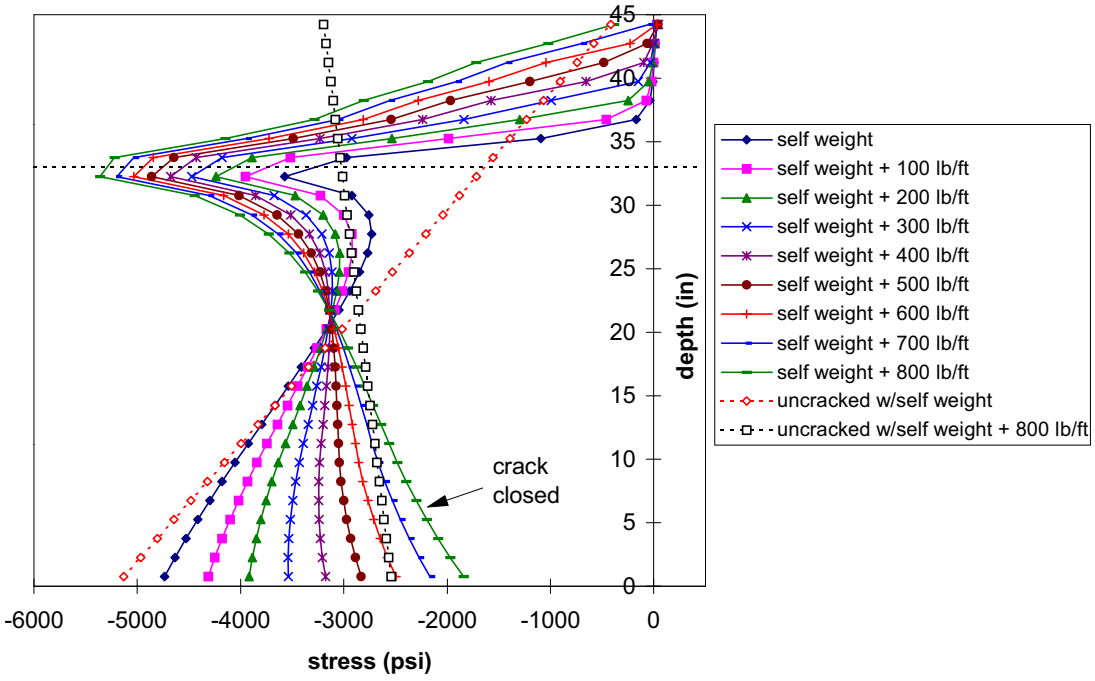

Figure 3.7 Stress Distribution at Midspan, Crack of 1/32" Width, 12" Depth

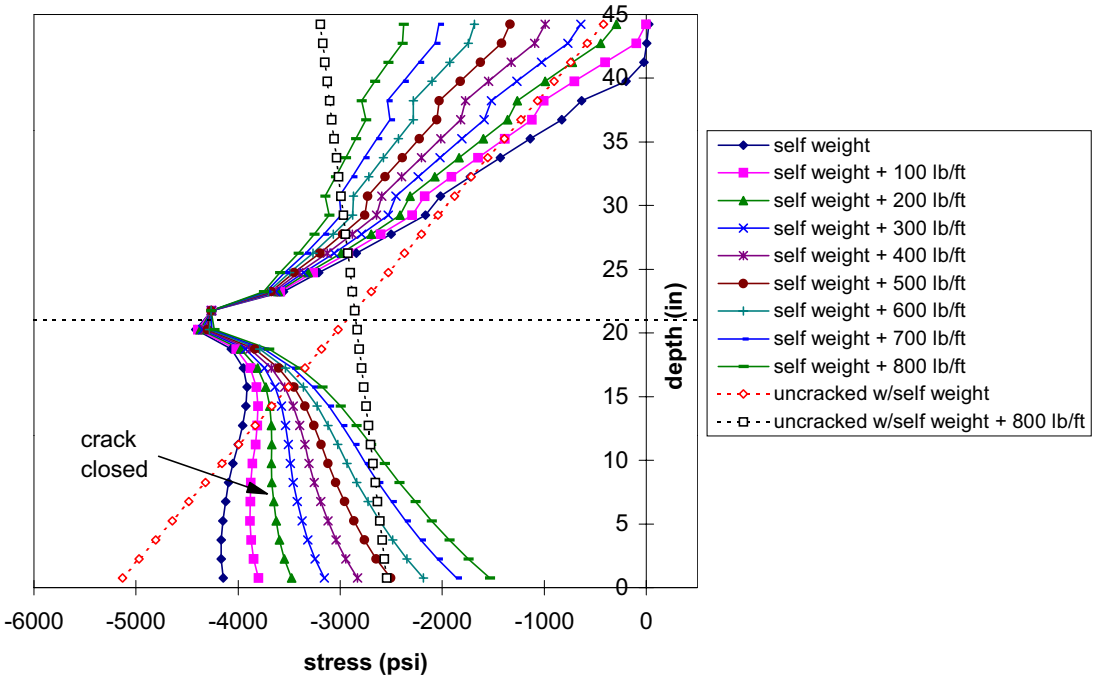

Figure 3.8 Stress Distribution at Midspan, Crack of 1/32" Width, 24" Depth

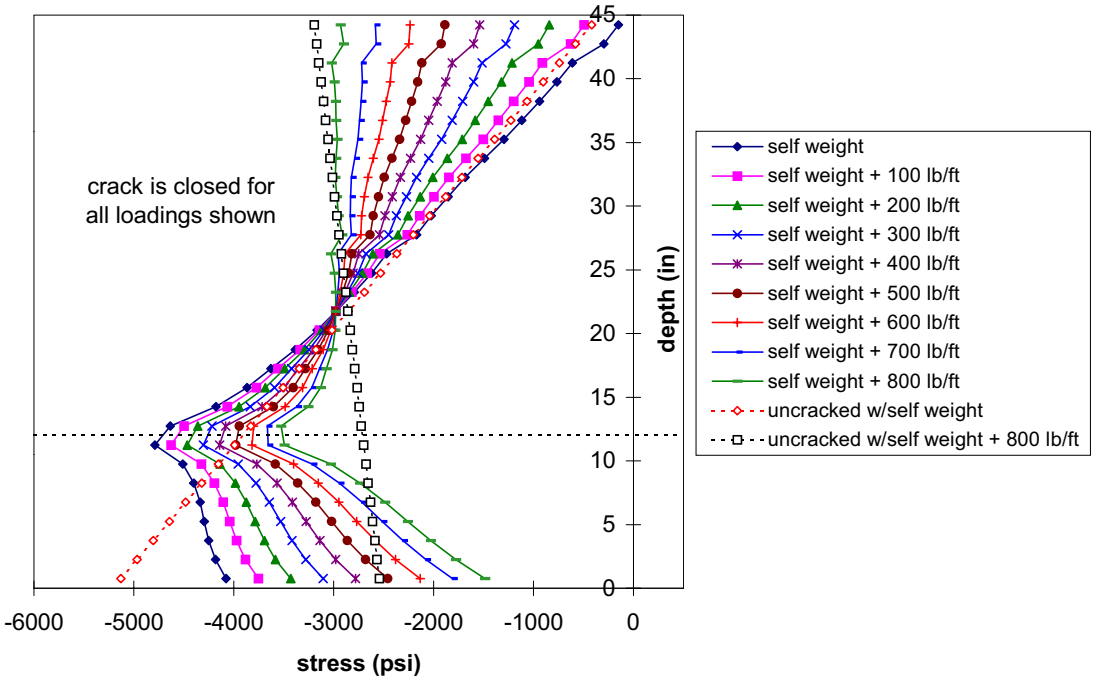

Figure 3.9 Stress Distribution at Midspan, Crack of 1/32" Width, 33" Depth

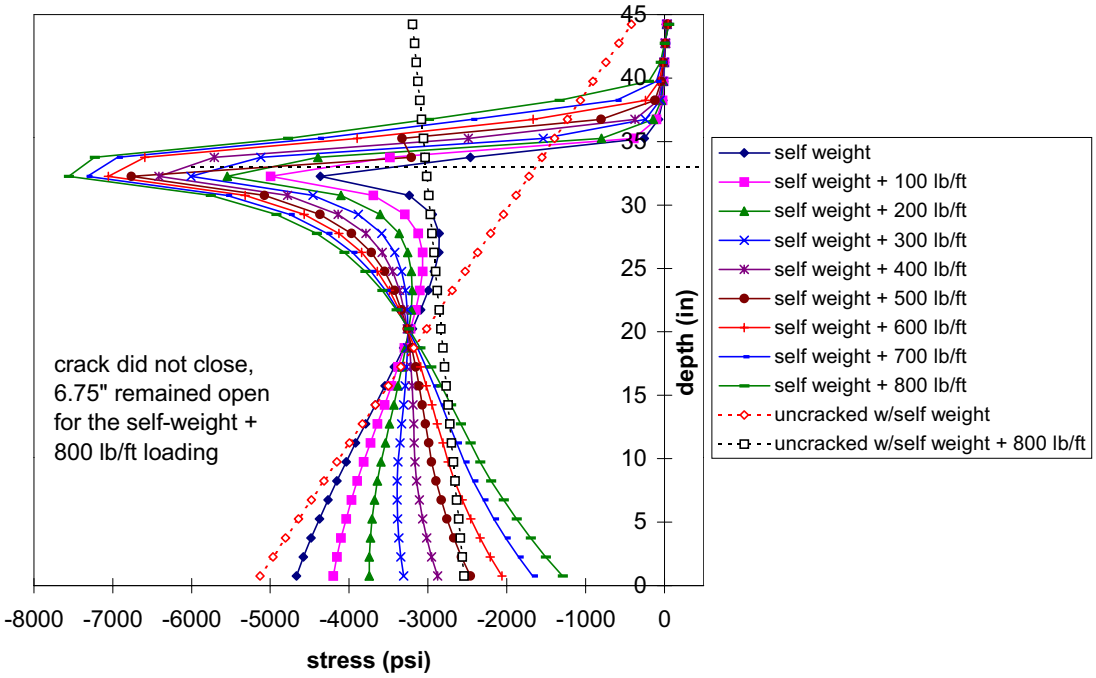

Figure 3.10 Stress Distribution at Midspan, Crack of 1/16" Width, 12" Depth

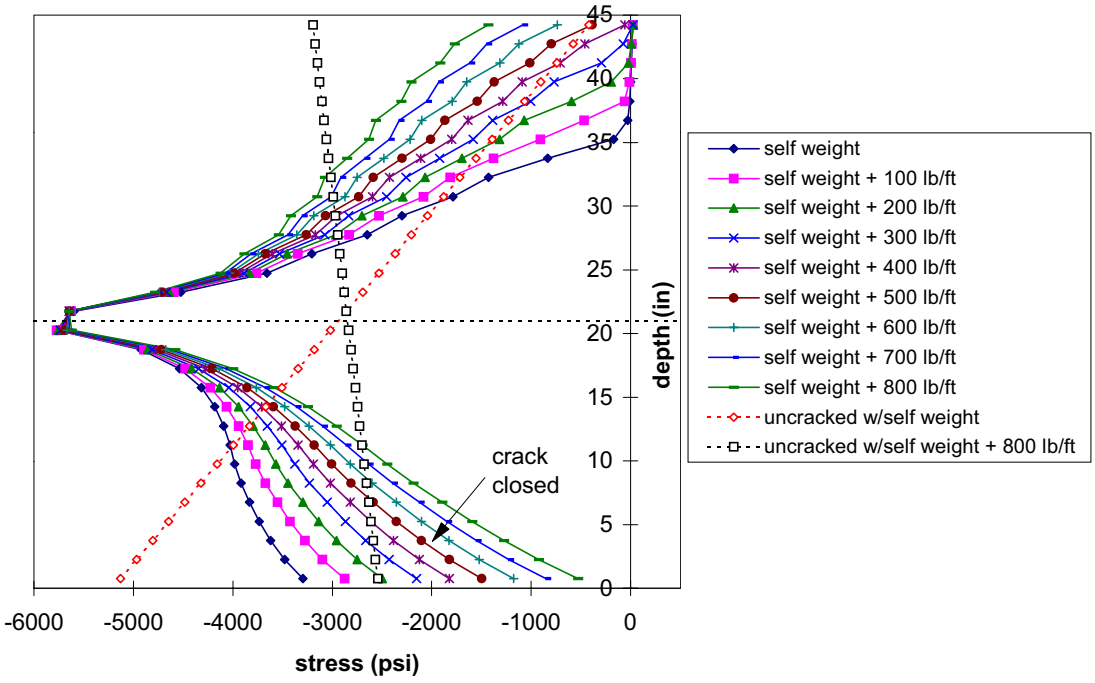

Figure 3.11 Stress Distribution at Midspan, Crack of 1/16" Width, 24" Depth

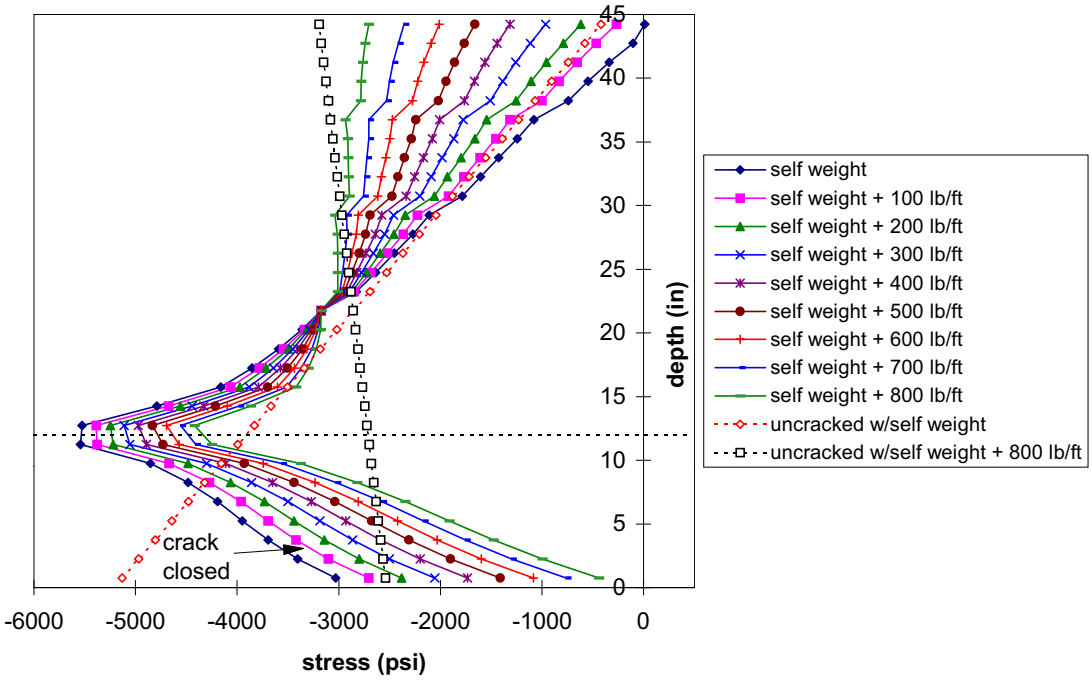

Figure 3.12 Stress Distribution at Midspan, Crack of 1/16" Width, 33" Depth

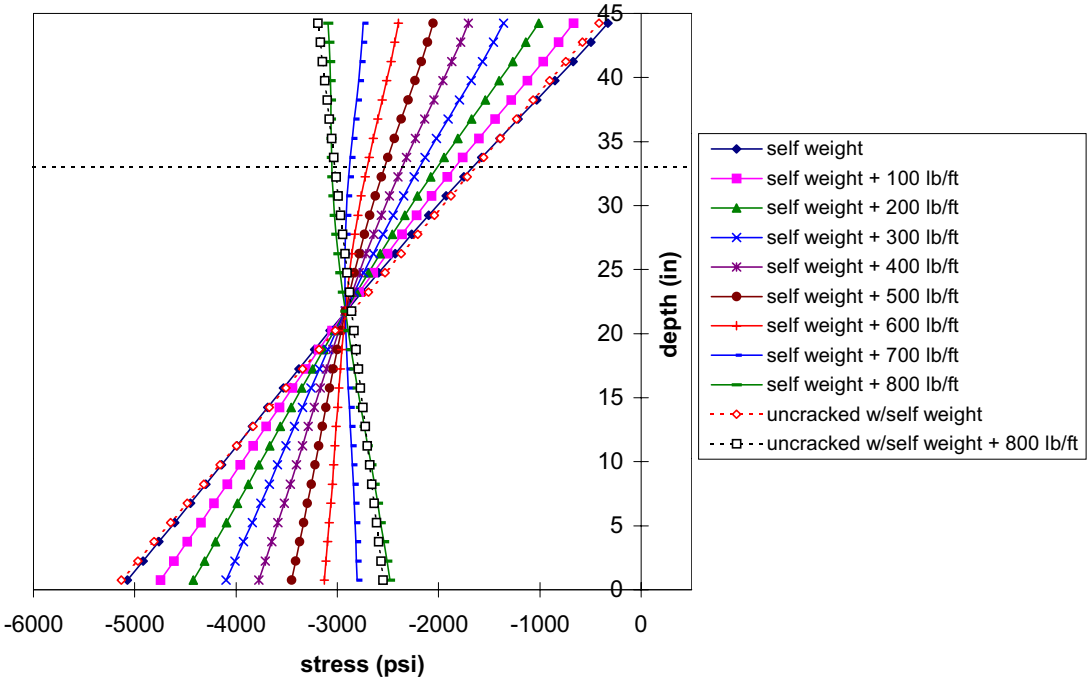

Figure 3.13 Stress Distribution 2 Feet Away from Midspan, Crack of 1/100" Width, 12" Depth

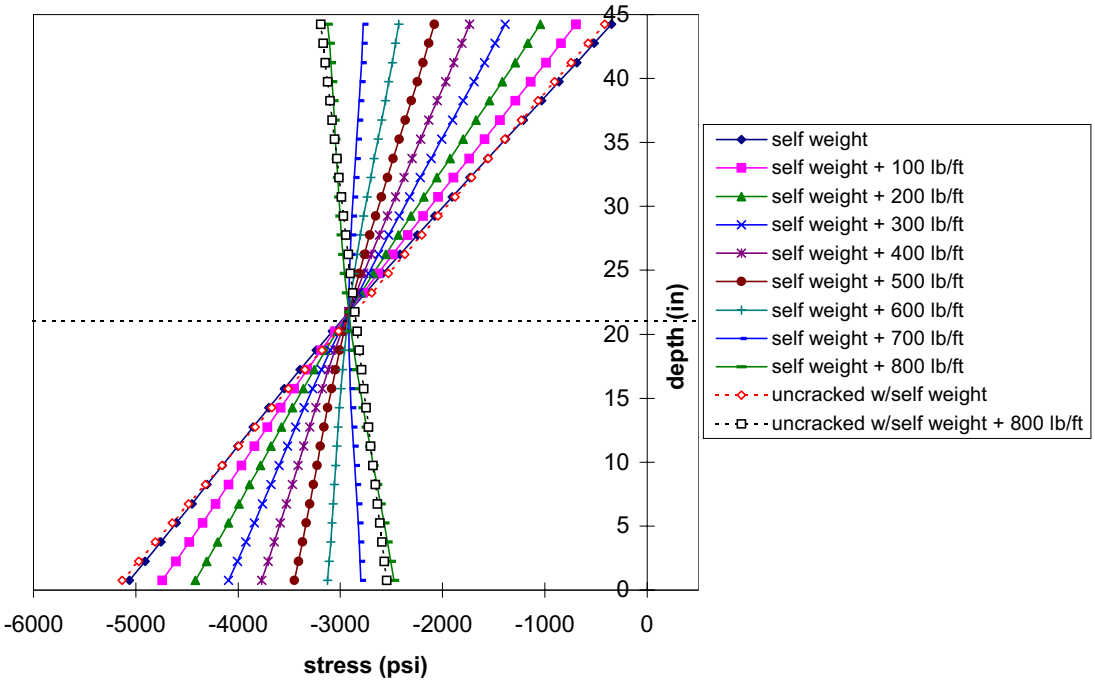

Figure 3.14 Stress Distribution 2 Feet Away from Midspan, Crack of 1/100" Width, 24" Depth

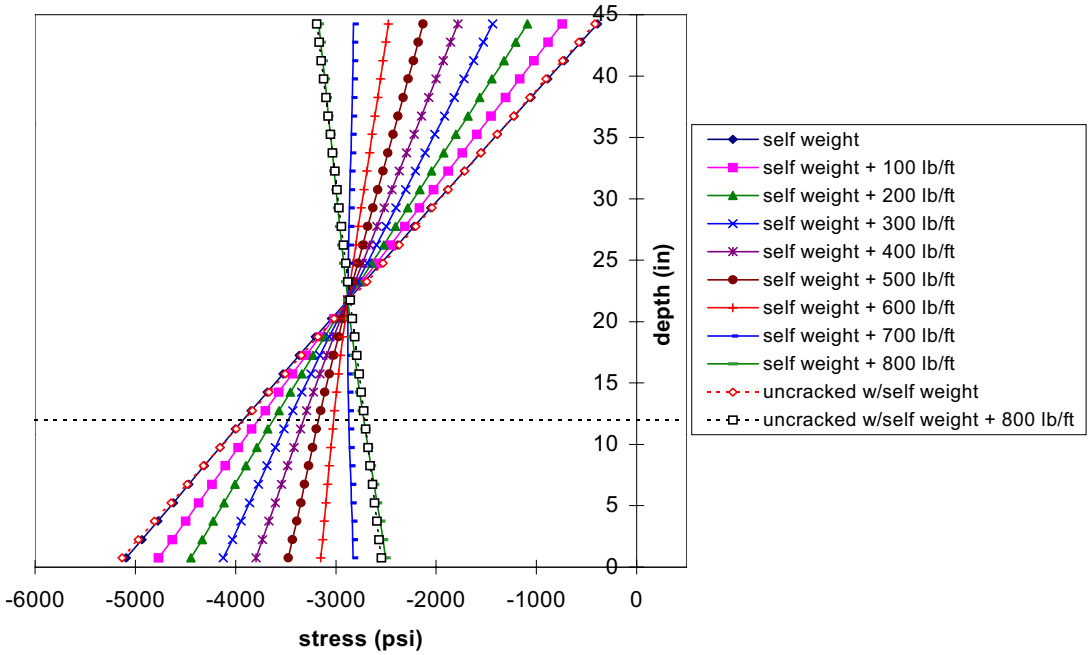

Figure 3.15 Stress Distribution 2 Feet Away from Midspan, Crack of 1/100" Width, 33" Depth

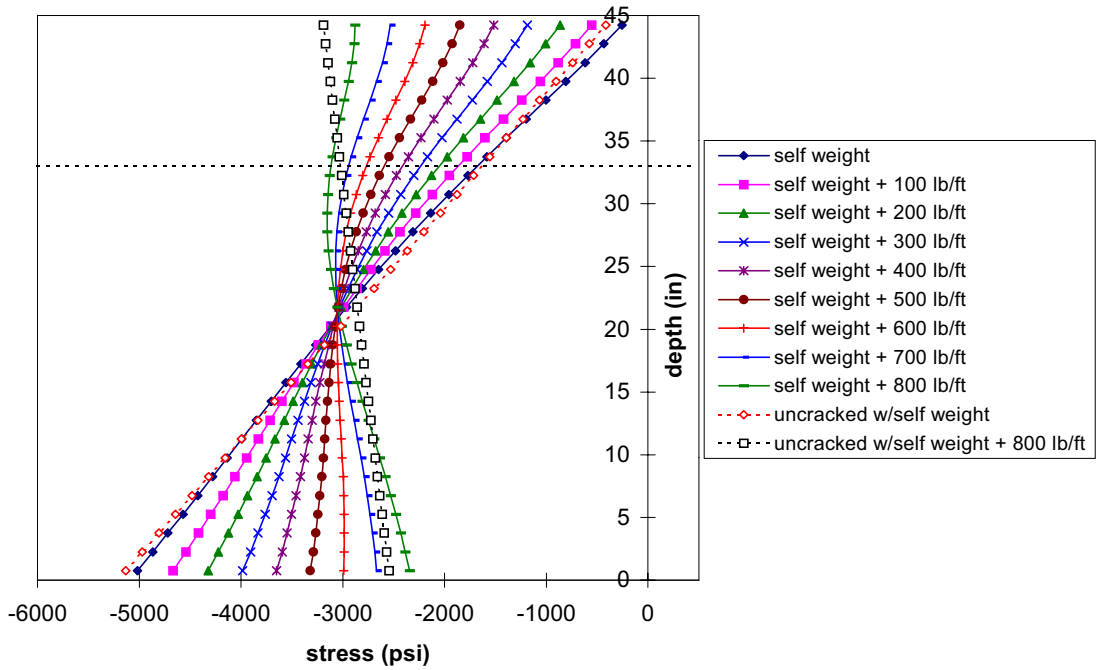

Figure 3.16 Stress Distribution 2 Feet Away from Midspan, Crack of 1/32" Width, 12" Depth

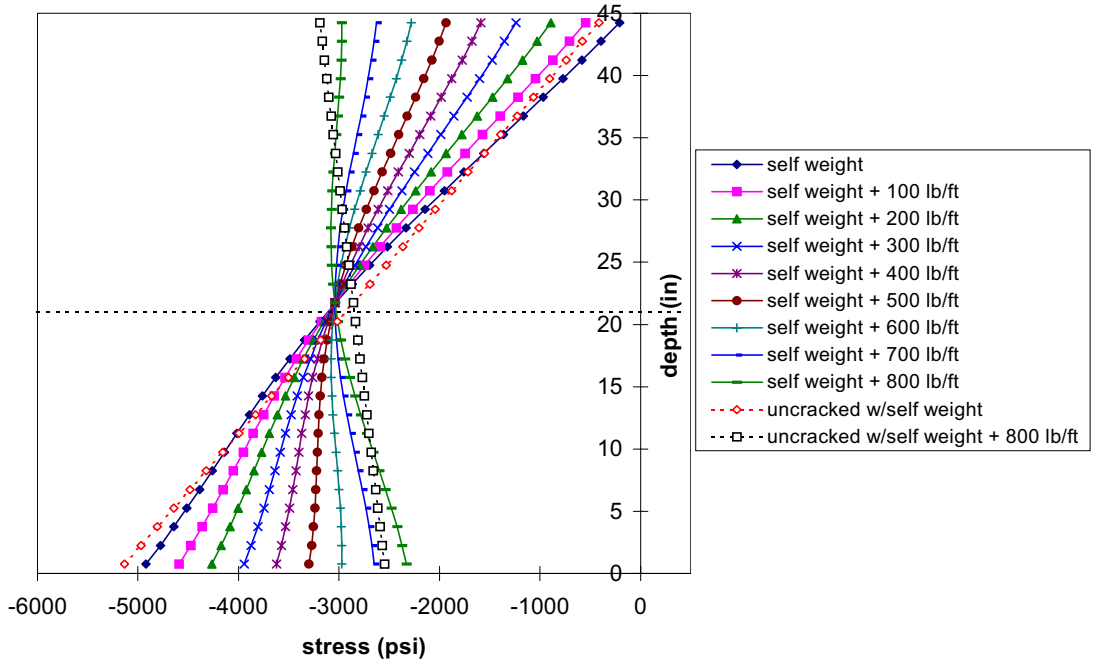

Figure 3.17 Stress Distribution 2 Feet Away from Midspan, Crack of 1/32" Width, 24" Depth

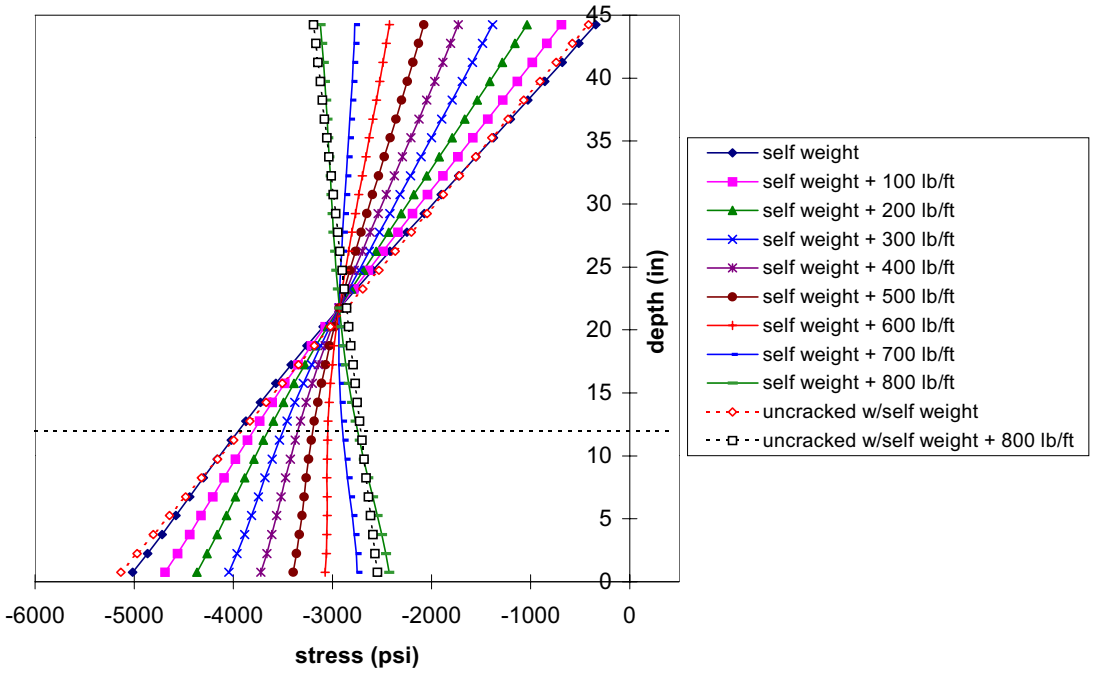

Figure 3.18 Stress Distribution 2 Feet Away from Midspan, Crack of 1/32" Width, 33" Depth

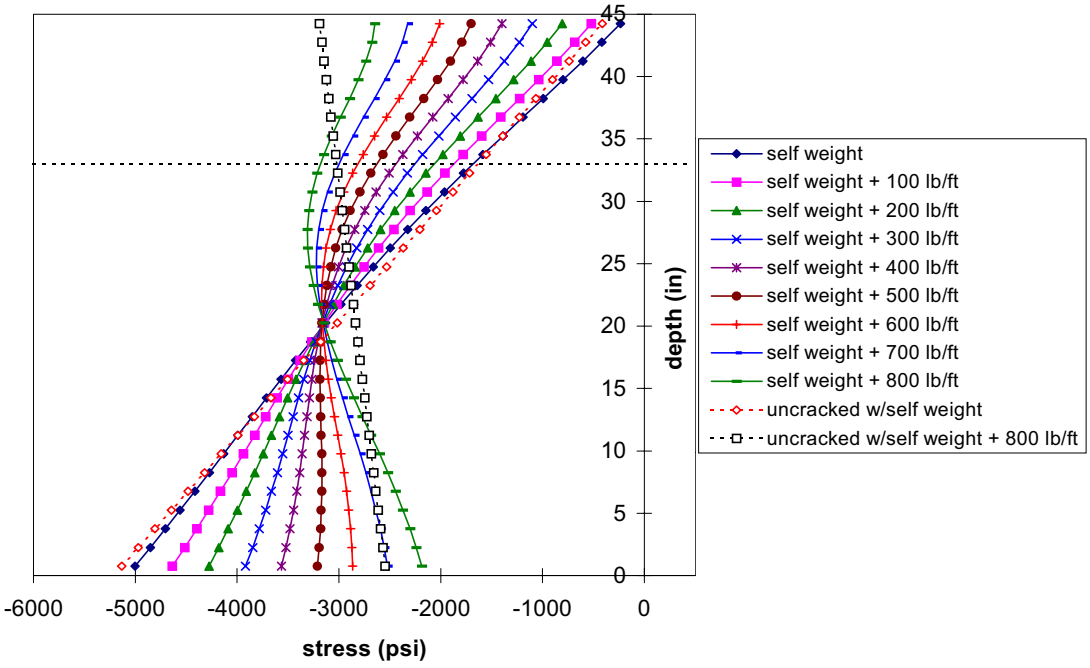

Figure 3.19 Stress Distribution 2 Feet Away from Midspan, Crack of 1/16" Width, 12" Depth

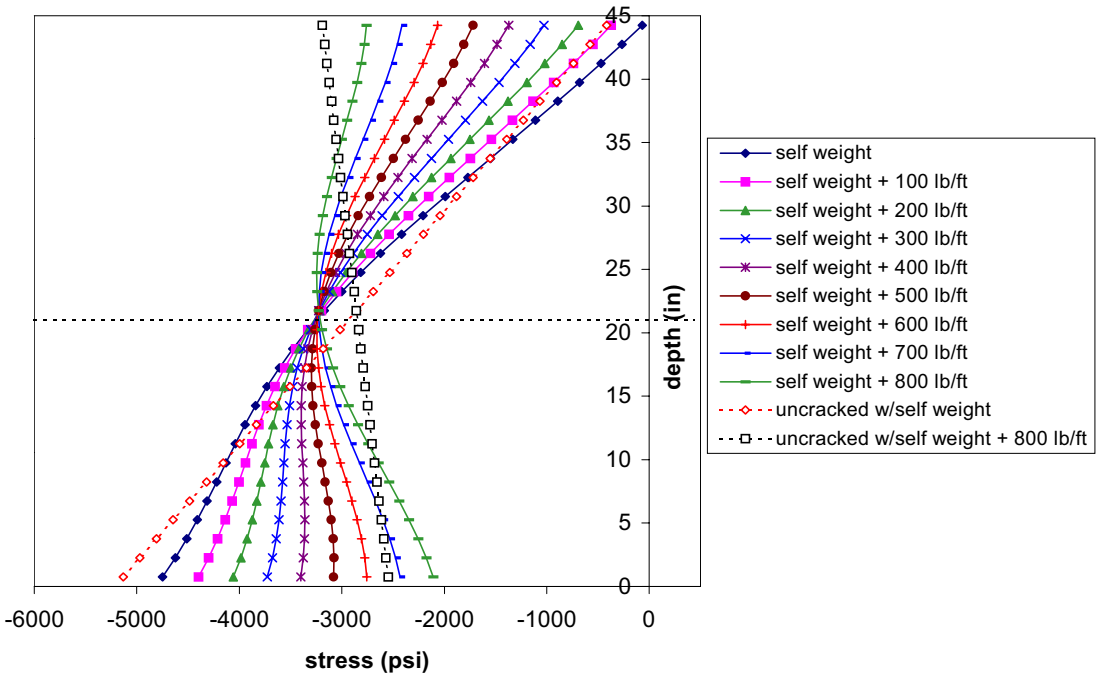

Figure 3.20 Stress Distribution 2 Feet Away from Midspan, Crack of 1/16" Width 24" Depth

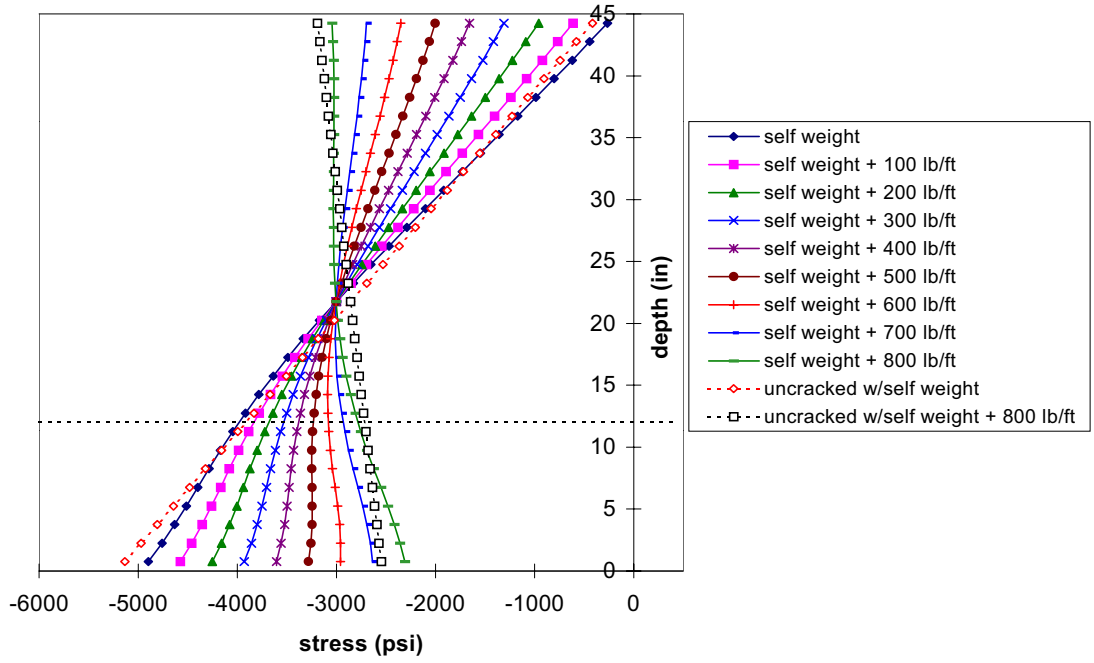

Figure 3.21 Stress Distribution 2 Feet Away from Midspan, Crack of 1/16" Width, 33" Depth

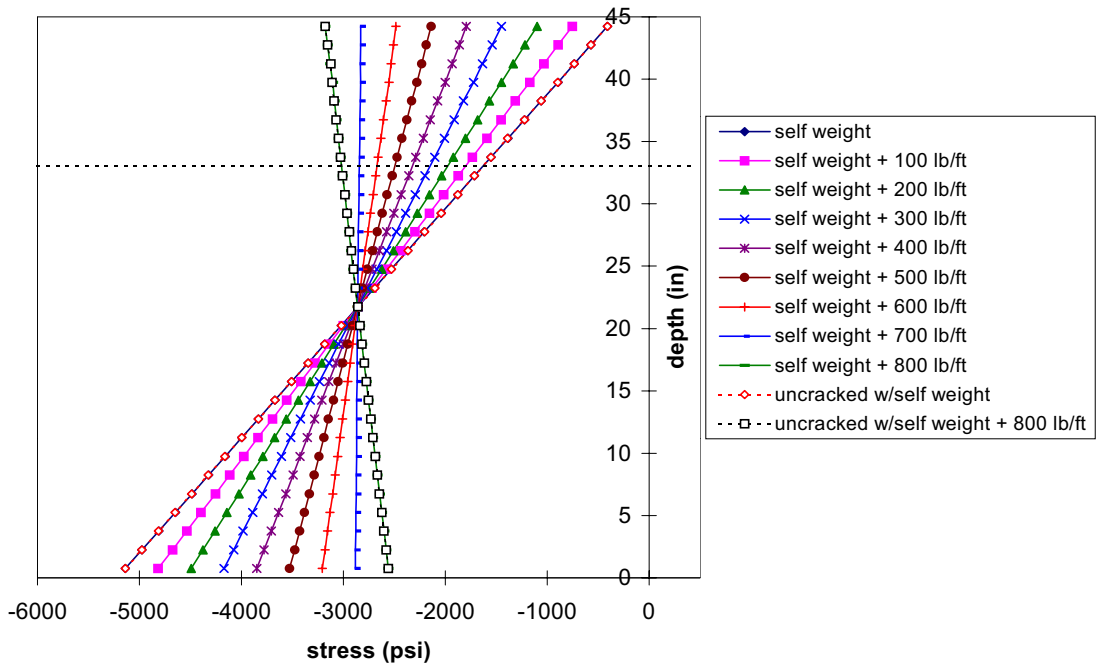

Figure 3.22 Stress Distribution 4 Feet Away from Midspan, Crack of 1/100" Width, 12" Depth

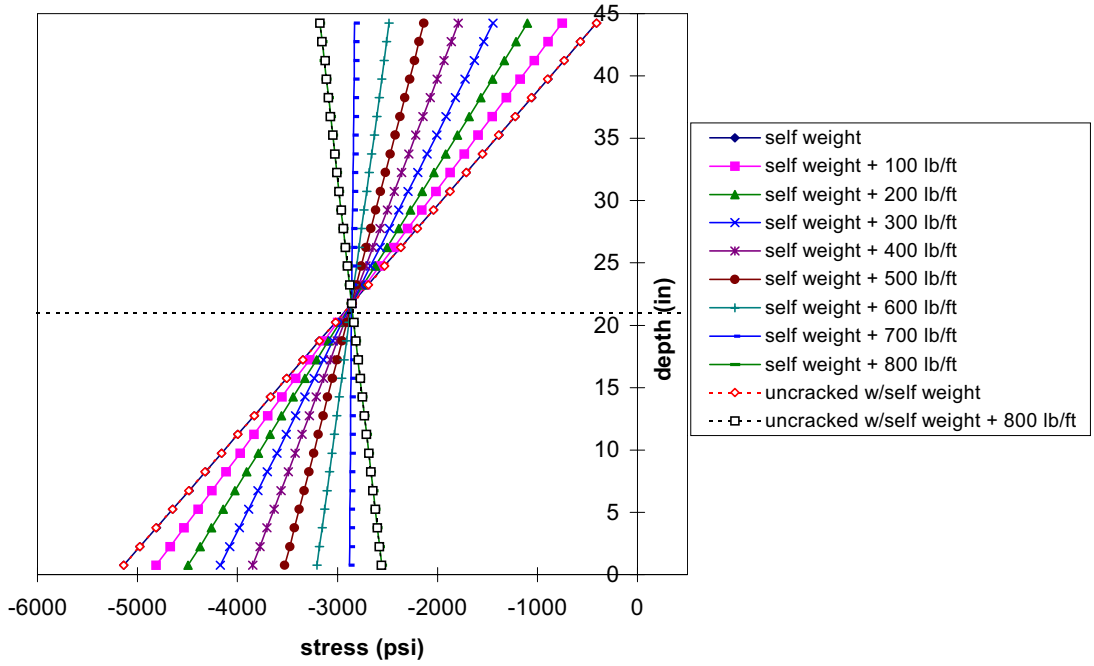

Figure 3.23 Stress Distribution 4 Feet Away from Midspan, Crack of 1/100" Width, 24" Depth

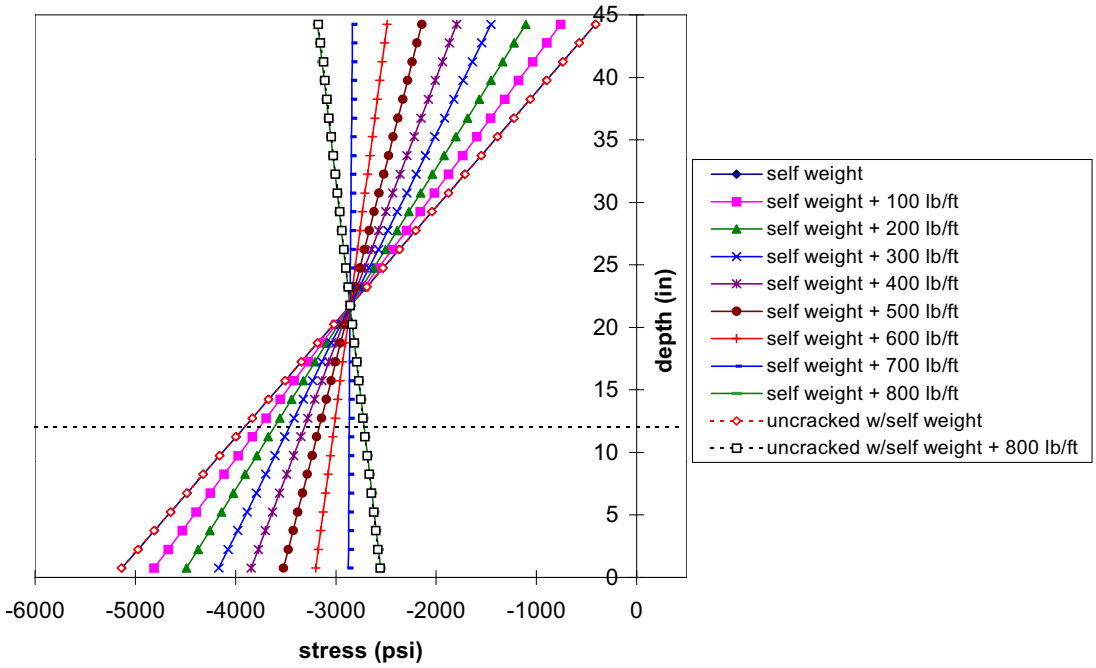

Figure 3.24 Stress Distribution 4 Feet Away from Midspan, Crack of 1/100" Width, 33" Depth

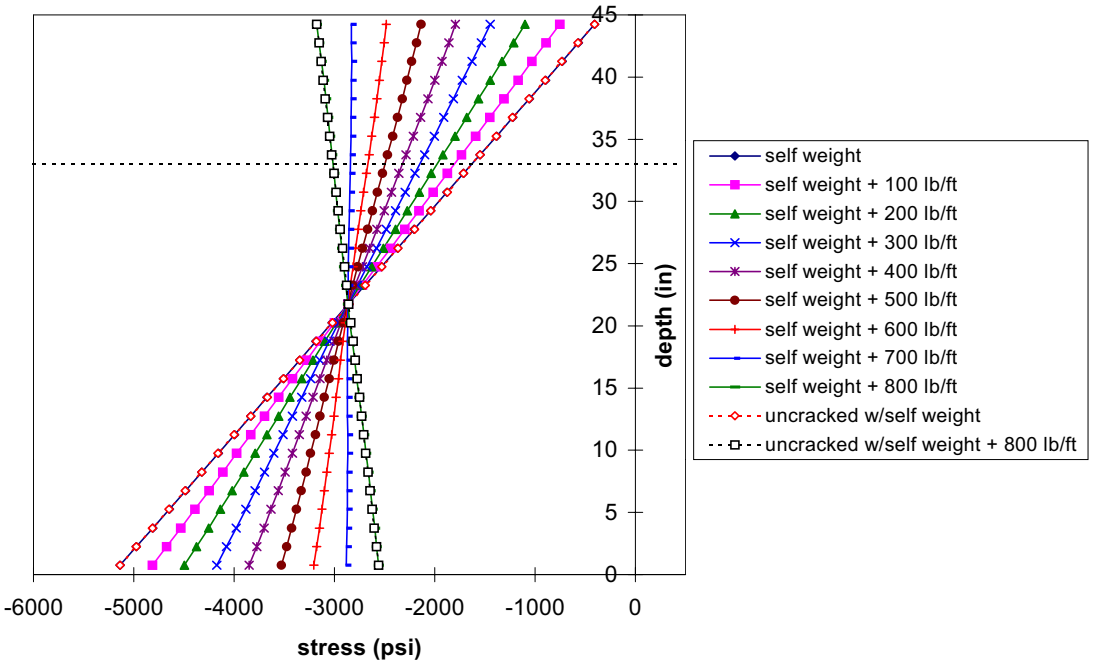

Figure 3.25 Stress Distribution 4 Feet Away from Midspan, Crack of 1/32" Width, 12" Depth

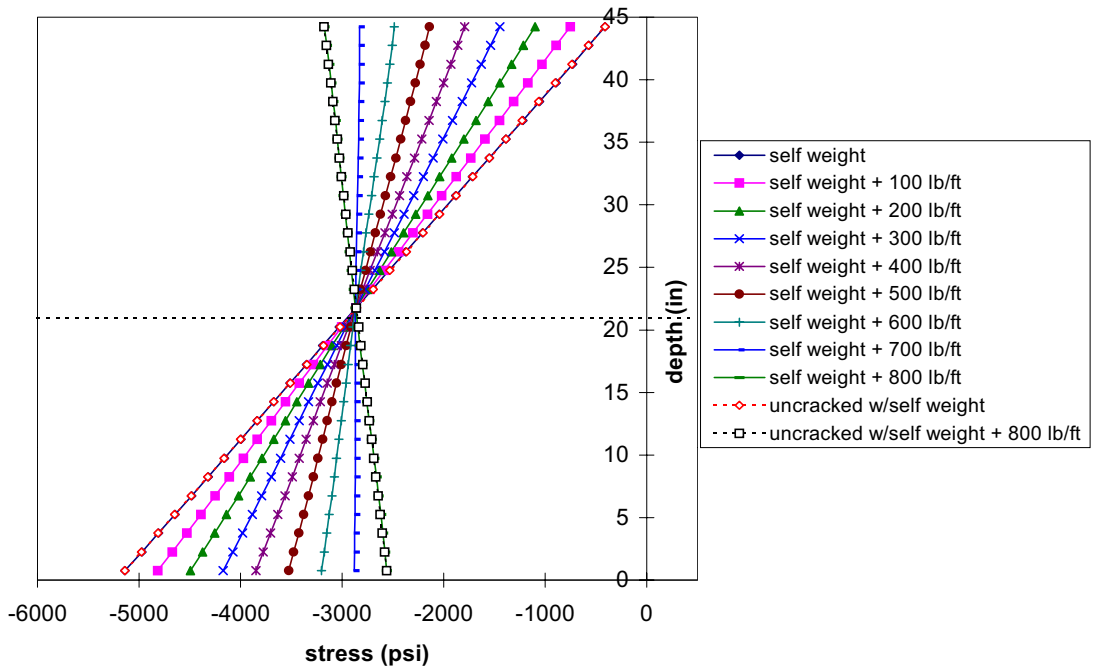

Figure 3.26 Stress Distribution 4 Feet Away from Midspan, Crack of 1/32" Width, 24" Depth

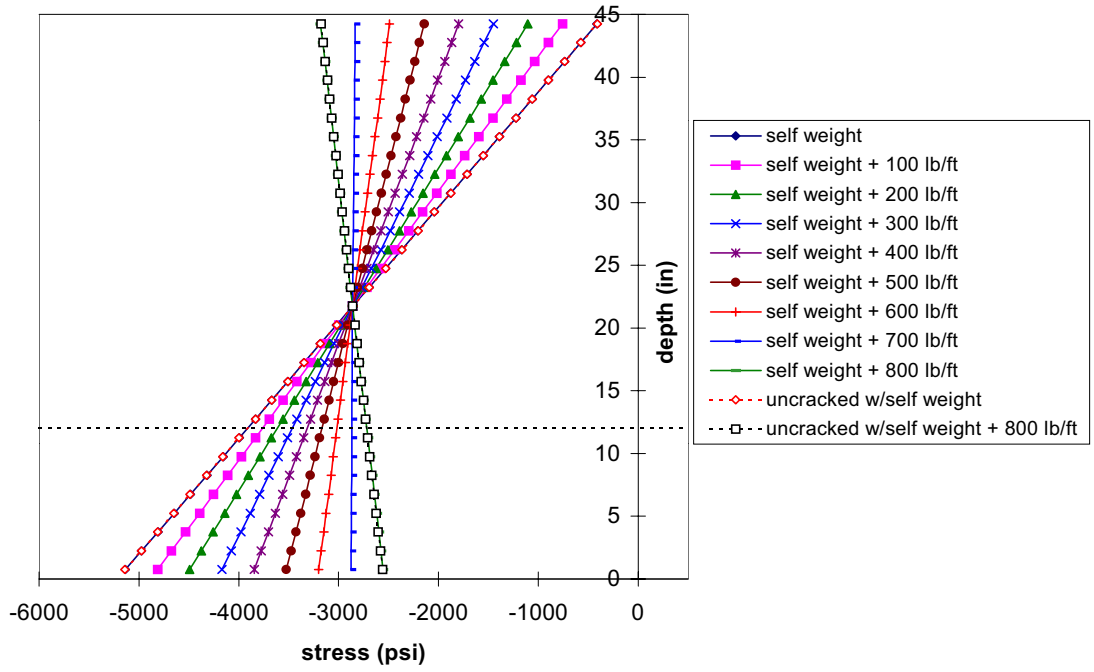

Figure 3.27 Stress Distribution 4 Feet Away from Midspan, Crack of 1/32" Width, 33" Depth

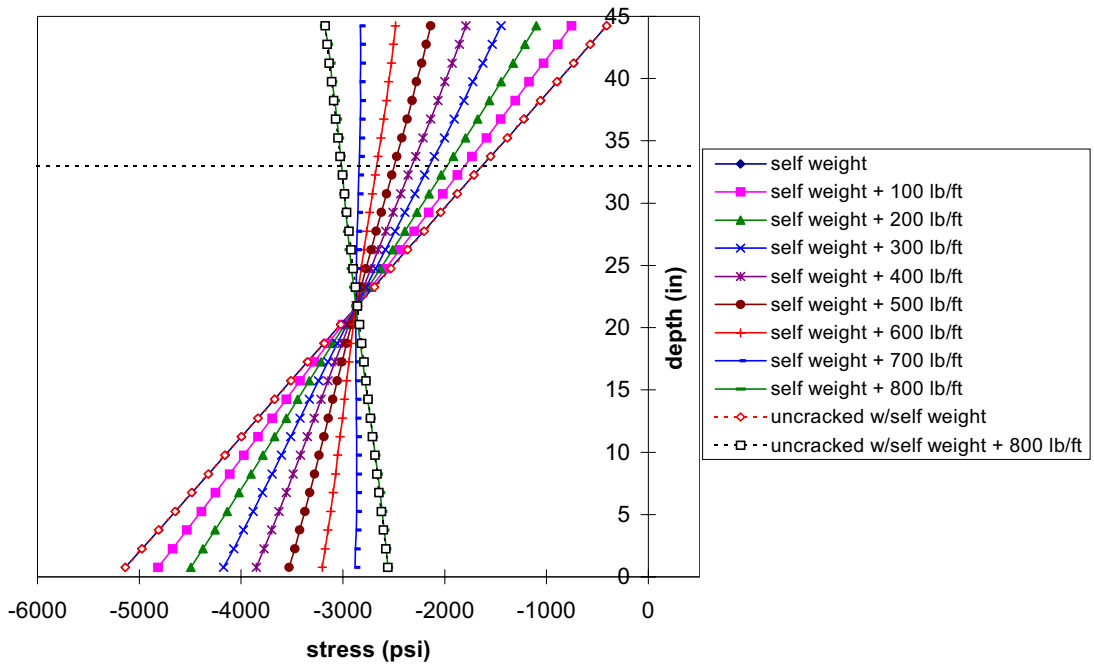

Figure 3.28 Stress Distribution 4 Feet Away from Midspan, Crack of 1/16" Width, 12" Depth

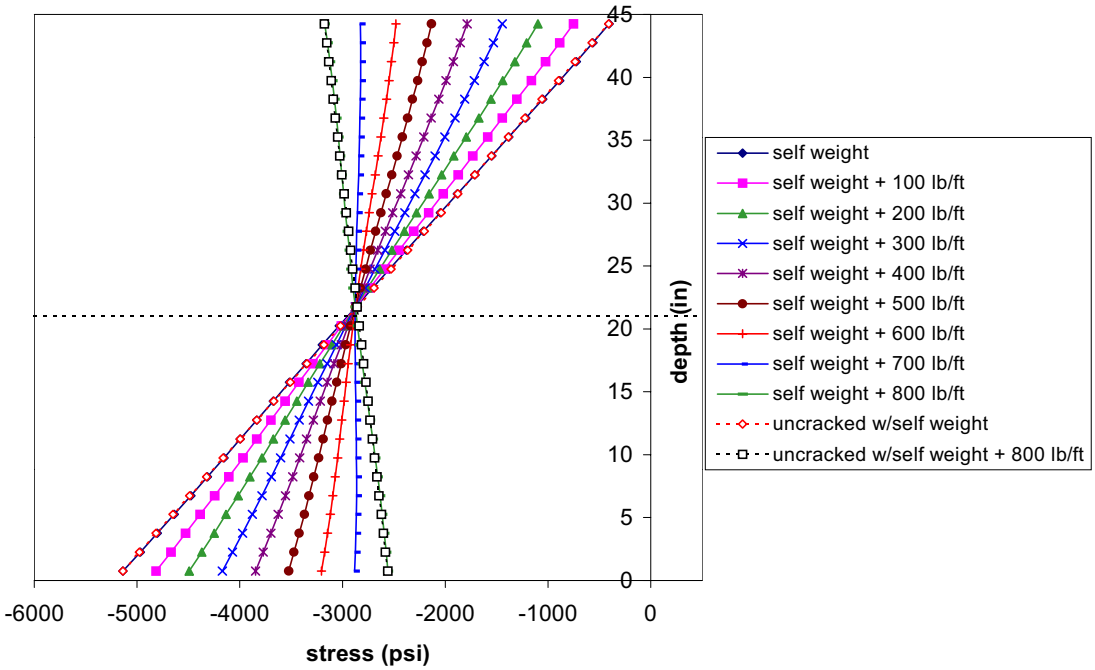

Figure 3.29 Stress Distribution 4 Feet Away from Midspan, Crack of 1/16" Width, 24" Depth

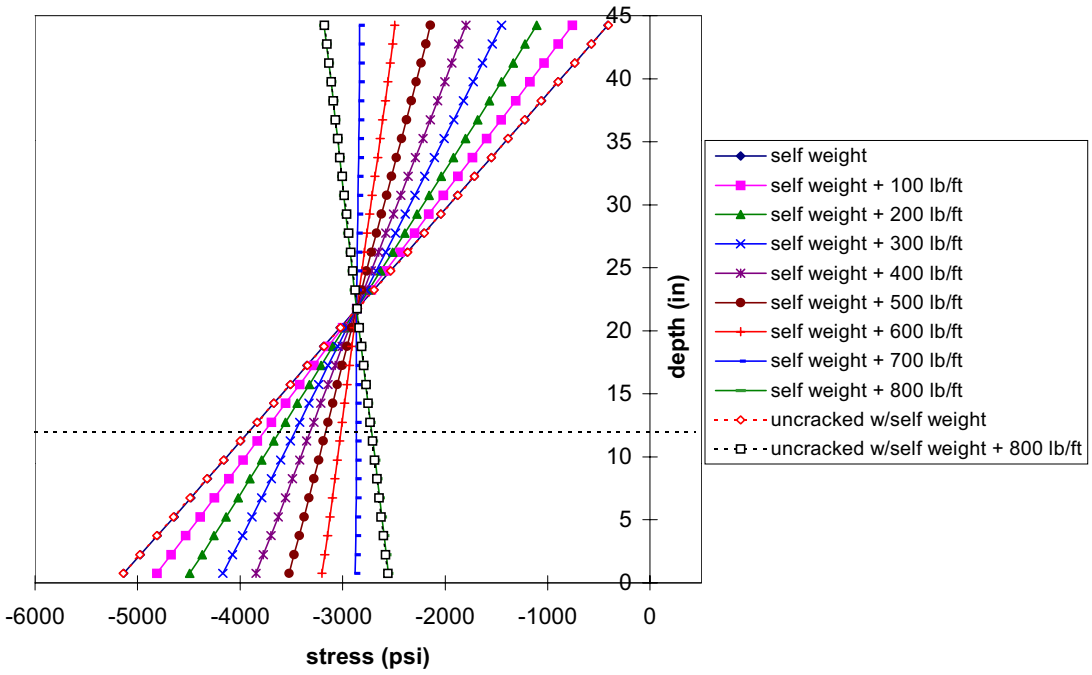

Figure 3.30 Stress Distribution 4 Feet Away from Midspan, Crack of 1/16" Width, 33" Depth

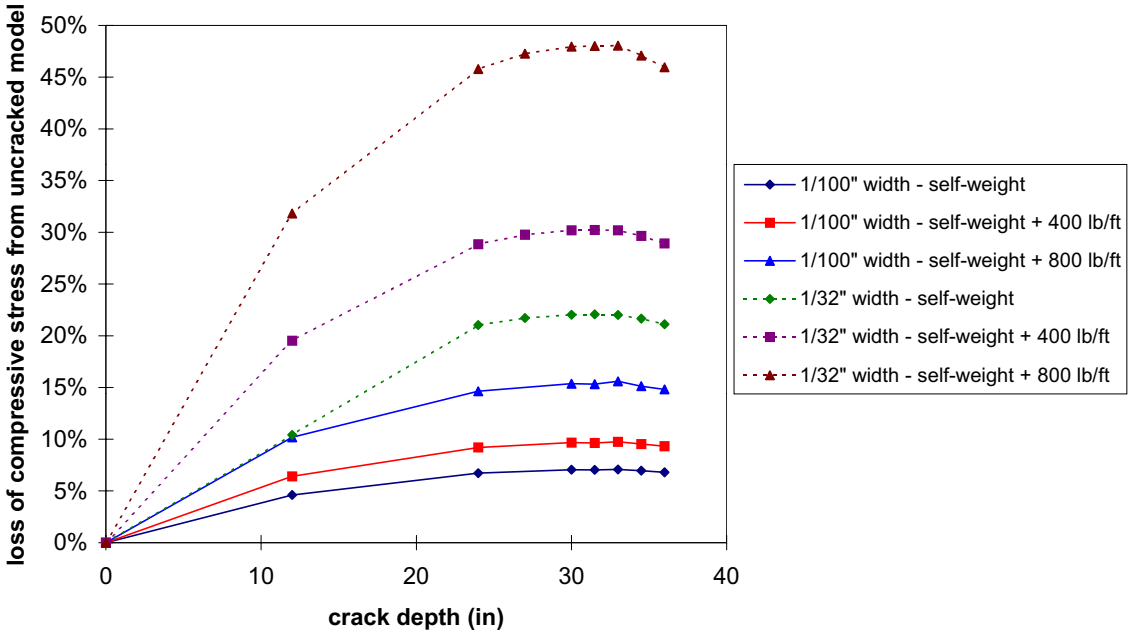

Figure 3.31 Crack Depth Effect on Bottom Element Stress

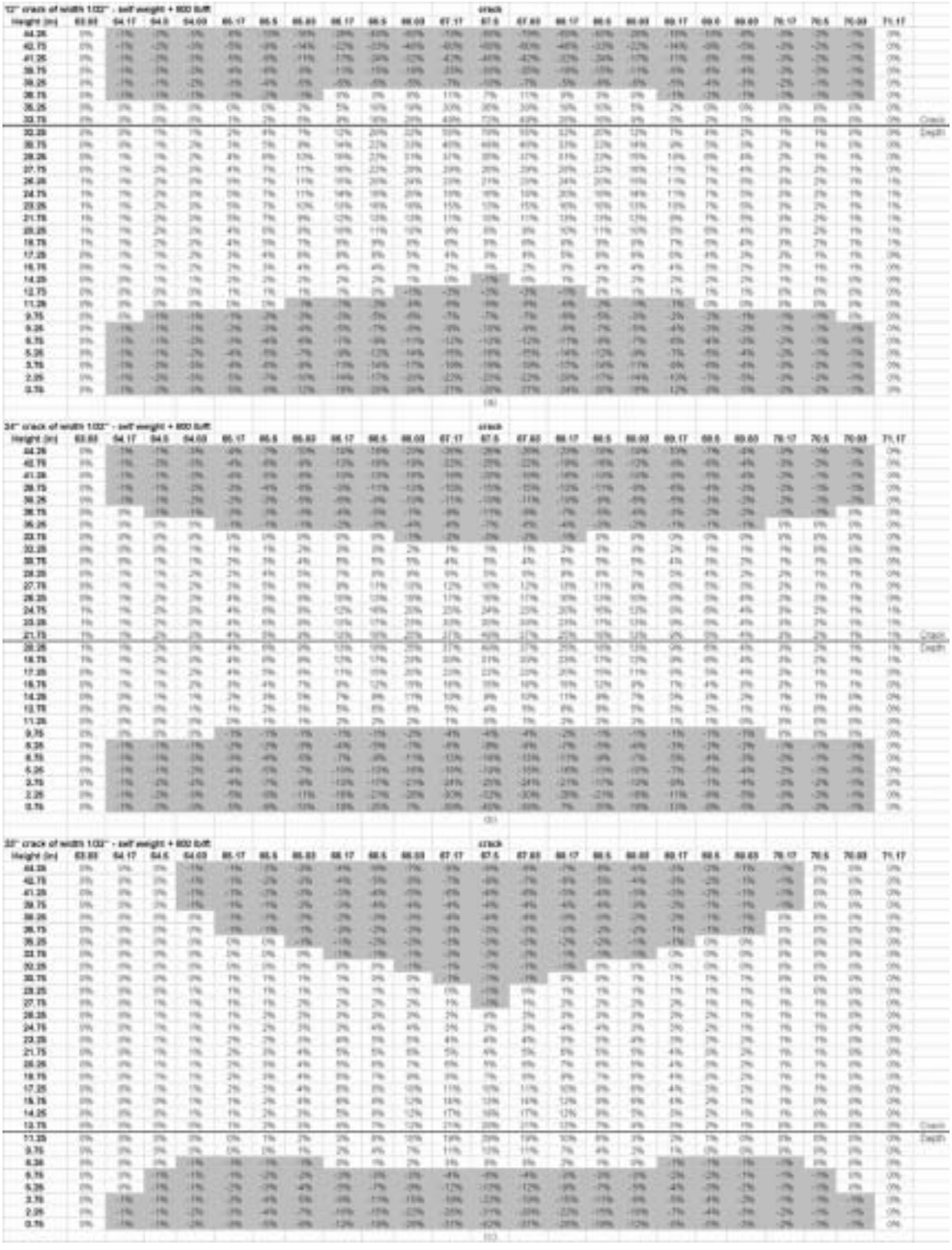

Figure 3.32 Crack Depth Effect

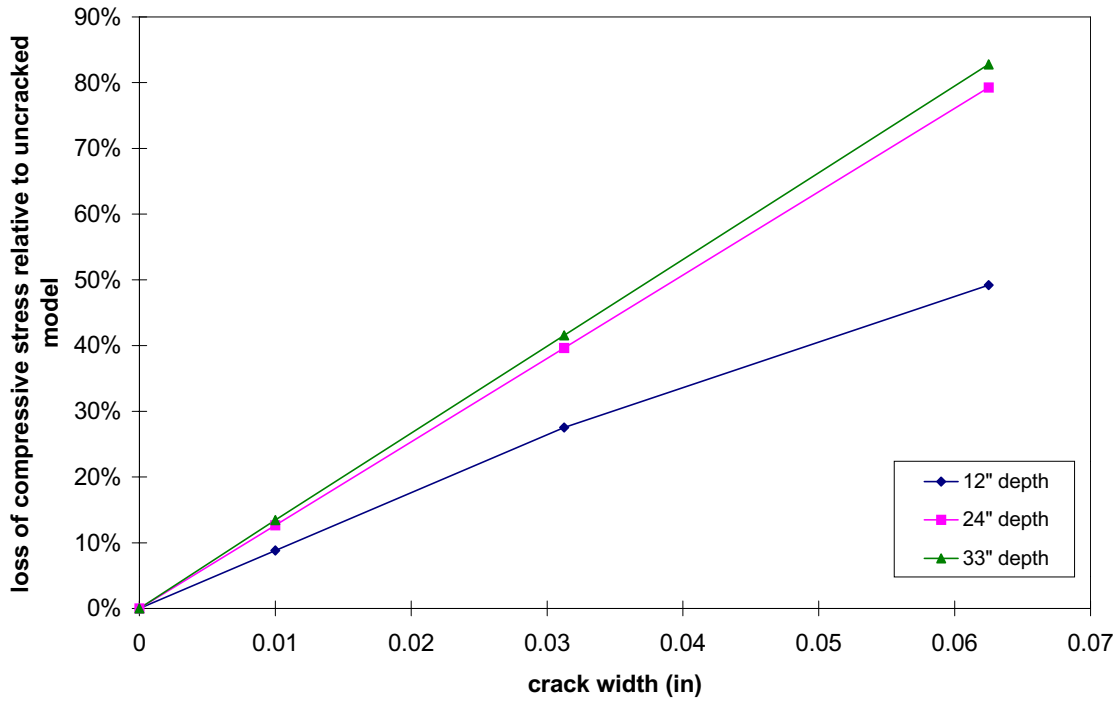

Figure 3.33 Crack Width Effect on Bottom Element Stress - self-weight + 800 lb/ft load

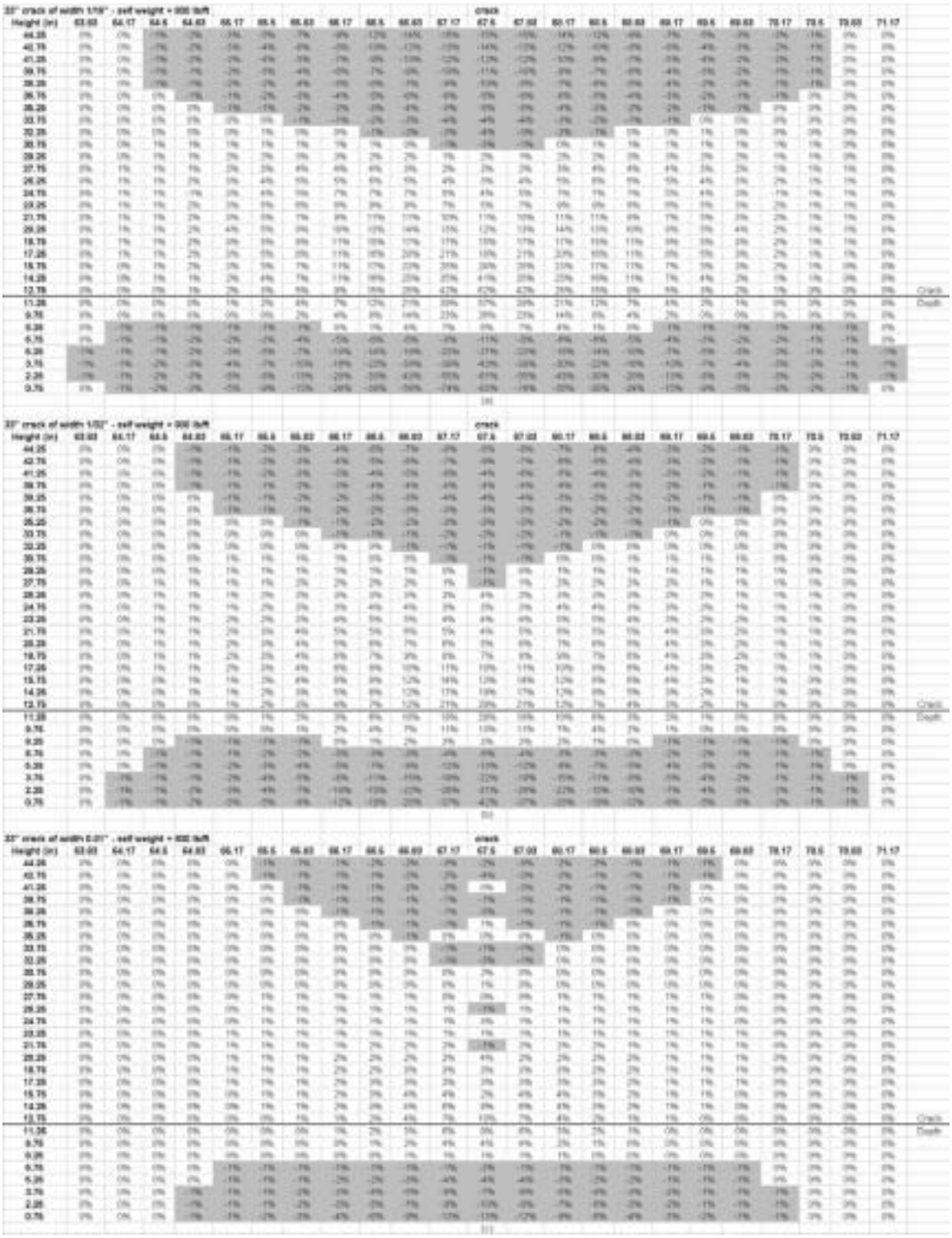

Figure 3.34 Crack Width Effect

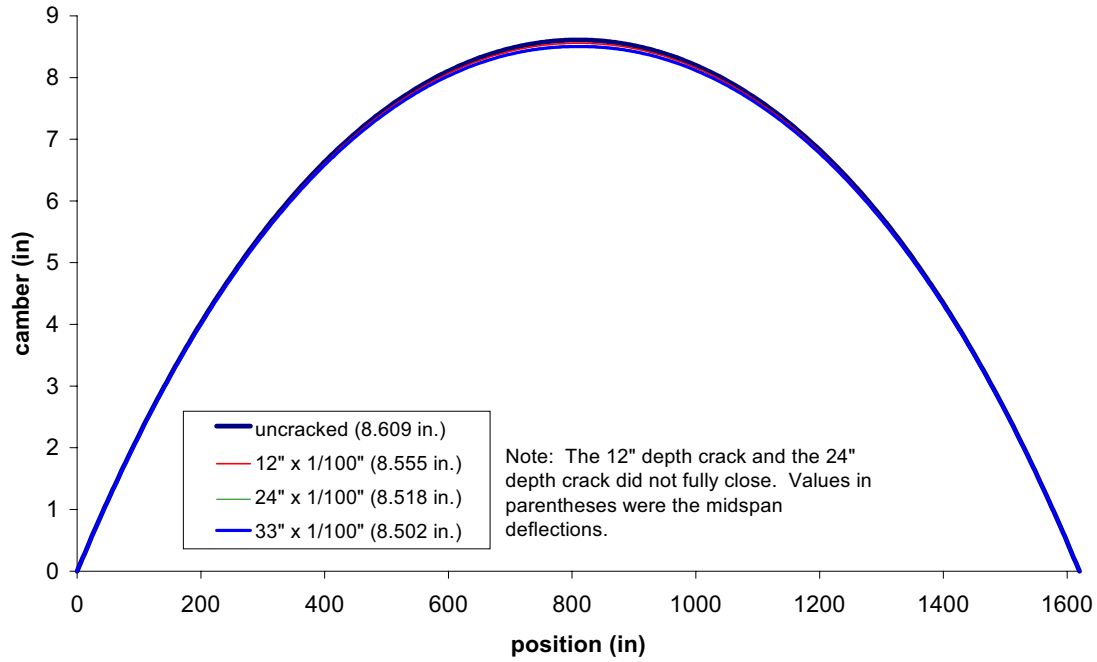

Figure 3.35 Camber for 1/100" Width Cracks Relative to Uncracked Case - self-weight load

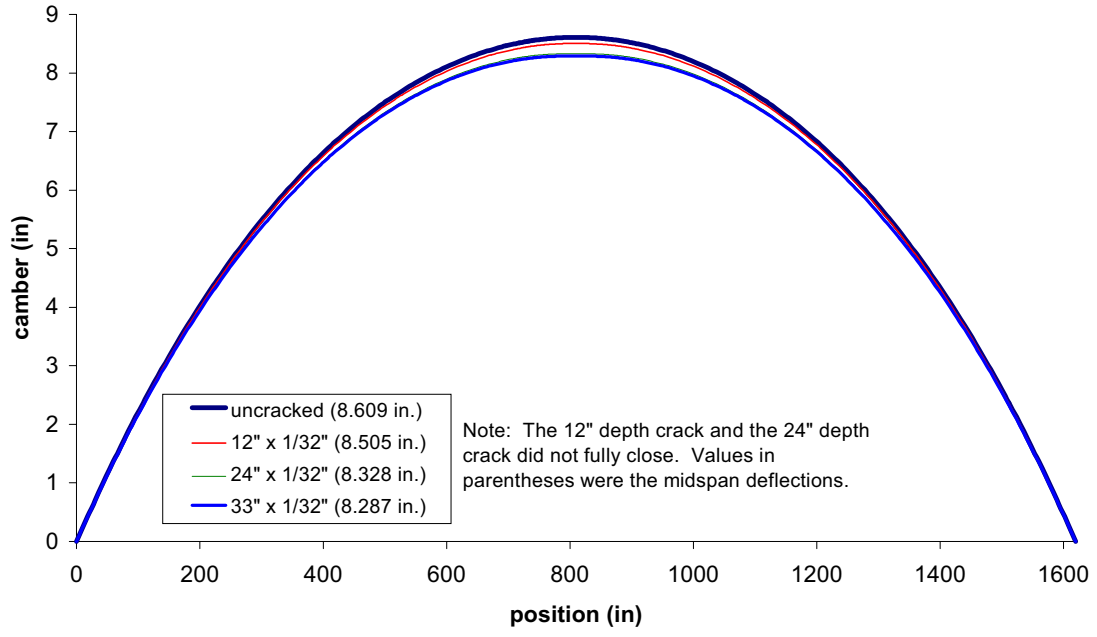

Figure 3.36 Camber for 1/32" Width Cracks Relative to Uncracked Case - self-weight load

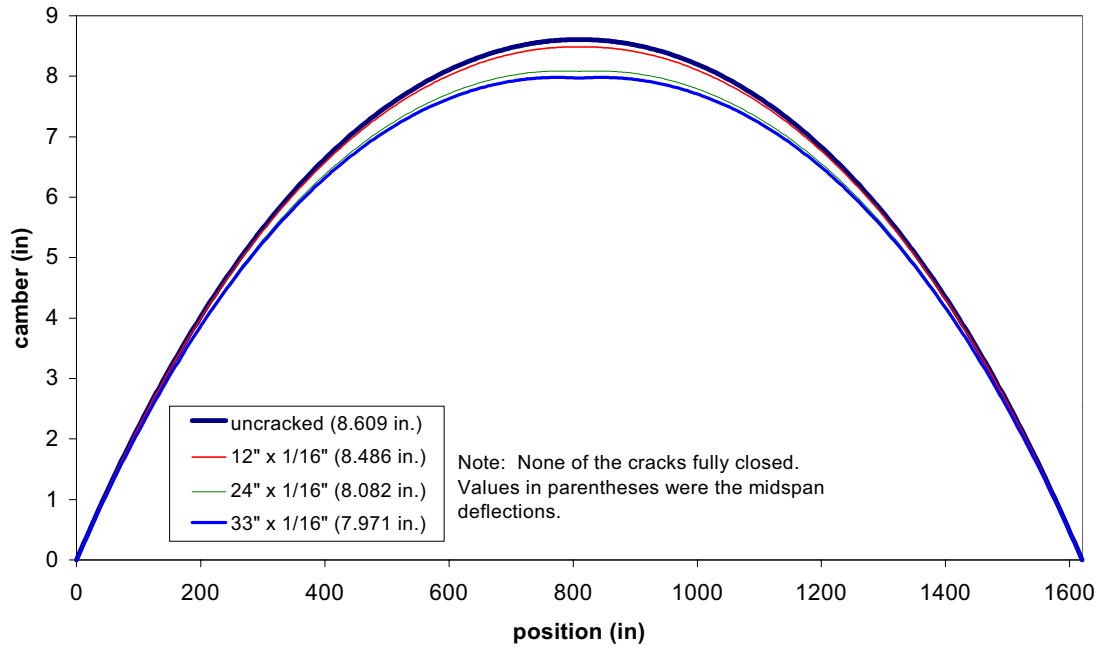

Figure 3.37 Camber for 1/16" Width Cracks Relative to Uncracked Case - self-weight load

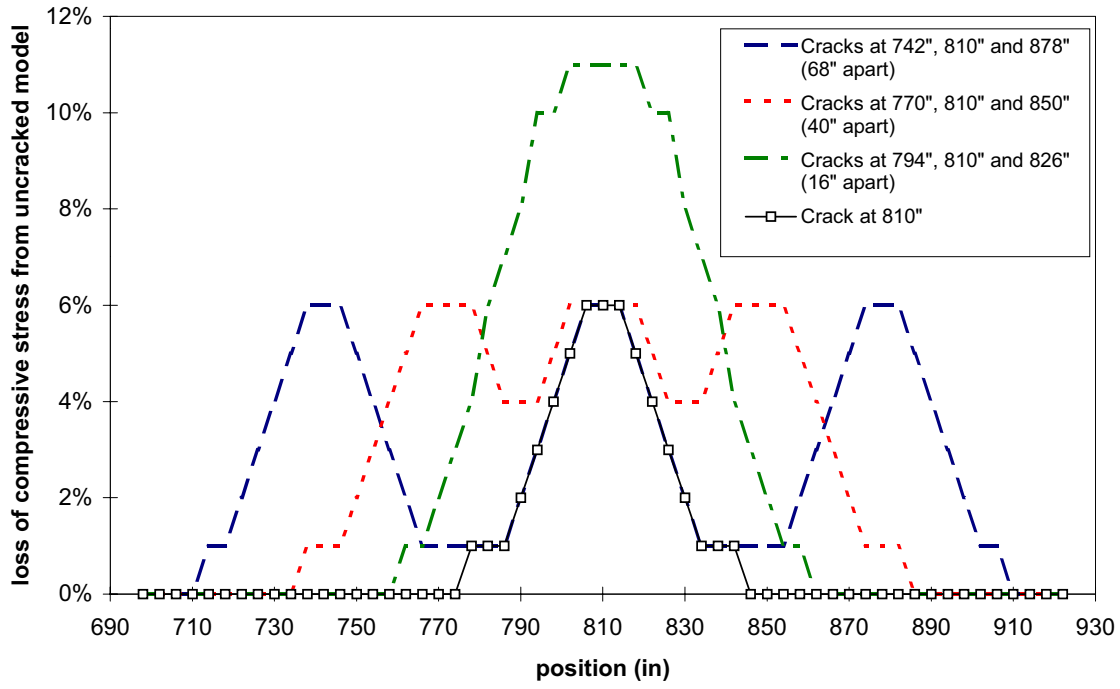

Figure 3.38 Bottom Element Stress Change Relative to Uncracked Case for 24" Cracks of 1/100" Width

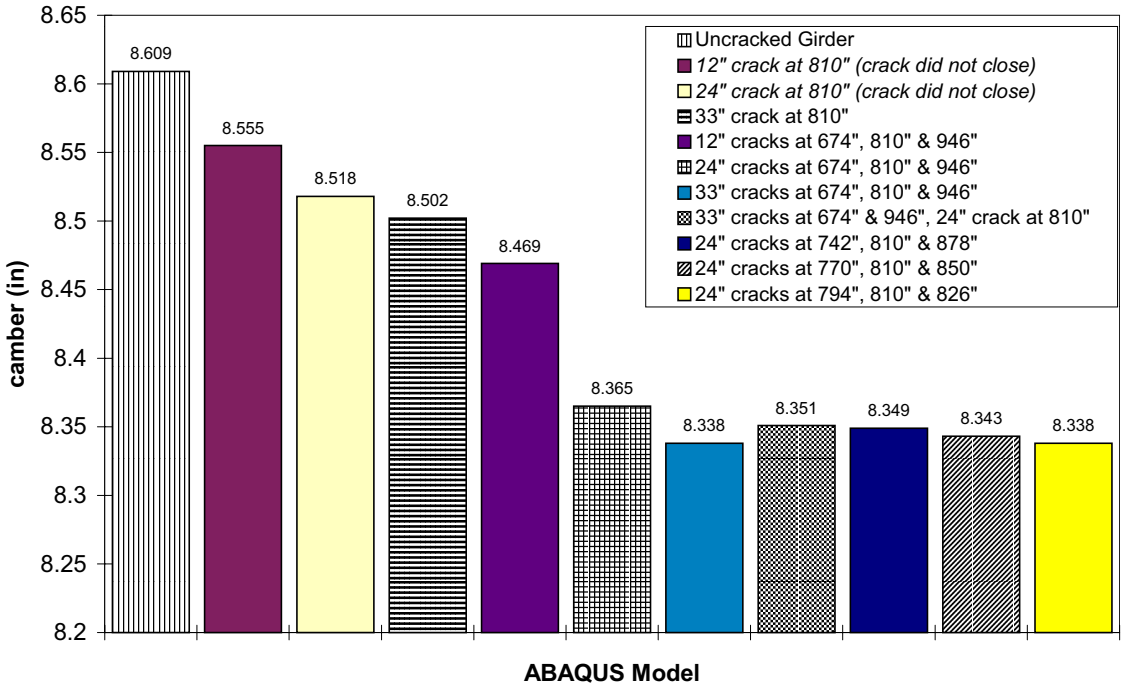

Figure 3.39 Midspan Camber

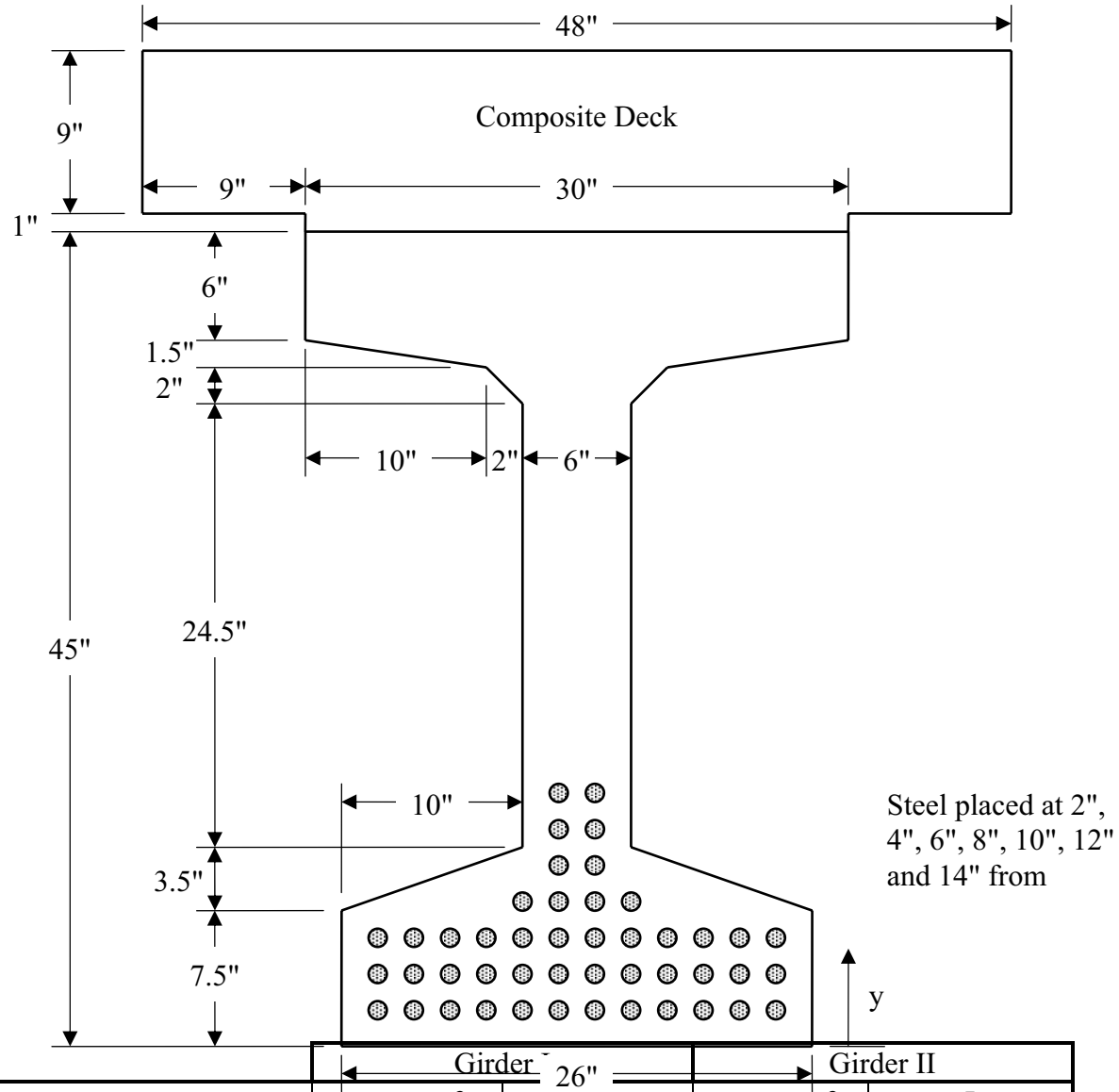

	Girder I		Girder II	
	center of gravity y[1]	I	center of gravity y	I
steel	5.391 in.		5.391 in.	
net section	22.635 in.	163,977 in.^{4}	22.635 in.	163,977 in.^{4}
Initial				
transformed, non-composite	20.892 in.	182,410 in.^{4}	21.015 in.	181,109 in.^{4}
Flexural Crack Testing				
transformed, composite	31.733 in.	396,945 in.^{4}	31.602 in.	392,373 in.^{4}

[1] measured from the bottom fiber

Figure 4.1 Mn/DOT 45M Section at Midspan

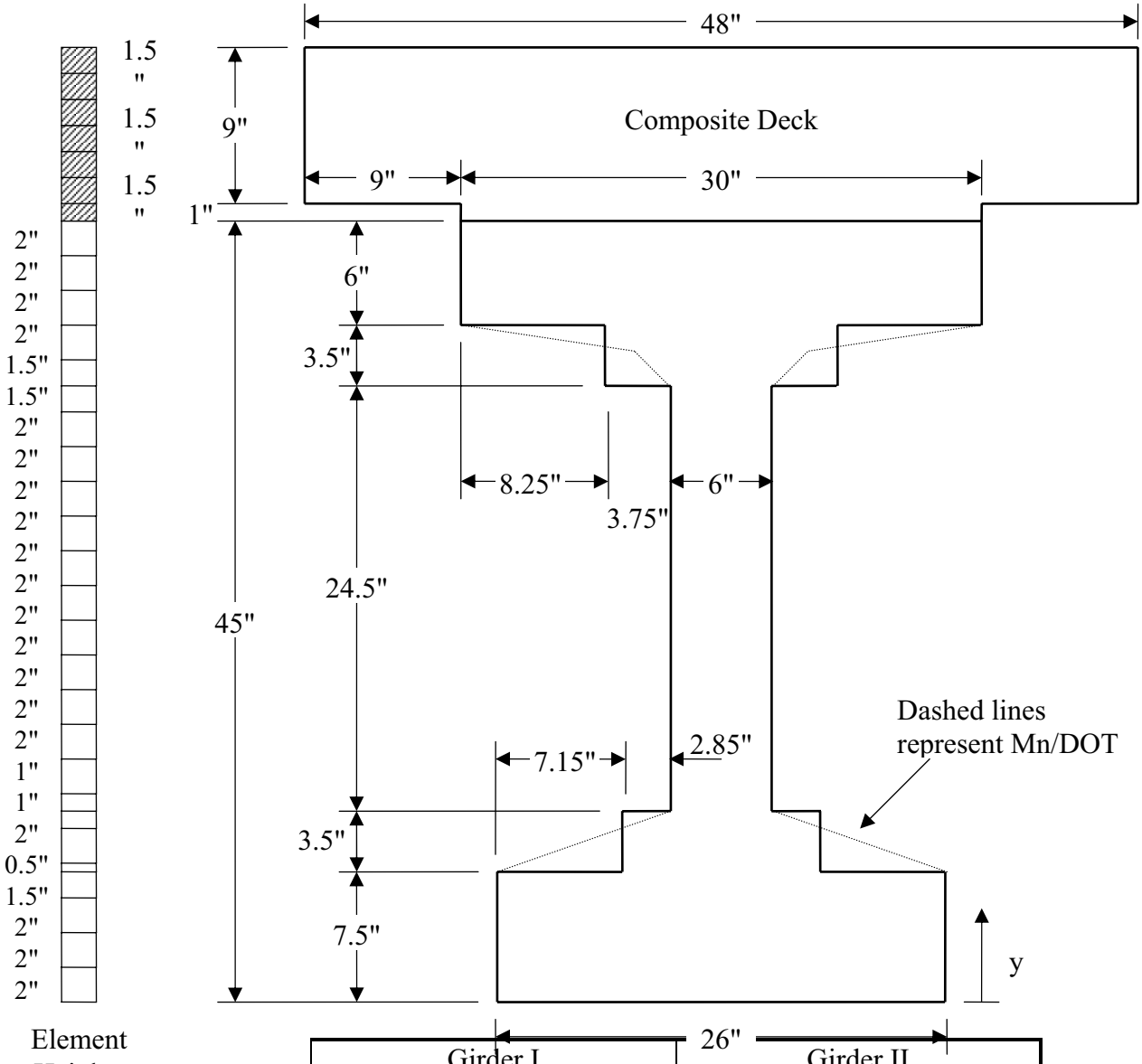

Element Heights

	Girder I		Girder II	
	center of gravity y^1	I	center of gravity y	I
steel	5.391 in.		5.391 in.	
net section	22.997 in.	160,231 in^4	22.997 in.	160,231 in^4
Initial				
transformed, non-composite	21.181 in.	179,401 in^4	21.309 in.	178,051 in^4
Flexural Crack Testing				
transformed, composite	32.057 in.	388,075 in^4	31.927 in.	383,592 in^4

[1] measured from the bottom fiber

Figure 4.2 ABAQUS Cross Section for Modeling crack in DOT 45M Section

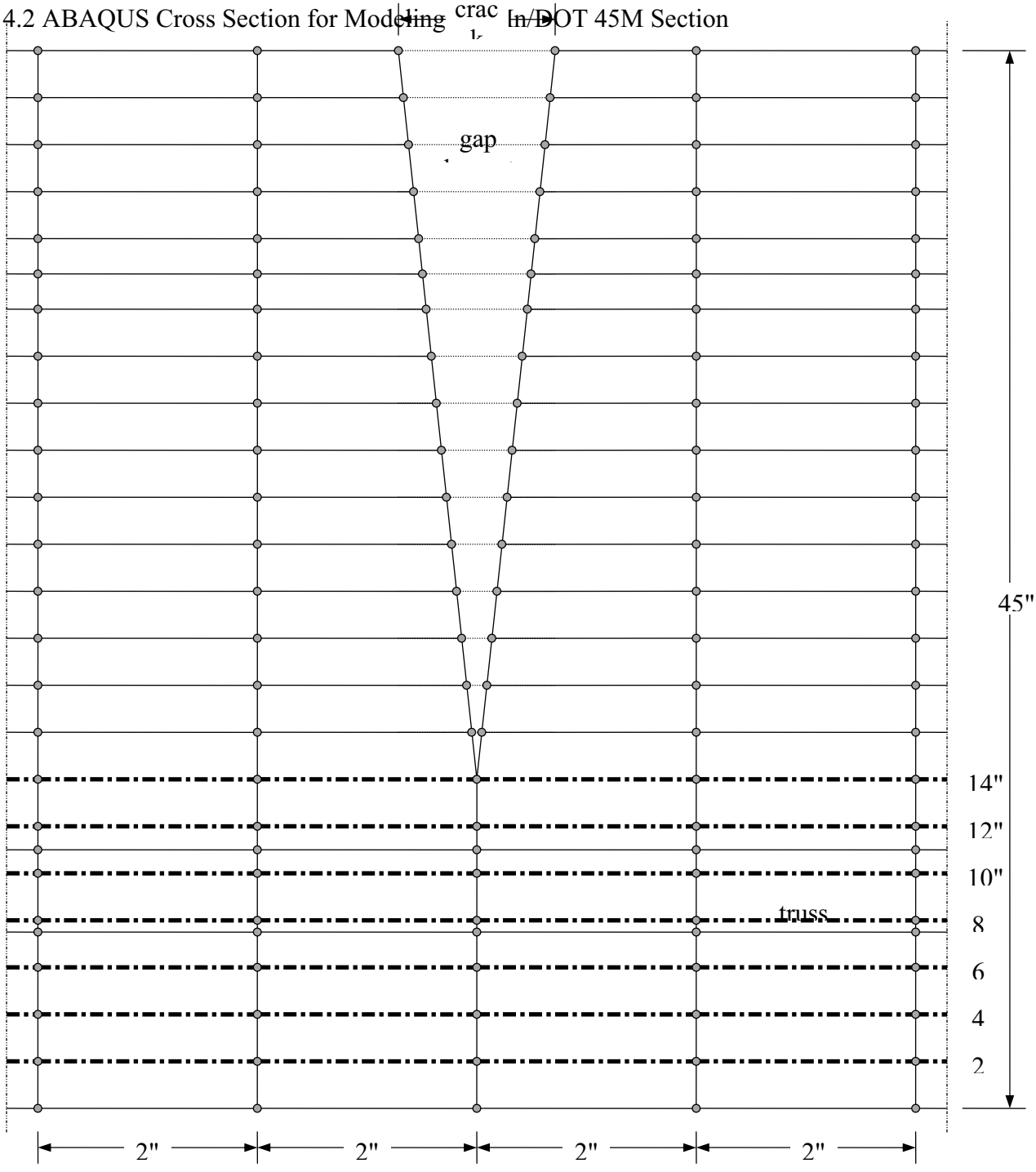

drawing not to scale

Figure 4.3 Pre-release Crack Modeling for Girder II

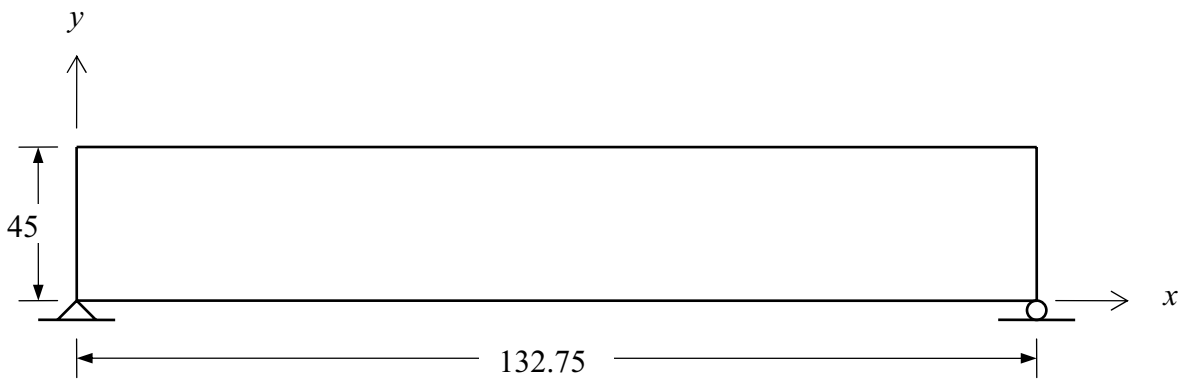

Drawing not to scale.

Figure 4.4 ABAQUS Boundary Conditions, Initial Condition

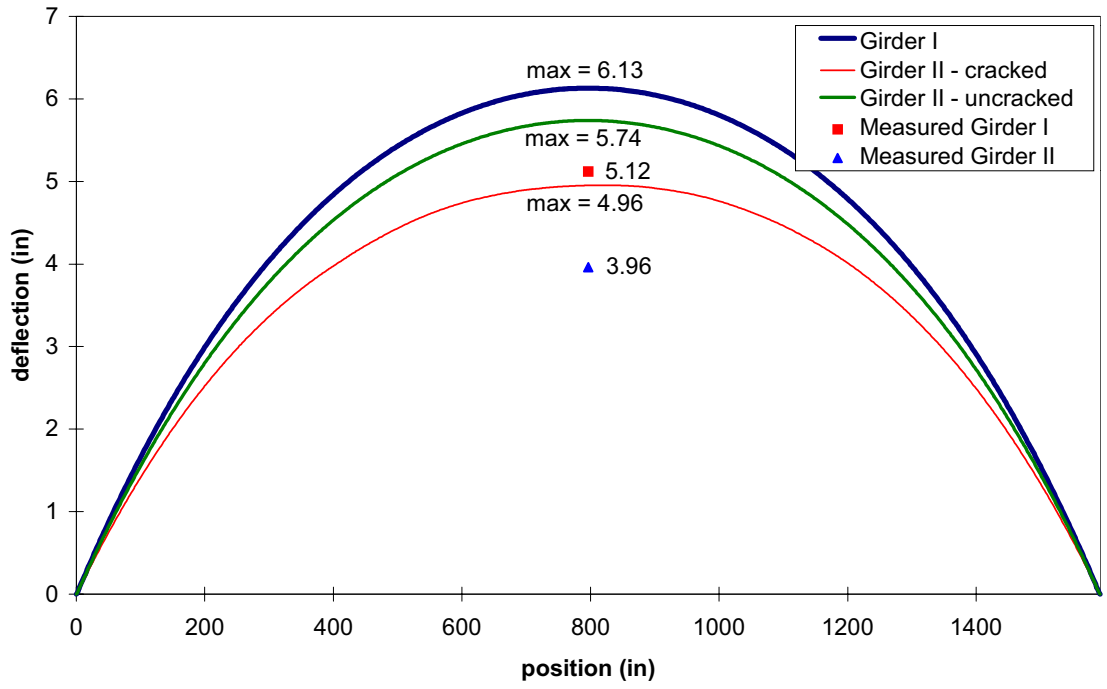

Figure 4.5 Initial Deflection of Girders I and II

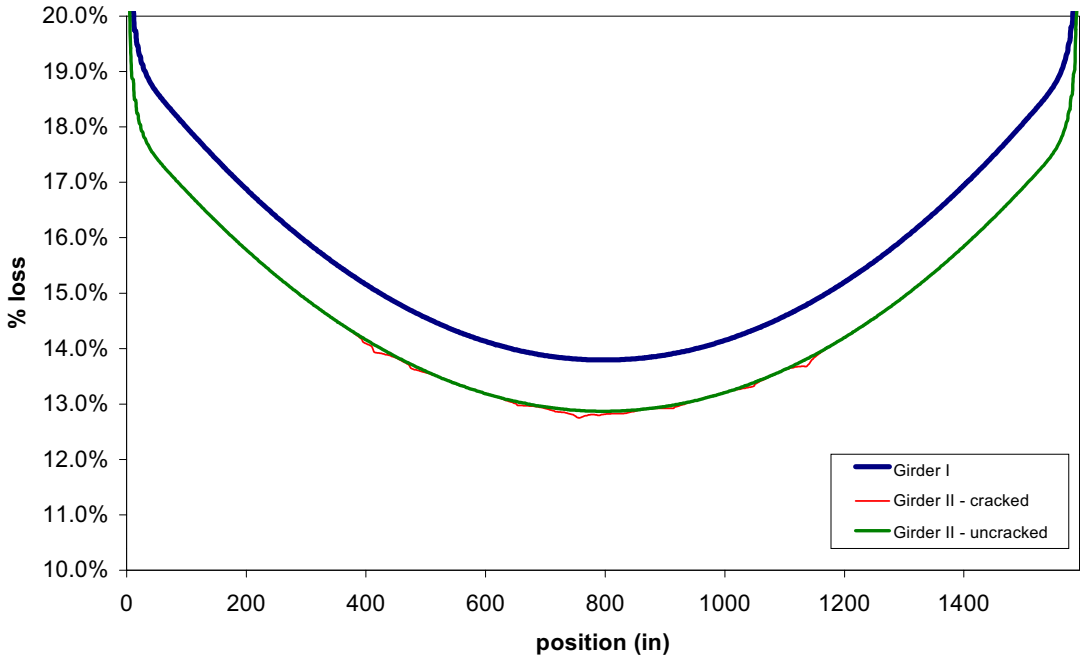

Figure 4.6 Initial Prestress Loss from ABAQUS for Girders I and II

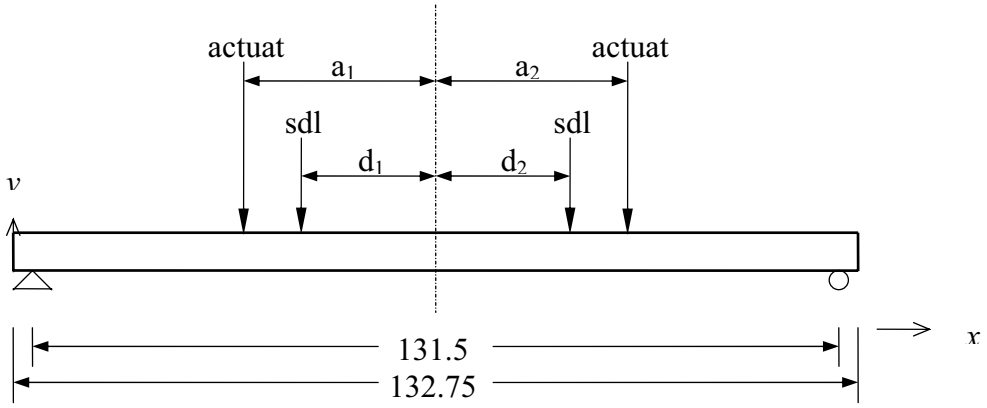

Girder	I - measured	II - measured	I - ABAQUS	II - ABAQUS
d_1	60"	78"	60.5"	77.5"
d_2	60"	66"	59.5"	66.5"
a_1	162"	157"	161.5"	157.5"
a_2	157"	159"	157.5"	158.5"

Notes: 1. Drawing not to scale
2. Total sdl load was 35.0 kips
3. Each actuator load ranged from 0 - 33.4 kips

Figure 4.7 Load Locations for Flexural Crack Testing

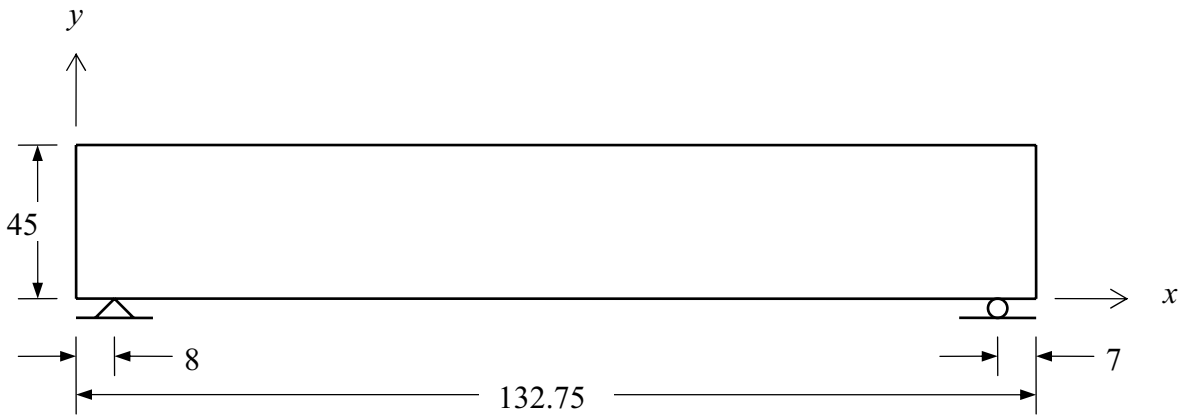

Drawing not to scale.

Figure 4.8 ABAQUS Boundary Conditions, Flexural Crack Testing

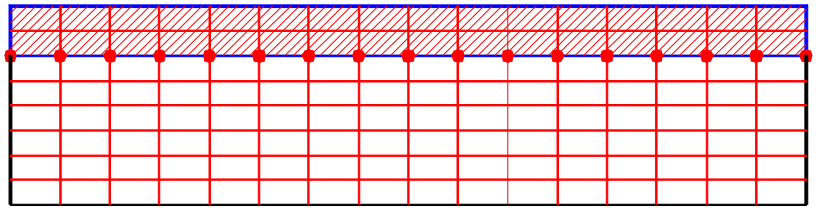

PRIOR TO ANALYSIS STEPS *Define nodes and elements*

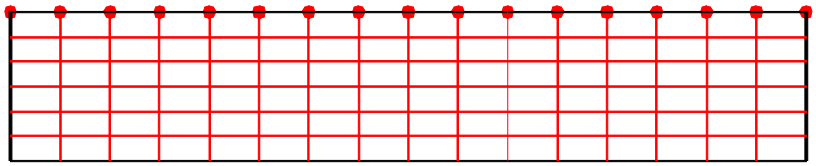

STEP 1 *Remove Deck Elements*

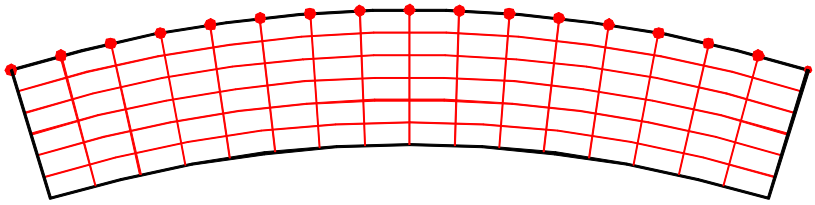

STEPS 2 & 3 *Girder Loaded with Prestress, Girder Self-Weight, and Deck Self-Weight*

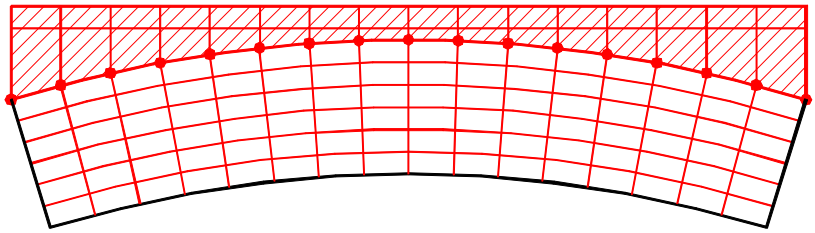

STEP 4 *Attach Deck in Strain-Free State to the Deformed Girder*

ADDITIONAL STEPS *Apply Superimposed Sustained Dead Loads and Actuator Loads*

Figure 4.9 ABAQUS Procedure for Adding the Composite Deck

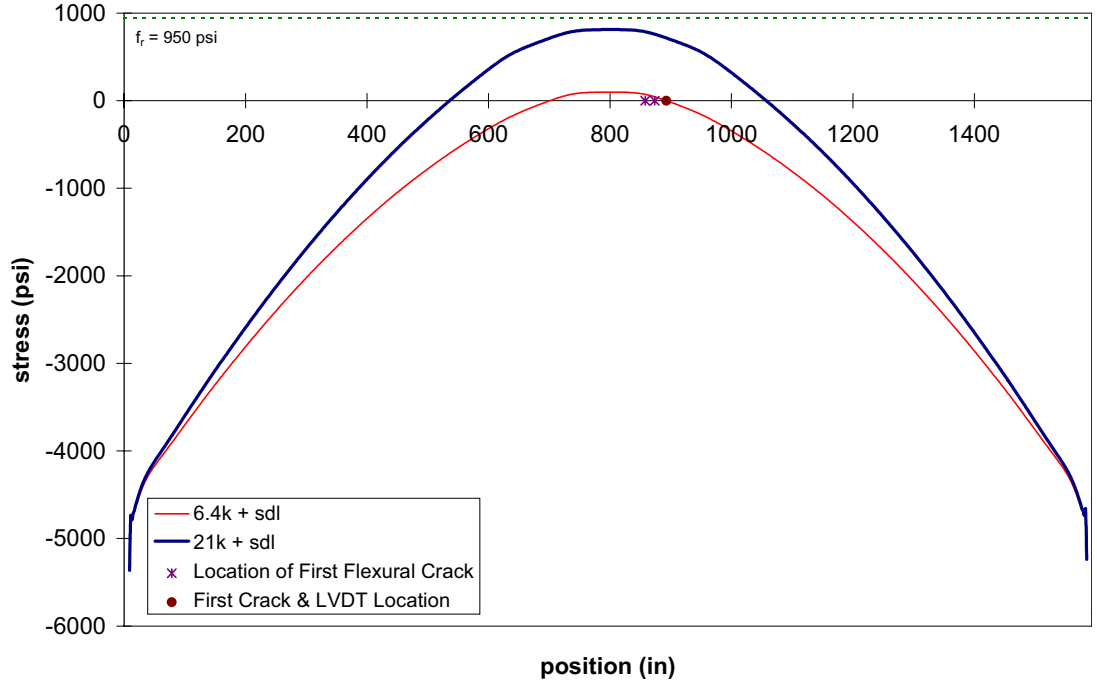

Figure 4.10 Bottom Element Stress at Crack Testing for Girder I - 36.3% Prestress Loss

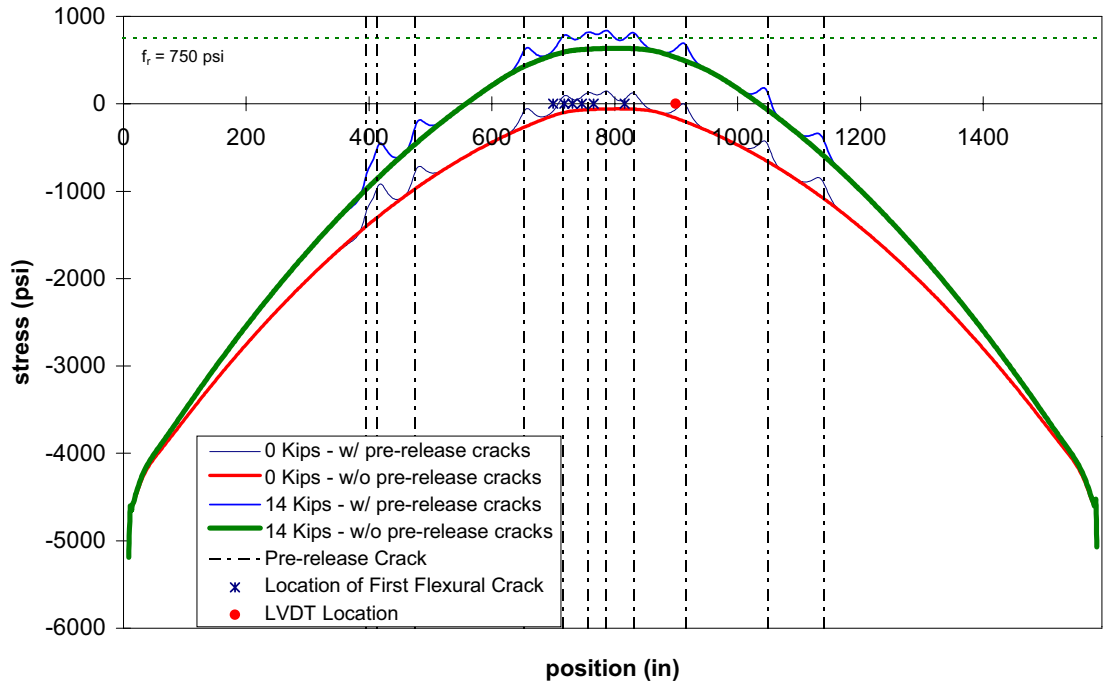

Figure 4.11 Bottom Element Stress at Crack Testing for Girder II - 38.0% Prestress Loss

Change in Stress from Uncracked Model for Girder II at Initial Flexural Cracking (14k+sdl)

(Cracked - Uncracked) / Uncracked

Position	Crack 1 394"	Crack 2 412"	Crack 3 474"	Crack 4 652"	Crack 5 716"	Crack 6 756"	Crack 7 786"	Crack 8 830"	Crack 9 916"	Crack 10 1050"	Crack 11 1140"
44	0%	-5%	-1%	-1%	-1%	-3%	-2%	-2%	-2%	-3%	-4%
42	-2%	-6%	-3%	-2%	-2%	-3%	-2%	-2%	-2%	-2%	-3%
40	-4%	-6%	-4%	-3%	-3%	-3%	13%	-3%	-3%	-3%	-3%
38	0%	-1%	0%	0%	0%	-1%	0%	1%	1%	1%	0%
36.25	10%	11%	10%	10%	9%	8%	9%	9%	10%	10%	8%
34.75	11%	12%	11%	10%	10%	11%	11%	10%	11%	11%	12%
33	3%	6%	3%	3%	3%	2%	4%	3%	3%	3%	2%
31	3%	7%	3%	3%	3%	7%	4%	3%	3%	3%	7%
29	2%	7%	2%	2%	3%	6%	4%	3%	2%	2%	5%
27	2%	9%	3%	3%	4%	8%	5%	3%	3%	3%	7%
25	0%	10%	1%	1%	2%	10%	5%	2%	1%	1%	8%
23	3%	15%	5%	6%	7%	14%	10%	6%	6%	5%	11%
21	7%	21%	10%	11%	12%	20%	16%	12%	11%	10%	15%
19	6%	23%	11%	12%	14%	36%	18%	14%	12%	11%	26%
17	9%	27%	14%	18%	20%	47%	24%	20%	18%	15%	31%
15	19%	37%	26%	36%	40%	32%	45%	41%	37%	30%	18%
13	20%	38%	29%	47%	53%	34%	59%	55%	49%	35%	16%
11.5	12%	29%	20%	37%	44%	36%	50%	46%	40%	25%	14%
10.5	9%	24%	16%	34%	42%	35%	49%	45%	37%	21%	11%
9	6%	17%	12%	55%	47%	39%	58%	53%	38%	17%	8%
7.75	4%	12%	9%	35%	65%	57%	95%	91%	44%	14%	6%
6.75	2%	6%	5%	29%	220%	-105%	-165%	-226%	45%	8%	2%
5	-2%	-5%	-4%	79%	17%	23%	18%	13%	29%	-6%	-5%
3	-7%	-20%	-17%	44%	27%	29%	28%	24%	35%	-43%	-15%
1	-14%	-39%	-39%	43%	31%	31%	33%	29%	38%	-236%	-30%
Crack Depth	31"	31"	31"	31"	31"	27"	31"	31"	31"	31"	27"

NOTE: Stress changes greater than 100% are because the denominator is very near zero.

these elements show a loss in compressive stress due to the pre-release cracks

these elements show an increase in tensile stress due to the pre-release cracks, however, the percentage is positive because the stress is tensile for both the cracked and uncracked models

Figure 4.12 Stress Difference at Pre-release Crack Locations with 38.0% Prestress Loss

APPENDIX A
SPAN OUTPUT FILE

A sample output file from the computer program SPAN (Leap Software, 1990) is included. This results of this program were used for determining steel stress ranges in the parametric study.

APPENDIX B
RESPONSE FILE

A sample input file for the computer program RESPONSE (Collins, 1990) is included. This program was used in the parametric study for determining steel stress ranges in partially cracked sections.

Response Version 1 Data-File

Name of Section: 81is1nt
Units M/U 'Metric/U.S.Customary': U
Number of Concrete Types (1-5): 2

Type Number	f'c [psi]	ec' [Milli-Strain]	fcr [psi]	Tension Stiffening Factor
1	7000	0.000	0	0.00
2	4000	0.000	0	0.00

Number of Rebar Types (1-5): 0
Number of Tendon Types (1-5): 1

Type Number	[Ramberg-Osgood-Factors--] A	B	C	Elastic Modulus [ksi]	fpu [ksi]	eprupt [Milli-Strain]
1	0.025	118.000	10.000	28500.00	270.00	40.000

Height of Section: 91.00 in
Distance to Moment Axis: 65.31 in
Shear Y/N 'Yes/No': N
Number of Concrete Layers (1-20): 8

Layer Number	y [in]	bottom width [in]	top width [in]	height [in]	Type Number
1	0.00	26.00	26.00	7.50	1
2	7.50	26.00	6.00	3.50	1
3	11.00	6.00	6.00	60.50	1
4	71.50	6.00	10.00	2.00	1
5	73.50	10.00	30.00	1.50	1
6	75.00	30.00	30.00	6.00	1
7	81.00	30.00	30.00	1.00	2
8	82.00	138.00	138.00	9.00	2

Number of Tendon Layers (0-10) : 5

Layer Number	y [in]	Area [in^2]	Prestrain [Milli-Strain]	Type Number
1	2.00	1.84	5.561	1
2	4.00	1.84	5.561	1
3	6.00	1.84	5.561	1
4	8.00	0.31	5.561	1
5	16.00	0.31	5.561	1

Consider displaced Concrete Y/N: Y

Tendon Layer	Concrete Type
1	1
2	1
3	1
4	1
5	1

Thermal & Shrinkage Strains Y/N : N
Initial Strains Y/N : Y

Concrete Layer	Bottom [--Milli-Strain----	Top]
1	-0.229	-0.236
2	-0.236	-0.239
3	-0.239	-0.294
4	-0.294	-0.296
5	-0.296	-0.297
6	-0.297	-0.303
7	0.000	0.000
8	0.000	0.000

Tendon Layer	Strain [Milli-Strain]
1	-0.231
2	-0.233
3	-0.235
4	-0.237
5	-0.244

APPENDIX C
ABAQUS INPUT FILE

A sample input file for the computer program ABAQUS (1994) is included. This finite element program was used to model pre-release cracks and determine crack effects on girder stress state and camber. The file included was a model of the experimental girder described in Chapter Four that developed pre-release cracks.

```
*HEADING
tess_max11cr_newloss.inp
**file changed 4-21-99 to use only 11 cracks
**uses Tess's plf weights from Table 6.10 for self weight applied
**girder = 716 lb/ft and deck = 479 lb/ft
**prestressing determined by LVDT stress=zero with no load, location = 898.8 in.
**new file 4-12-99 that changes sdl load to 17510 lbs at each loading point
*NODE, NSET=BEAM
    1,    0.,   0.
  797, 1592.,   0.
  798, 1593.,   0.
 1001,    0.,   2.
 1797, 1592.,   2.
 1798, 1593.,   2.
 2001,    0.,   4.
 2797, 1592.,   4.
 2798, 1593.,   4.
 3001,    0.,   6.
 3797, 1592.,   6.
 3798, 1593.,   6.
 4001,    0.,  7.5
 4797, 1592.,  7.5
 4798, 1593.,  7.5
 5001,    0.,   8.
 5797, 1592.,   8.
 5798, 1593.,   8.
 6001,    0.,  10.
 6797, 1592.,  10.
 6798, 1593.,  10.
 7001,    0.,  11.
 7797, 1592.,  11.
 7798, 1593.,  11.
 8001,    0.,  12.
 8797, 1592.,  12.
 8798, 1593.,  12.
 9001,    0.,  14.
 9797, 1592.,  14.
 9798, 1593.,  14.
10001,    0.,  16.
10797, 1592.,  16.
10798, 1593.,  16.
11001,    0.,  18.
11797, 1592.,  18.
11798, 1593.,  18.
12001,    0.,  20.
12797, 1592.,  20.
```

```
12798, 1593.,  20.
13001,    0.,  22.
13797, 1592.,  22.
13798, 1593.,  22.
14001,    0.,  24.
14797, 1592.,  24.
14798, 1593.,  24.
15001,    0.,  26.
15797, 1592.,  26.
15798, 1593.,  26.
16001,    0.,  28.
16797, 1592.,  28.
16798, 1593.,  28.
17001,    0.,  30.
17797, 1592.,  30.
17798, 1593.,  30.
18001,    0.,  32.
18797, 1592.,  32.
18798, 1593.,  32.
19001,    0.,  34.
19797, 1592.,  34.
19798, 1593.,  34.
20001,    0., 35.5
20797, 1592., 35.5
20798, 1593., 35.5
21001,    0.,  37.
21797, 1592.,  37.
21798, 1593.,  37.
22001,    0.,  39.
22797, 1592.,  39.
22798, 1593.,  39.
23001,    0.,  41.
23797, 1592.,  41.
23798, 1593.,  41.
24001,    0.,  43.
24797, 1592.,  43.
24798, 1593.,  43.
25001,    0.,  45.
25797, 1592.,  45.
25798, 1593.,  45.
*NGEN, NSET=BEAM
    1,   797
 1001,  1797
 2001,  2797
 3001,  3797
 4001,  4797
```

```
 5001,  5797
 6001,  6797
 7001,  7797
 8001,  8797
 9001,  9797
10001, 10797
11001, 11797
12001, 12797
13001, 13797
14001, 14797
15001, 15797
16001, 16797
17001, 17797
18001, 18797
19001, 19797
20001, 20797
21001, 21797
22001, 22797
23001, 23797
24001, 24797
25001, 25797
*NODE, NSET=BEAM
 10198, 393.9997,  16.
 11198, 393.9994,  18.
 12198, 393.9991,  20.
 13198, 393.9988,  22.
 14198, 393.9984,  24.
 15198, 393.9981,  26.
 16198, 393.9978,  28.
 17198, 393.9975,  30.
 18198, 393.9972,  32.
 19198, 393.9969,  34.
 20198, 393.9966,  36.
 21198, 393.9963, 37.5
 22198, 393.9959,  39.
 23198, 393.9956,  41.
 24198, 393.9953,  43.
 25198, 393.9950,  45.
 10207, 411.9997,  16.
 11207, 411.9994,  18.
 12207, 411.9991,  20.
 13207, 411.9988,  22.
 14207, 411.9984,  24.
 15207, 411.9981,  26.
 16207, 411.9978,  28.
 17207, 411.9975,  30.
```

18207, 411.9972, 32.
19207, 411.9969, 34.
20207, 411.9966, 36.
21207, 411.9963, 37.5
22207, 411.9959, 39.
23207, 411.9956, 41.
24207, 411.9953, 43.
25207, 411.9950, 45.
10238, 473.9997, 16.
11238, 473.9994, 18.
12238, 473.9991, 20.
13238, 473.9988, 22.
14238, 473.9984, 24.
15238, 473.9981, 26.
16238, 473.9978, 28.
17238, 473.9975, 30.
18238, 473.9972, 32.
19238, 473.9969, 34.
20238, 473.9966, 36.
21238, 473.9963, 37.5
22238, 473.9959, 39.
23238, 473.9956, 41.
24238, 473.9953, 43.
25238, 473.9950, 45.
10327, 651.9997, 16.
11327, 651.9994, 18.
12327, 651.9991, 20.
13327, 651.9988, 22.
14327, 651.9984, 24.
15327, 651.9981, 26.
16327, 651.9978, 28.
17327, 651.9975, 30.
18327, 651.9972, 32.
19327, 651.9969, 34.
20327, 651.9966, 36.
21327, 651.9963, 37.5
22327, 651.9959, 39.
23327, 651.9956, 41.
24327, 651.9953, 43.
25327, 651.9950, 45.
10359, 715.9997, 16.
11359, 715.9994, 18.
12359, 715.9991, 20.
13359, 715.9988, 22.
14359, 715.9984, 24.
15359, 715.9981, 26.

16359, 715.9978, 28.
17359, 715.9975, 30.
18359, 715.9972, 32.
19359, 715.9969, 34.
20359, 715.9966, 36.
21359, 715.9963, 37.5
22359, 715.9959, 39.
23359, 715.9956, 41.
24359, 715.9953, 43.
25359, 715.9950, 45.
12379, 755.9996, 20.
13379, 755.9993, 22.
14379, 755.9989, 24.
15379, 755.9986, 26.
16379, 755.9982, 28.
17379, 755.9979, 30.
18379, 755.9975, 32.
19379, 755.9971, 34.
20379, 755.9968, 36.
21379, 755.9964, 37.5
22379, 755.9961, 39.
23379, 755.9957, 41.
24379, 755.9954, 43.
25379, 755.9950, 45.
10394, 785.9997, 16.
11394, 785.9994, 18.
12394, 785.9991, 20.
13394, 785.9988, 22.
14394, 785.9984, 24.
15394, 785.9981, 26.
16394, 785.9978, 28.
17394, 785.9975, 30.
18394, 785.9972, 32.
19394, 785.9969, 34.
20394, 785.9966, 36.
21394, 785.9963, 37.5
22394, 785.9959, 39.
23394, 785.9956, 41.
24394, 785.9953, 43.
25394, 785.9950, 45.
10416, 829.9997, 16.
11416, 829.9994, 18.
12416, 829.9991, 20.
13416, 829.9988, 22.
14416, 829.9984, 24.
15416, 829.9981, 26.

16416, 829.9978, 28.
17416, 829.9975, 30.
18416, 829.9972, 32.
19416, 829.9969, 34.
20416, 829.9966, 36.
21416, 829.9963, 37.5
22416, 829.9959, 39.
23416, 829.9956, 41.
24416, 829.9953, 43.
25416, 829.9950, 45.
10459, 915.9997, 16.
11459, 915.9994, 18.
12459, 915.9991, 20.
13459, 915.9988, 22.
14459, 915.9984, 24.
15459, 915.9981, 26.
16459, 915.9978, 28.
17459, 915.9975, 30.
18459, 915.9972, 32.
19459, 915.9969, 34.
20459, 915.9966, 36.
21459, 915.9963, 37.5
22459, 915.9959, 39.
23459, 915.9956, 41.
24459, 915.9953, 43.
25459, 915.9950, 45.
10526, 1049.9997, 16.
11526, 1049.9994, 18.
12526, 1049.9991, 20.
13526, 1049.9988, 22.
14526, 1049.9984, 24.
15526, 1049.9981, 26.
16526, 1049.9978, 28.
17526, 1049.9975, 30.
18526, 1049.9972, 32.
19526, 1049.9969, 34.
20526, 1049.9966, 36.
21526, 1049.9963, 37.5
22526, 1049.9959, 39.
23526, 1049.9956, 41.
24526, 1049.9953, 43.
25526, 1049.9950, 45.
12571, 1139.9996, 20.
13571, 1139.9993, 22.
14571, 1139.9989, 24.
15571, 1139.9986, 26.

16571, 1139.9982, 28.
17571, 1139.9979, 30.
18571, 1139.9975, 32.
19571, 1139.9971, 34.
20571, 1139.9968, 36.
21571, 1139.9964, 37.5
22571, 1139.9961, 39.
23571, 1139.9957, 41.
24571, 1139.9954, 43.
25571, 1139.9950, 45.
40101, 394.0003, 16.
40102, 394.0006, 18.
40103, 394.0009, 20.
40104, 394.0012, 22.
40105, 394.0016, 24.
40106, 394.0019, 26.
40107, 394.0022, 28.
40108, 394.0025, 30.
40109, 394.0028, 32.
40110, 394.0031, 34.
40111, 394.0034, 36.
40112, 394.0037, 37.5
40113, 394.0041, 39.
40114, 394.0044, 41.
40115, 394.0047, 43.
40116, 394.0050, 45.
40301, 412.0003, 16.
40302, 412.0006, 18.
40303, 412.0009, 20.
40304, 412.0012, 22.
40305, 412.0016, 24.
40306, 412.0019, 26.
40307, 412.0022, 28.
40308, 412.0025, 30.
40309, 412.0028, 32.
40310, 412.0031, 34.
40311, 412.0034, 36.
40312, 412.0037, 37.5
40313, 412.0041, 39.
40314, 412.0044, 41.
40315, 412.0047, 43.
40316, 412.0050, 45.
40401, 474.0003, 16.
40402, 474.0006, 18.
40403, 474.0009, 20.
40404, 474.0012, 22.

40405, 474.0016, 24.
40406, 474.0019, 26.
40407, 474.0022, 28.
40408, 474.0025, 30.
40409, 474.0028, 32.
40410, 474.0031, 34.
40411, 474.0034, 36.
40412, 474.0037, 37.5
40413, 474.0041, 39.
40414, 474.0044, 41.
40415, 474.0047, 43.
40416, 474.0050, 45.
40501, 652.0003, 16.
40502, 652.0006, 18.
40503, 652.0009, 20.
40504, 652.0012, 22.
40505, 652.0016, 24.
40506, 652.0019, 26.
40507, 652.0022, 28.
40508, 652.0025, 30.
40509, 652.0028, 32.
40510, 652.0031, 34.
40511, 652.0034, 36.
40512, 652.0037, 37.5
40513, 652.0041, 39.
40514, 652.0044, 41.
40515, 652.0047, 43.
40516, 652.0050, 45.
40601, 716.0003, 16.
40602, 716.0006, 18.
40603, 716.0009, 20.
40604, 716.0012, 22.
40605, 716.0016, 24.
40606, 716.0019, 26.
40607, 716.0022, 28.
40608, 716.0025, 30.
40609, 716.0028, 32.
40610, 716.0031, 34.
40611, 716.0034, 36.
40612, 716.0037, 37.5
40613, 716.0041, 39.
40614, 716.0044, 41.
40615, 716.0047, 43.
40616, 716.0050, 45.
40701, 756.0004, 20.
40702, 756.0007, 22.

40703, 756.0011, 24.
40704, 756.0014, 26.
40705, 756.0018, 28.
40706, 756.0021, 30.
40707, 756.0025, 32.
40708, 756.0029, 34.
40709, 756.0032, 36.
40710, 756.0036, 37.5
40711, 756.0039, 39.
40712, 756.0043, 41.
40713, 756.0046, 43.
40714, 756.0050, 45.
40801, 786.0003, 16.
40802, 786.0006, 18.
40803, 786.0009, 20.
40804, 786.0012, 22.
40805, 786.0016, 24.
40806, 786.0019, 26.
40807, 786.0022, 28.
40808, 786.0025, 30.
40809, 786.0028, 32.
40810, 786.0031, 34.
40811, 786.0034, 36.
40812, 786.0037, 37.5
40813, 786.0041, 39.
40814, 786.0044, 41.
40815, 786.0047, 43.
40816, 786.0050, 45.
40901, 830.0003, 16.
40902, 830.0006, 18.
40903, 830.0009, 20.
40904, 830.0012, 22.
40905, 830.0016, 24.
40906, 830.0019, 26.
40907, 830.0022, 28.
40908, 830.0025, 30.
40909, 830.0028, 32.
40910, 830.0031, 34.
40911, 830.0034, 36.
40912, 830.0037, 37.5
40913, 830.0041, 39.
40914, 830.0044, 41.
40915, 830.0047, 43.
40916, 830.0050, 45.
41001, 916.0003, 16.
41002, 916.0006, 18.

```
41003, 916.0009,  20.
41004, 916.0012,  22.
41005, 916.0016,  24.
41006, 916.0019,  26.
41007, 916.0022,  28.
41008, 916.0025,  30.
41009, 916.0028,  32.
41010, 916.0031,  34.
41011, 916.0034,  36.
41012, 916.0037, 37.5
41013, 916.0041,  39.
41014, 916.0044,  41.
41015, 916.0047,  43.
41016, 916.0050,  45.
41101, 1050.0003,  16.
41102, 1050.0006,  18.
41103, 1050.0009,  20.
41104, 1050.0012,  22.
41105, 1050.0016,  24.
41106, 1050.0019,  26.
41107, 1050.0022,  28.
41108, 1050.0025,  30.
41109, 1050.0028,  32.
41110, 1050.0031,  34.
41111, 1050.0034,  36.
41112, 1050.0037, 37.5
41113, 1050.0041,  39.
41114, 1050.0044,  41.
41115, 1050.0047,  43.
41116, 1050.0050,  45.
41201, 1140.0004,  20.
41202, 1140.0007,  22.
41203, 1140.0011,  24.
41204, 1140.0014,  26.
41205, 1140.0018,  28.
41206, 1140.0021,  30.
41207, 1140.0025,  32.
41208, 1140.0029,  34.
41209, 1140.0032,  36.
41210, 1140.0036, 37.5
41211, 1140.0039,  39.
41212, 1140.0043,  41.
41213, 1140.0046,  43.
41214, 1140.0050,  45.
*NODE, NSET=DECK
26001,    0.,  45.
```

```
 26797, 1592.,  45.
 26798, 1593.,  45.
 27001,    0.,  46.
 27797, 1592.,  46.
 27798, 1593.,  46.
 28001,    0., 47.5
 28797, 1592., 47.5
 28798, 1593., 47.5
 29001,    0.,  49.
 29797, 1592.,  49.
 29798, 1593.,  49.
 30001,    0., 50.5
 30797, 1592., 50.5
 30798, 1593., 50.5
 31001,    0.,  52.
 31797, 1592.,  52.
 31798, 1593.,  52.
 32001,    0., 53.5
 32797, 1592., 53.5
 32798, 1593., 53.5
 33001,    0.,  55.
 33797, 1592.,  55.
 33798, 1593.,  55.
*NGEN, NSET=DECK
 26001, 26797, 1
 27001, 27797, 1
 28001, 28797, 1
 29001, 29797, 1
 30001, 30797, 1
 31001, 31797, 1
 32001, 32797, 1
 33001, 33797, 1
*NODE, NSET=DUM
 34001,    0., 45.
 34797, 1592., 45.
 34798, 1593., 45.
*NGEN, NSET=DUM
 34001, 34797, 1
*ELEMENT, TYPE=CPS4R, ELSET=BOTFLA
 1, 1, 2, 1002, 1001
*ELGEN, ELSET=BOTFLA
 1, 797, 1, 1, 4, 1000, 1000
*ELEMENT, TYPE=CPS4R, ELSET=BOTWEB
 4001, 4001, 4002, 5002, 5001
*ELGEN, ELSET=BOTWEB
 4001, 797, 1, 1, 3, 1000, 1000
```

```
*ELEMENT, TYPE=CPS4R, ELSET=WEB
 7001, 7001, 7002, 8002, 8001
*ELGEN, ELSET=WEB
 7001, 797, 1, 1, 13, 1000, 1000
*ELEMENT, TYPE=CPS4R, ELSET=WEB
  9198,  9198,  9199, 10199, 40101
 10198, 40101, 10199, 11199, 40102
 11198, 40102, 11199, 12199, 40103
 12198, 40103, 12199, 13199, 40104
 13198, 40104, 13199, 14199, 40105
 14198, 40105, 14199, 15199, 40106
 15198, 40106, 15199, 16199, 40107
 16198, 40107, 16199, 17199, 40108
 17198, 40108, 17199, 18199, 40109
 18198, 40109, 18199, 19199, 40110
 19198, 40110, 19199, 20199, 40111
  9207,  9207,  9208, 10208, 40301
 10207, 40301, 10208, 11208, 40302
 11207, 40302, 11208, 12208, 40303
 12207, 40303, 12208, 13208, 40304
 13207, 40304, 13208, 14208, 40305
 14207, 40305, 14208, 15208, 40306
 15207, 40306, 15208, 16208, 40307
 16207, 40307, 16208, 17208, 40308
 17207, 40308, 17208, 18208, 40309
 18207, 40309, 18208, 19208, 40310
 19207, 40310, 19208, 20208, 40311
  9238,  9238,  9239, 10239, 40401
 10238, 40401, 10239, 11239, 40402
 11238, 40402, 11239, 12239, 40403
 12238, 40403, 12239, 13239, 40404
 13238, 40404, 13239, 14239, 40405
 14238, 40405, 14239, 15239, 40406
 15238, 40406, 15239, 16239, 40407
 16238, 40407, 16239, 17239, 40408
 17238, 40408, 17239, 18239, 40409
 18238, 40409, 18239, 19239, 40410
 19238, 40410, 19239, 20239, 40411
  9327,  9327,  9328, 10328, 40501
 10327, 40501, 10328, 11328, 40502
 11327, 40502, 11328, 12328, 40503
 12327, 40503, 12328, 13328, 40504
 13327, 40504, 13328, 14328, 40505
 14327, 40505, 14328, 15328, 40506
 15327, 40506, 15328, 16328, 40507
 16327, 40507, 16328, 17328, 40508
```

17327, 40508, 17328, 18328, 40509
18327, 40509, 18328, 19328, 40510
19327, 40510, 19328, 20328, 40511
9359, 9359, 9360, 10360, 40601
10359, 40601, 10360, 11360, 40602
11359, 40602, 11360, 12360, 40603
12359, 40603, 12360, 13360, 40604
13359, 40604, 13360, 14360, 40605
14359, 40605, 14360, 15360, 40606
15359, 40606, 15360, 16360, 40607
16359, 40607, 16360, 17360, 40608
17359, 40608, 17360, 18360, 40609
18359, 40609, 18360, 19360, 40610
19359, 40610, 19360, 20360, 40611
11379, 11379, 11380, 12380, 40701
12379, 40701, 12380, 13380, 40702
13379, 40702, 13380, 14380, 40703
14379, 40703, 14380, 15380, 40704
15379, 40704, 15380, 16380, 40705
16379, 40705, 16380, 17380, 40706
17379, 40706, 17380, 18380, 40707
18379, 40707, 18380, 19380, 40708
19379, 40708, 19380, 20380, 40709
9394, 9394, 9395, 10395, 40801
10394, 40801, 10395, 11395, 40802
11394, 40802, 11395, 12395, 40803
12394, 40803, 12395, 13395, 40804
13394, 40804, 13395, 14395, 40805
14394, 40805, 14395, 15395, 40806
15394, 40806, 15395, 16395, 40807
16394, 40807, 16395, 17395, 40808
17394, 40808, 17395, 18395, 40809
18394, 40809, 18395, 19395, 40810
19394, 40810, 19395, 20395, 40811
9416, 9416, 9417, 10417, 40901
10416, 40901, 10417, 11417, 40902
11416, 40902, 11417, 12417, 40903
12416, 40903, 12417, 13417, 40904
13416, 40904, 13417, 14417, 40905
14416, 40905, 14417, 15417, 40906
15416, 40906, 15417, 16417, 40907
16416, 40907, 16417, 17417, 40908
17416, 40908, 17417, 18417, 40909
18416, 40909, 18417, 19417, 40910
19416, 40910, 19417, 20417, 40911
9459, 9459, 9460, 10460, 41001

10459, 41001, 10460, 11460, 41002
11459, 41002, 11460, 12460, 41003
12459, 41003, 12460, 13460, 41004
13459, 41004, 13460, 14460, 41005
14459, 41005, 14460, 15460, 41006
15459, 41006, 15460, 16460, 41007
16459, 41007, 16460, 17460, 41008
17459, 41008, 17460, 18460, 41009
18459, 41009, 18460, 19460, 41010
19459, 41010, 19460, 20460, 41011
9526, 9526, 9527, 10527, 41101
10526, 41101, 10527, 11527, 41102
11526, 41102, 11527, 12527, 41103
12526, 41103, 12527, 13527, 41104
13526, 41104, 13527, 14527, 41105
14526, 41105, 14527, 15527, 41106
15526, 41106, 15527, 16527, 41107
16526, 41107, 16527, 17527, 41108
17526, 41108, 17527, 18527, 41109
18526, 41109, 18527, 19527, 41110
19526, 41110, 19527, 20527, 41111
11571, 11571, 11572, 12572, 41201
12571, 41201, 12572, 13572, 41202
13571, 41202, 13572, 14572, 41203
14571, 41203, 14572, 15572, 41204
15571, 41204, 15572, 16572, 41205
16571, 41205, 16572, 17572, 41206
17571, 41206, 17572, 18572, 41207
18571, 41207, 18572, 19572, 41208
19571, 41208, 19572, 20572, 41209
*ELEMENT, TYPE=CPS4R, ELSET=TOPWEB
20001, 20001, 20002, 21002, 21001
*ELGEN, ELSET=TOPWEB
20001, 797, 1, 1, 2, 1000, 1000
*ELEMENT, TYPE=CPS4R, ELSET=TOPWEB
20198, 40111, 20199, 21199, 40112
21198, 40112, 21199, 22199, 40113
20207, 40311, 20208, 21208, 40312
21207, 40312, 21208, 22208, 40313
20238, 40411, 20239, 21239, 40412
21238, 40412, 21239, 22239, 40413
20327, 40511, 20328, 21328, 40512
21327, 40512, 21328, 22328, 40513
20359, 40611, 20360, 21360, 40612
21359, 40612, 21360, 22360, 40613
20379, 40709, 20380, 21380, 40710

21379, 40710, 21380, 22380, 40711
20394, 40811, 20395, 21395, 40812
21394, 40812, 21395, 22395, 40813
20416, 40911, 20417, 21417, 40912
21416, 40912, 21417, 22417, 40913
20459, 41011, 20460, 21460, 41012
21459, 41012, 21460, 22460, 41013
20526, 41111, 20527, 21527, 41112
21526, 41112, 21527, 22527, 41113
20571, 41209, 20572, 21572, 41210
21571, 41210, 21572, 22572, 41211
*ELEMENT, TYPE=CPS4R, ELSET=TOPFLA
22001, 22001, 22002, 23002, 23001
*ELGEN, ELSET=TOPFLA
22001, 797, 1, 1, 3, 1000, 1000
*ELEMENT, TYPE=CPS4R, ELSET=TOPFLA
22198, 40113, 22199, 23199, 40114
23198, 40114, 23199, 24199, 40115
24198, 40115, 24199, 25199, 40116
22207, 40313, 22208, 23208, 40314
23207, 40314, 23208, 24208, 40315
24207, 40315, 24208, 25208, 40316
22238, 40413, 22239, 23239, 40414
23238, 40414, 23239, 24239, 40415
24238, 40415, 24239, 25239, 40416
22327, 40513, 22328, 23328, 40514
23327, 40514, 23328, 24328, 40515
24327, 40515, 24328, 25328, 40516
22359, 40613, 22360, 23360, 40614
23359, 40614, 23360, 24360, 40615
24359, 40615, 24360, 25360, 40616
22379, 40711, 22380, 23380, 40712
23379, 40712, 23380, 24380, 40713
24379, 40713, 24380, 25380, 40714
22394, 40813, 22395, 23395, 40814
23394, 40814, 23395, 24395, 40815
24394, 40815, 24395, 25395, 40816
22416, 40913, 22417, 23417, 40914
23416, 40914, 23417, 24417, 40915
24416, 40915, 24417, 25417, 40916
22459, 41013, 22460, 23460, 41014
23459, 41014, 23460, 24460, 41015
24459, 41015, 24460, 25460, 41016
22526, 41113, 22527, 23527, 41114
23526, 41114, 23527, 24527, 41115
24526, 41115, 24527, 25527, 41116

22571, 41211, 22572, 23572, 41212
23571, 41212, 23572, 24572, 41213
24571, 41213, 24572, 25572, 41214
*ELEMENT, TYPE=CPS4R, ELSET=DK30
25001, 26001, 26002, 27002, 27001
*ELGEN, ELSET=DK30
25001, 797
*ELEMENT, TYPE=CPS4R, ELSET=DK48
26001, 27001, 27002, 28002, 28001
*ELGEN, ELSET=DK48
26001, 797, 1, 1, 6, 1000, 1000
*ELEMENT, TYPE=T2D2, ELSET=TRUSS2
32001, 1001, 1002
*ELGEN, ELSET=TRUSS2
32001, 797
*ELEMENT, TYPE=T2D2, ELSET=TRUSS4
33001, 2001, 2002
*ELGEN, ELSET=TRUSS4
33001, 797
*ELEMENT, TYPE=T2D2, ELSET=TRUSS6
34001, 3001, 3002
*ELGEN, ELSET=TRUSS6
34001, 797
*ELEMENT, TYPE=T2D2, ELSET=TRUSS8
35001, 5001, 5002
*ELGEN, ELSET=TRUSS8
35001, 797
*ELEMENT, TYPE=T2D2, ELSET=TRUSS10
36001, 6001, 6002
*ELGEN, ELSET=TRUSS10
36001, 797
*ELEMENT, TYPE=T2D2, ELSET=TRUSS12
37001, 8001, 8002
*ELGEN, ELSET=TRUSS12
37001, 797
*ELEMENT, TYPE=T2D2, ELSET=TRUSS14
38001, 9001, 9002
*ELGEN, ELSET=TRUSS14
38001, 797
*ELEMENT, TYPE=GAPUNI, ELSET=GAPS1
40101, 10198, 40101
40301, 10207, 40301
40401, 10238, 40401
40501, 10327, 40501
40601, 10359, 40601
40801, 10394, 40801

40901, 10416, 40901
41001, 10459, 41001
41101, 10526, 41101
*ELEMENT, TYPE=GAPUNI, ELSET=GAPS2
40102, 11198, 40102
40302, 11207, 40302
40402, 11238, 40402
40502, 11327, 40502
40602, 11359, 40602
40802, 11394, 40802
40902, 11416, 40902
41002, 11459, 41002
41102, 11526, 41102
*ELEMENT, TYPE=GAPUNI, ELSET=GAPS3
40103, 12198, 40103
40303, 12207, 40303
40403, 12238, 40403
40503, 12327, 40503
40603, 12359, 40603
40803, 12394, 40803
40903, 12416, 40903
41003, 12459, 41003
41103, 12526, 41103
*ELEMENT, TYPE=GAPUNI, ELSET=GAPS4
40104, 13198, 40104
40304, 13207, 40304
40404, 13238, 40404
40504, 13327, 40504
40604, 13359, 40604
40804, 13394, 40804
40904, 13416, 40904
41004, 13459, 41004
41104, 13526, 41104
*ELEMENT, TYPE=GAPUNI, ELSET=GAPS5
40105, 14198, 40105
40305, 14207, 40305
40405, 14238, 40405
40505, 14327, 40505
40605, 14359, 40605
40805, 14394, 40805
40905, 14416, 40905
41005, 14459, 41005
41105, 14526, 41105
*ELEMENT, TYPE=GAPUNI, ELSET=GAPS6
40106, 15198, 40106
40306, 15207, 40306

40406, 15238, 40406
40506, 15327, 40506
40606, 15359, 40606
40806, 15394, 40806
40906, 15416, 40906
41006, 15459, 41006
41106, 15526, 41106
*ELEMENT, TYPE=GAPUNI, ELSET=GAPS7
40107, 16198, 40107
40307, 16207, 40307
40407, 16238, 40407
40507, 16327, 40507
40607, 16359, 40607
40807, 16394, 40807
40907, 16416, 40907
41007, 16459, 41007
41107, 16526, 41107
*ELEMENT, TYPE=GAPUNI, ELSET=GAPS8
40108, 17198, 40108
40308, 17207, 40308
40408, 17238, 40408
40508, 17327, 40508
40608, 17359, 40608
40808, 17394, 40808
40908, 17416, 40908
41008, 17459, 41008
41108, 17526, 41108
*ELEMENT, TYPE=GAPUNI, ELSET=GAPS9
40109, 18198, 40109
40309, 18207, 40309
40409, 18238, 40409
40509, 18327, 40509
40609, 18359, 40609
40809, 18394, 40809
40909, 18416, 40909
41009, 18459, 41009
41109, 18526, 41109
*ELEMENT, TYPE=GAPUNI, ELSET=GAPS10
40110, 19198, 40110
40310, 19207, 40310
40410, 19238, 40410
40510, 19327, 40510
40610, 19359, 40610
40810, 19394, 40810
40910, 19416, 40910
41010, 19459, 41010

41110, 19526, 41110
*ELEMENT, TYPE=GAPUNI, ELSET=GAPS11
40111, 20198, 40111
40311, 20207, 40311
40411, 20238, 40411
40511, 20327, 40511
40611, 20359, 40611
40811, 20394, 40811
40911, 20416, 40911
41011, 20459, 41011
41111, 20526, 41111
*ELEMENT, TYPE=GAPUNI, ELSET=GAPS12
40112, 21198, 40112
40312, 21207, 40312
40412, 21238, 40412
40512, 21327, 40512
40612, 21359, 40612
40812, 21394, 40812
40912, 21416, 40912
41012, 21459, 41012
41112, 21526, 41112
*ELEMENT, TYPE=GAPUNI, ELSET=GAPS13
40113, 22198, 40113
40313, 22207, 40313
40413, 22238, 40413
40513, 22327, 40513
40613, 22359, 40613
40813, 22394, 40813
40913, 22416, 40913
41013, 22459, 41013
41113, 22526, 41113
*ELEMENT, TYPE=GAPUNI, ELSET=GAPS14
40114, 23198, 40114
40314, 23207, 40314
40414, 23238, 40414
40514, 23327, 40514
40614, 23359, 40614
40814, 23394, 40814
40914, 23416, 40914
41014, 23459, 41014
41114, 23526, 41114
*ELEMENT, TYPE=GAPUNI, ELSET=GAPS15
40115, 24198, 40115
40315, 24207, 40315
40415, 24238, 40415
40515, 24327, 40515

40615, 24359, 40615
40815, 24394, 40815
40915, 24416, 40915
41015, 24459, 41015
41115, 24526, 41115
*ELEMENT, TYPE=GAPUNI, ELSET=GAPS16
40116, 25198, 40116
40316, 25207, 40316
40416, 25238, 40416
40516, 25327, 40516
40616, 25359, 40616
40816, 25394, 40816
40916, 25416, 40916
41016, 25459, 41016
41116, 25526, 41116
*ELEMENT, TYPE=GAPUNI, ELSET=GAPS201
40701, 12379, 40701
41201, 12571, 41201
*ELEMENT, TYPE=GAPUNI, ELSET=GAPS202
40702, 13379, 40702
41202, 13571, 41202
*ELEMENT, TYPE=GAPUNI, ELSET=GAPS203
40703, 14379, 40703
41203, 14571, 41203
*ELEMENT, TYPE=GAPUNI, ELSET=GAPS204
40704, 15379, 40704
41204, 15571, 41204
*ELEMENT, TYPE=GAPUNI, ELSET=GAPS205
40705, 16379, 40705
41205, 16571, 41205
*ELEMENT, TYPE=GAPUNI, ELSET=GAPS206
40706, 17379, 40706
41206, 17571, 41206
*ELEMENT, TYPE=GAPUNI, ELSET=GAPS207
40707, 18379, 40707
41207, 18571, 41207
*ELEMENT, TYPE=GAPUNI, ELSET=GAPS208
40708, 19379, 40708
41208, 19571, 41208
*ELEMENT, TYPE=GAPUNI, ELSET=GAPS209
40709, 20379, 40709
41209, 20571, 41209
*ELEMENT, TYPE=GAPUNI, ELSET=GAPS210
40710, 21379, 40710
41210, 21571, 41210
*ELEMENT, TYPE=GAPUNI, ELSET=GAPS211

40711, 22379, 40711
41211, 22571, 41211
*ELEMENT, TYPE=GAPUNI, ELSET=GAPS212
40712, 23379, 40712
41212, 23571, 41212
*ELEMENT, TYPE=GAPUNI, ELSET=GAPS213
40713, 24379, 40713
41213, 24571, 41213
*ELEMENT, TYPE=GAPUNI, ELSET=GAPS214
40714, 25379, 40714
41214, 25571, 41214
*NSET, NSET=II, GENERATE
25001, 25798
*NSET, NSET=JJ, GENERATE
26001, 26798
*NSET, NSET=KK, GENERATE
34001, 34798
*NSET, NSET=TOP_5
25798
*NSET, NSET=TOP1_5
25797
*NSET, NSET=TOP1
25001, 25198, 25207, 25238, 25327, 25359, 25379, 25394,
25416, 25459, 25526, 25571, 40116, 40316, 40416, 40516,
40616, 40714, 40816, 40916, 41016, 41116, 41214
*NSET, NSET=TOP2, GENERATE
25002, 25197
25199, 25206
25208, 25237
25239, 25326
25328, 25358
25360, 25378
25380, 25393
25395, 25415
25417, 25458
25460, 25525
25527, 25570
25572, 25796
*NSET, NSET=DKSDL
33360, 33432
*NSET, NSET=DKLL
33321, 33479
*NSET, NSET=TOPROW, GENERATE
25001, 25798
*NSET, NSET=BOTROW, GENERATE
1, 798

```
*ELSET, ELSET=BOTELE, GENERATE
 1, 797
*ELSET, ELSET=LVDT
 450, 456
*ELSET, ELSET=GAPS, GENERATE
 40101, 40116
 40301, 40316
 40401, 40416
 40501, 40516
 40601, 40616
 40701, 40714
 40801, 40816
 40901, 40916
 41001, 41016
 41101, 41116
 41201, 41214
*ELSET, ELSET=CRACK1
   197,   198,  1197,  1198,  2197,  2198,  3197,  3198,
  4197,  4198,  5197,  5198,  6197,  6198,  7197,  7198,
  8197,  8198,  9197,  9198, 10197, 10198, 11197, 11198,
 12197, 12198, 13197, 13198, 14197, 14198, 15197, 15198,
 16197, 16198, 17197, 17198, 18197, 18198, 19197, 19198,
 20197, 20198, 21197, 21198, 22197, 22198, 23197, 23198,
 24197, 24198
*ELSET, ELSET=CRACK3
   206,   207,  1206,  1207,  2206,  2207,  3206,  3207,
  4206,  4207,  5206,  5207,  6206,  6207,  7206,  7207,
  8206,  8207,  9206,  9207, 10206, 10207, 11206, 11207,
 12206, 12207, 13206, 13207, 14206, 14207, 15206, 15207,
 16206, 16207, 17206, 17207, 18206, 18207, 19206, 19207,
 20206, 20207, 21206, 21207, 22206, 22207, 23206, 23207,
 24206, 24207
*ELSET, ELSET=CRACK4
   237,   238,  1237,  1238,  2237,  2238,  3237,  3238,
  4237,  4238,  5237,  5238,  6237,  6238,  7237,  7238,
  8237,  8238,  9237,  9238, 10237, 10238, 11237, 11238,
 12237, 12238, 13237, 13238, 14237, 14238, 15237, 15238,
 16237, 16238, 17237, 17238, 18237, 18238, 19237, 19238,
 20237, 20238, 21237, 21238, 22237, 22238, 23237, 23238,
 24237, 24238
*ELSET, ELSET=CRACK5
   326,   327,  1326,  1327,  2326,  2327,  3326,  3327,
  4326,  4327,  5326,  5327,  6326,  6327,  7326,  7327,
  8326,  8327,  9326,  9327, 10326, 10327, 11326, 11327,
 12326, 12327, 13326, 13327, 14326, 14327, 15326, 15327,
 16326, 16327, 17326, 17327, 18326, 18327, 19326, 19327,
```

20326, 20327, 21326, 21327, 22326, 22327, 23326, 23327,
24326, 24327
*ELSET, ELSET=CRACK6
358, 359, 1358, 1359, 2358, 2359, 3358, 3359,
4358, 4359, 5358, 5359, 6358, 6359, 7358, 7359,
8358, 8359, 9358, 9359, 10358, 10359, 11358, 11359,
12358, 12359, 13358, 13359, 14358, 14359, 15358, 15359,
16358, 16359, 17358, 17359, 18358, 18359, 19358, 19359,
20358, 20359, 21358, 21359, 22358, 22359, 23358, 23359,
24358, 24359
*ELSET, ELSET=CRACK7
378, 379, 1378, 1379, 2378, 2379, 3378, 3379,
4378, 4379, 5378, 5379, 6378, 6379, 7378, 7379,
8378, 8379, 9378, 9379, 10378, 10379, 11378, 11379,
12378, 12379, 13378, 13379, 14378, 14379, 15378, 15379,
16378, 16379, 17378, 17379, 18378, 18379, 19378, 19379,
20378, 20379, 21378, 21379, 22378, 22379, 23378, 23379,
24378, 24379
*ELSET, ELSET=CRACK8
393, 394, 1393, 1394, 2393, 2394, 3393, 3394,
4393, 4394, 5393, 5394, 6393, 6394, 7393, 7394,
8393, 8394, 9393, 9394, 10393, 10394, 11393, 11394,
12393, 12394, 13393, 13394, 14393, 14394, 15393, 15394,
16393, 16394, 17393, 17394, 18393, 18394, 19393, 19394,
20393, 20394, 21393, 21394, 22393, 22394, 23393, 23394,
24393, 24394
*ELSET, ELSET=CRACK9
415, 416, 1415, 1416, 2415, 2416, 3415, 3416,
4415, 4416, 5415, 5416, 6415, 6416, 7415, 7416,
8415, 8416, 9415, 9416, 10415, 10416, 11415, 11416,
12415, 12416, 13415, 13416, 14415, 14416, 15415, 15416,
16415, 16416, 17415, 17416, 18415, 18416, 19415, 19416,
20415, 20416, 21415, 21416, 22415, 22416, 23415, 23416,
24415, 24416
*ELSET, ELSET=CRACK10
458, 459, 1458, 1459, 2458, 2459, 3458, 3459,
4458, 4459, 5458, 5459, 6458, 6459, 7458, 7459,
8458, 8459, 9458, 9459, 10458, 10459, 11458, 11459,
12458, 12459, 13458, 13459, 14458, 14459, 15458, 15459,
16458, 16459, 17458, 17459, 18458, 18459, 19458, 19459,
20458, 20459, 21458, 21459, 22458, 22459, 23458, 23459,
24458, 24459
*ELSET, ELSET=CRACK11
525, 526, 1525, 1526, 2525, 2526, 3525, 3526,
4525, 4526, 5525, 5526, 6525, 6526, 7525, 7526,
8525, 8526, 9525, 9526, 10525, 10526, 11525, 11526,

12525, 12526, 13525, 13526, 14525, 14526, 15525, 15526,
16525, 16526, 17525, 17526, 18525, 18526, 19525, 19526,
20525, 20526, 21525, 21526, 22525, 22526, 23525, 23526,
24525, 24526
*ELSET, ELSET=CRACK12
570, 571, 1570, 1571, 2570, 2571, 3570, 3571,
4570, 4571, 5570, 5571, 6570, 6571, 7570, 7571,
8570, 8571, 9570, 9571, 10570, 10571, 11570, 11571,
12570, 12571, 13570, 13571, 14570, 14571, 15570, 15571,
16570, 16571, 17570, 17571, 18570, 18571, 19570, 19571,
20570, 20571, 21570, 21571, 22570, 22571, 23570, 23571,
24570, 24571
*ELSET, ELSET=GAGES
1356, 1398, 1437, 1440, 2356, 2398, 2437, 2440,
23398
*SOLID SECTION, MATERIAL=GIRCON, ELSET=BOTFLA
26.
*SOLID SECTION, MATERIAL=GIRCON, ELSET=BOTWEB
11.7
*SOLID SECTION, MATERIAL=GIRCON, ELSET=WEB
6.
*SOLID SECTION, MATERIAL=GIRCON, ELSET=TOPWEB
13.5
*SOLID SECTION, MATERIAL=GIRCON, ELSET=TOPFLA
30.
*SOLID SECTION, MATERIAL=DKCON, ELSET=DK30
30.
*SOLID SECTION, MATERIAL=DKCON, ELSET=DK48
48.
*SOLID SECTION, MATERIAL=STEEL, ELSET=TRUSS2
2.737
*SOLID SECTION, MATERIAL=STEEL, ELSET=TRUSS4
2.737
*SOLID SECTION, MATERIAL=STEEL, ELSET=TRUSS6
2.737
*SOLID SECTION, MATERIAL=STEEL, ELSET=TRUSS8
0.912
*SOLID SECTION, MATERIAL=STEEL, ELSET=TRUSS10
0.456
*SOLID SECTION, MATERIAL=STEEL, ELSET=TRUSS12
0.456
*SOLID SECTION, MATERIAL=STEEL, ELSET=TRUSS14
0.456
*MATERIAL, NAME=DKCON
*ELASTIC
4.0E+6, 0.2

```
*DENSITY
 2.2465E-4
*MATERIAL, NAME=GIRCON
*ELASTIC
 4.8E+6, 0.2
*DENSITY
 2.3214E-4
*MATERIAL, NAME=STEEL
*ELASTIC
 2.88E+7, 0.3
*DENSITY
 7.3545E-4
*GAP, ELSET=GAPS1
 0.0006, 1., 0., 0.
*GAP, ELSET=GAPS2
 0.0012, 1., 0., 0.
*GAP, ELSET=GAPS3
 0.0018, 1., 0., 0.
*GAP, ELSET=GAPS4
 0.0024, 1., 0., 0.
*GAP, ELSET=GAPS5
 0.0032, 1., 0., 0.
*GAP, ELSET=GAPS6
 0.0038, 1., 0., 0.
*GAP, ELSET=GAPS7
 0.0044, 1., 0., 0.
*GAP, ELSET=GAPS8
 0.0050, 1., 0., 0.
*GAP, ELSET=GAPS9
 0.0056, 1., 0., 0.
*GAP, ELSET=GAPS10
 0.0062, 1., 0., 0.
*GAP, ELSET=GAPS11
 0.0068, 1., 0., 0.
*GAP, ELSET=GAPS12
 0.0074, 1., 0., 0.
*GAP, ELSET=GAPS13
 0.0082, 1., 0., 0.
*GAP, ELSET=GAPS14
 0.0088, 1., 0., 0.
*GAP, ELSET=GAPS15
 0.0094, 1., 0., 0.
*GAP, ELSET=GAPS16
 0.0100, 1., 0., 0.
*GAP, ELSET=GAPS201
 0.0008, 1., 0., 0.
```

```
*GAP, ELSET=GAPS202
 0.0014, 1., 0., 0.
*GAP, ELSET=GAPS203
 0.0022, 1., 0., 0.
*GAP, ELSET=GAPS204
 0.0028, 1., 0., 0.
*GAP, ELSET=GAPS205
 0.0036, 1., 0., 0.
*GAP, ELSET=GAPS206
 0.0042, 1., 0., 0.
*GAP, ELSET=GAPS207
 0.0050, 1., 0., 0.
*GAP, ELSET=GAPS208
 0.0058, 1., 0., 0.
*GAP, ELSET=GAPS209
 0.0064, 1., 0., 0.
*GAP, ELSET=GAPS210
 0.0072, 1., 0., 0.
*GAP, ELSET=GAPS211
 0.0078, 1., 0., 0.
*GAP, ELSET=GAPS212
 0.0086, 1., 0., 0.
*GAP, ELSET=GAPS213
 0.0092, 1., 0., 0.
*GAP, ELSET=GAPS214
 0.0100, 1., 0., 0.
*INITIAL CONDITIONS, TYPE=STRESS
  TRUSS2, 132753.
  TRUSS4, 132753.
  TRUSS6, 132753.
  TRUSS8, 132753.
 TRUSS10, 132753.
 TRUSS12, 132753.
 TRUSS14, 132753.
*EQUATION
3
II, 1, 1., JJ, 1, -1., KK, 1, -1.
3
II, 2, 1., JJ, 2, -1., KK, 2, -1.
*BOUNDARY
   5, 1, 2
 794, 2
*PREPRINT, ECHO=NO, MODEL=NO
*RESTART, WRITE, FREQ=10

**STEP 1, REMOVE DECK
```

```
*STEP
 STEP 1 - REMOVE DECK
*STATIC
 0.2, 1., 0.01, 0.4
*MODEL CHANGE, REMOVE
 DK30
 DK48
*BOUNDARY
 DECK, 1, 2
*NODE PRINT, NSET=BOTROW, FREQ=10
U
*NODE FILE, NSET=BOTROW, FREQ=10
U
*EL PRINT, POSITION=CENTROIDAL, ELSET=BOTELE, FREQ=10
S
*EL FILE, POSITION=CENTROIDAL, ELSET=BOTELE, FREQ=10
S
*END STEP

**STEP2, ADD SELF-WEIGHT OF GIRDER
*STEP
 STEP 2 - GIRDER SLF-WT
*STATIC
 0.2, 1., 0.01, 0.4
*CLOAD, OP=NEW
 TOP_5,  2,  -29.8333
 TOP1,   2,  -59.6667
 TOP1_5, 2,     -89.5
 TOP2,   2, -119.3333
*NODE PRINT, FREQ=10, NSET=BOTROW
U
*NODE FILE, FREQ=10, NSET=BOTROW
U
*EL PRINT, POSITION=CENTROIDAL, FREQ=10, ELSET=BOTELE
S
*EL FILE, POSITION=CENTROIDAL, FREQ=10, ELSET=BOTELE
S
*EL PRINT, POSITION=CENTROIDAL, ELSET=TRUSS2, FREQ=10
S
*EL FILE, POSITION=CENTROIDAL, ELSET=TRUSS2, FREQ=10
S
*EL PRINT, POSITION=CENTROIDAL, ELSET=TRUSS4, FREQ=10
S
*EL FILE, POSITION=CENTROIDAL, ELSET=TRUSS4, FREQ=10
S
*EL PRINT, POSITION=CENTROIDAL, ELSET=TRUSS6, FREQ=10
```

```
S
*EL FILE, POSITION=CENTROIDAL, ELSET=TRUSS6, FREQ=10
S
*EL PRINT, POSITION=CENTROIDAL, ELSET=TRUSS8, FREQ=10
S
*EL FILE, POSITION=CENTROIDAL, ELSET=TRUSS8, FREQ=10
S
*EL PRINT, POSITION=CENTROIDAL, ELSET=TRUSS10, FREQ=10
S
*EL FILE, POSITION=CENTROIDAL, ELSET=TRUSS10, FREQ=10
S
*EL PRINT, POSITION=CENTROIDAL, ELSET=TRUSS12, FREQ=10
S
*EL FILE, POSITION=CENTROIDAL, ELSET=TRUSS12, FREQ=10
S
*EL PRINT, POSITION=CENTROIDAL, ELSET=TRUSS14, FREQ=10
S
*EL FILE, POSITION=CENTROIDAL, ELSET=TRUSS14, FREQ=10
S
*EL PRINT, POSITION=AVERAGED AT NODES, FREQ=0
*EL FILE, POSITION=AVERAGED AT NODES, FREQ=0
*MODAL PRINT, FREQ=99999
*MODAL FILE, FREQ=99999
*ENERGY PRINT, FREQ=0
*ENERGY FILE, FREQ=0
*PRINT, FREQ=1
*END STEP

**STEP 3 - ADD DECK WEIGHT TO GIRDER
*STEP
 STEP 3 - DECK WEIGHT ON GIRDER
*STATIC
 0.2, 1., 0.01, 0.4
*CLOAD, OP=NEW
 TOP_5,  2,  -49.7917
 TOP1,   2,  -99.5833
 TOP1_5, 2,  -149.375
 TOP2,   2, -199.1667
*NODE PRINT, FREQ=10, NSET=BOTROW
U
*NODE FILE, FREQ=10, NSET=BOTROW
U
*EL PRINT, POSITION=CENTROIDAL, FREQ=10, ELSET=BOTELE
S
*EL FILE, POSITION=CENTROIDAL, FREQ=10, ELSET=BOTELE
S
```

```
*EL PRINT, POSITION=AVERAGED AT NODES, FREQ=0
*EL FILE, POSITION=AVERAGED AT NODES, FREQ=0
*MODAL PRINT, FREQ=99999
*MODAL FILE, FREQ=99999
*ENERGY PRINT, FREQ=0
*ENERGY FILE, FREQ=0
*PRINT, FREQ=1
*END STEP

**STEP 4 - ADD DECK
*STEP
 STEP 4 - ADD DECK
*STATIC
 0.2, 1., 0.01, 0.4
*MODEL CHANGE, INCLUDE
 DK30
 DK48
*BOUNDARY, OP=NEW
   5, 1, 2
 794, 2
*BOUNDARY, FIXED, OP=NEW
 KK, 1, 2
*NODE PRINT, FREQ=10, NSET=BOTROW
U
*NODE FILE, FREQ=10, NSET=BOTROW
U
*EL PRINT, POSITION=CENTROIDAL, FREQ=10, ELSET=BOTELE
S
*EL FILE, POSITION=CENTROIDAL, FREQ=10, ELSET=BOTELE
S
*END STEP

**STEP 5 - LOAD SUSTAINED DEAD LOAD
*STEP
 STEP 5 - SUSTAINED DEAD LOAD
*STATIC
 0.2, 1., 0.01, 0.4
*CLOAD, OP=MOD
 DKSDL, 2, -17510.
*NODE PRINT, FREQ=10, NSET=BOTROW
U
*NODE FILE, FREQ=10, NSET=BOTROW
U
*EL PRINT, POSITION=CENTROIDAL, FREQ=10, ELSET=BOTELE
S
*EL FILE, POSITION=CENTROIDAL, FREQ=10, ELSET=BOTELE
```

```
S
*EL PRINT, POSITION=CENTROIDAL, FREQ=10, ELSET=LVDT
S
*EL FILE, POSITION=CENTROIDAL, FREQ=10, ELSET=LVDT
S
*EL PRINT, POSITION=CENTROIDAL, ELSET=GAPS, FREQ=0
E
*EL FILE, POSITION=CENTROIDAL, ELSET=GAPS, FREQ=0
E
*EL PRINT, POSITION=CENTROIDAL, FREQ=10, ELSET=CRACK1
S
*EL FILE, POSITION=CENTROIDAL, FREQ=10, ELSET=CRACK1
S
*EL PRINT, POSITION=CENTROIDAL, FREQ=10, ELSET=CRACK3
S
*EL FILE, POSITION=CENTROIDAL, FREQ=10, ELSET=CRACK3
S
*EL PRINT, POSITION=CENTROIDAL, FREQ=10, ELSET=CRACK4
S
*EL FILE, POSITION=CENTROIDAL, FREQ=10, ELSET=CRACK4
S
*EL PRINT, POSITION=CENTROIDAL, FREQ=10, ELSET=CRACK5
S
*EL FILE, POSITION=CENTROIDAL, FREQ=10, ELSET=CRACK5
S
*EL PRINT, POSITION=CENTROIDAL, FREQ=10, ELSET=CRACK6
S
*EL FILE, POSITION=CENTROIDAL, FREQ=10, ELSET=CRACK6
S
*EL PRINT, POSITION=CENTROIDAL, FREQ=10, ELSET=CRACK7
S
*EL FILE, POSITION=CENTROIDAL, FREQ=10, ELSET=CRACK7
S
*EL PRINT, POSITION=CENTROIDAL, FREQ=10, ELSET=CRACK8
S
*EL FILE, POSITION=CENTROIDAL, FREQ=10, ELSET=CRACK8
S
*EL PRINT, POSITION=CENTROIDAL, FREQ=10, ELSET=CRACK9
S
*EL FILE, POSITION=CENTROIDAL, FREQ=10, ELSET=CRACK9
S
*EL PRINT, POSITION=CENTROIDAL, FREQ=10, ELSET=CRACK10
S
*EL FILE, POSITION=CENTROIDAL, FREQ=10, ELSET=CRACK10
S
*EL PRINT, POSITION=CENTROIDAL, FREQ=10, ELSET=CRACK11
```

```
S
*EL FILE, POSITION=CENTROIDAL, FREQ=10, ELSET=CRACK11
S
*EL PRINT, POSITION=CENTROIDAL, FREQ=10, ELSET=CRACK12
S
*EL FILE, POSITION=CENTROIDAL, FREQ=10, ELSET=CRACK12
S
*EL PRINT, POSITION=AVERAGED AT NODES, FREQ=0
*EL FILE, POSITION=AVERAGED AT NODES, FREQ=0
*MODAL PRINT, FREQ=99999
*MODAL FILE, FREQ=99999
*ENERGY PRINT, FREQ=0
*ENERGY FILE, FREQ=0
*PRINT, FREQ=1
*END STEP

**STEP 6 - LOAD 14 KIP ACTUATOR LOAD
*STEP
 STEP 6 - ACTUATOR LOAD
*STATIC
 0.2, 1., 0.01, 0.4
*CLOAD, OP=MOD
 DKLL, 2, -14000.
*NODE PRINT, FREQ=10, NSET=BOTROW
U
*NODE FILE, FREQ=10, NSET=BOTROW
U
*EL PRINT, POSITION=CENTROIDAL, FREQ=10, ELSET=BOTELE
S
*EL FILE, POSITION=CENTROIDAL, FREQ=10, ELSET=BOTELE
S
*EL PRINT, POSITION=CENTROIDAL, FREQ=10, ELSET=LVDT
S
*EL FILE, POSITION=CENTROIDAL, FREQ=10, ELSET=LVDT
S
*EL PRINT, POSITION=CENTROIDAL, ELSET=GAPS, FREQ=0
E
*EL FILE, POSITION=CENTROIDAL, ELSET=GAPS, FREQ=0
E
*EL PRINT, POSITION=CENTROIDAL, FREQ=10, ELSET=CRACK1
S
*EL FILE, POSITION=CENTROIDAL, FREQ=10, ELSET=CRACK1
S
*EL PRINT, POSITION=CENTROIDAL, FREQ=10, ELSET=CRACK3
S
*EL FILE, POSITION=CENTROIDAL, FREQ=10, ELSET=CRACK3
```

```
S
*EL PRINT, POSITION=CENTROIDAL, FREQ=10, ELSET=CRACK4
S
*EL FILE, POSITION=CENTROIDAL, FREQ=10, ELSET=CRACK4
S
*EL PRINT, POSITION=CENTROIDAL, FREQ=10, ELSET=CRACK5
S
*EL FILE, POSITION=CENTROIDAL, FREQ=10, ELSET=CRACK5
S
*EL PRINT, POSITION=CENTROIDAL, FREQ=10, ELSET=CRACK6
S
*EL FILE, POSITION=CENTROIDAL, FREQ=10, ELSET=CRACK6
S
*EL PRINT, POSITION=CENTROIDAL, FREQ=10, ELSET=CRACK7
S
*EL FILE, POSITION=CENTROIDAL, FREQ=10, ELSET=CRACK7
S
*EL PRINT, POSITION=CENTROIDAL, FREQ=10, ELSET=CRACK8
S
*EL FILE, POSITION=CENTROIDAL, FREQ=10, ELSET=CRACK8
S
*EL PRINT, POSITION=CENTROIDAL, FREQ=10, ELSET=CRACK9
S
*EL FILE, POSITION=CENTROIDAL, FREQ=10, ELSET=CRACK9
S
*EL PRINT, POSITION=CENTROIDAL, FREQ=10, ELSET=CRACK10
S
*EL FILE, POSITION=CENTROIDAL, FREQ=10, ELSET=CRACK10
S
*EL PRINT, POSITION=CENTROIDAL, FREQ=10, ELSET=CRACK11
S
*EL FILE, POSITION=CENTROIDAL, FREQ=10, ELSET=CRACK11
S
*EL PRINT, POSITION=CENTROIDAL, FREQ=10, ELSET=CRACK12
S
*EL FILE, POSITION=CENTROIDAL, FREQ=10, ELSET=CRACK12
S
*EL PRINT, POSITION=AVERAGED AT NODES, FREQ=0
*EL FILE, POSITION=AVERAGED AT NODES, FREQ=0
*MODAL PRINT, FREQ=99999
*MODAL FILE, FREQ=99999
*ENERGY PRINT, FREQ=0
*ENERGY FILE, FREQ=0
*PRINT, FREQ=1
*END STEP
```

APPENDIX D
LOWER BOUND PRESTRESS LOSSES

An accurate prediction of the level of prestress in a girder at any given time is a difficult parameter to determine due to the time dependent properties of both the prestressing strand and the concrete in a prestressed girder. Prior to release, the concrete is restrained from shrinkage by the prestressing strands and the steel strands expand due to the heat of hydration from curing and the greater thermal coefficient of steel than concrete. The traditional method used in industry for predicting prestress loss is to assume the concrete stress at the time of release is zero. This assumption does not account for any time or temperature dependent properties of the concrete or the steel that occur before release.

Ahlborn (1998) determined the prestress losses using the above assumption for the two girders discussed in Chapter 4. The change in strain since the time of release was measured using vibrating wire strain gages placed in the concrete near the location of the center of gravity of the prestressing strands. Using the data recorded with the vibrating wire gages with the assumption that the initial concrete stress at release was zero, the prestress losses at the time of flexural crack testing were calculated to be 26.6% for Girder I and 25.8% for Girder II. These losses were assumed to be a lower bound because the assumption of zero concrete stress at the time of release underestimates the prestress loss (relative to the case where the concrete stress may initially be tensile).

ABAQUS models incorporating the lower bound prestress losses were made of the two experimental girders. Figures D.1 and D.2 show plots of the stress in the bottom element along the length of each girder. Each plot includes the stresses from two loads. The larger load was the measured initial flexural cracking load determined from acoustic emission (AE) monitoring equipment and the smaller load was the crack reopening load determined using LVDTs . The load corresponds to each of the two actuator loads applied to each girder in addition to the superimposed sustained dead load. These loads were described in Section 4.3. Data points were included in each figure denoting the location of the first flexural cracks and the LVDT locations. Figure D.2 also includes dashed lines for the locations of the eleven pre-release cracks. The bottom element stress along the length of Girder II for the ABAQUS model which did not include pre-release cracks is also shown in Figure D.2. The local stress changes at the pre-

release crack locations are illustrated in the comparison of the results from the two models of Girder II.

The bottom element stress at the first flexural crack locations and at the location of maximum stress are tabulated in Table D.1 for Girder I and D.2 for Girder II. The maximum stress in Girder I from the cracking load was +46.7 psi which was well below +950 psi, the 28-day modulus of rupture. The maximum stress from the reopening load was -687.2 psi which was well below zero, the bottom element stress at crack reopening. The results from Girder II were also much lower than the 28-day modulus of rupture (+750 psi) and zero. The maximum stress from the cracking load was -130.0 psi and from the reopening load was -823.2 psi.

The finite element analyses of the two girders emphasizes the belief that there was initial tensile stress in the concrete prior to release. A greater prestress loss was present at the time of flexural crack testing than was predicted assuming zero stress in the concrete at release. This correlates with the results of Ahlborn (1998). More accurate results were obtained by calibrating the models to the reopening load for each girder because the concrete stress prior to release was not known. This procedure and the results using the calibrated models were included in Section 4.3.

Table D.1 Girder I - Bottom Element Stresses at the First Crack Locations and at the Location of Maximum Stress using Lower Bound Prestress Loss (26.6%)

Crack Location (in.)	ABAQUS Stress (psi) Cracking Load - (21k+sdl)	ABAQUS Stress (psi) Reopening Load (6.4k + sdl)
893	-49.9	-784.8
874	-6.14	-740.5
858	+21.2	-713.0
max. ABAQUS stress [1]	*+46.7*	*-687.2*

[1] Maximum midspan bottom fiber stress.

Table D.2 Girder II - Bottom Element Stresses at the First Crack Locations and at the Location of Maximum Stress using Lower Bound Prestress Loss (25.8%)

Crack Location (in.)	ABAQUS Stress (psi) Cracking Load - (14k + sdl)	ABAQUS Stress (psi) Reopening Load - (0k + sdl)
700	-357.9 [-411.9][1]	-1051.2 [-1104.8]
718	-186.5 [-376.1]	-878.9 [-1068.8]
731	-224.3 [-359.3]	-916.6 [-1051.2]
746	-196.1 [-349.1]	-888.4 [-1040.3]
766	-164.6 [-340.7]	-856.9 [-1033.0]
816	-222.9 [-336.0]	-915.1 [-1028]
max. ABAQUS stress [2]	*-130.9 [-335.5]*	*-823.2 [-1028.0]*

[1] Bracketed terms are the stresses in the Girder II model without pre-release cracks.

[2] Maximum stress which occurred at the pre-release crack location of 785 in. in the model with pre-release cracks and at midspan [803 in.] in the model without pre-release cracks.

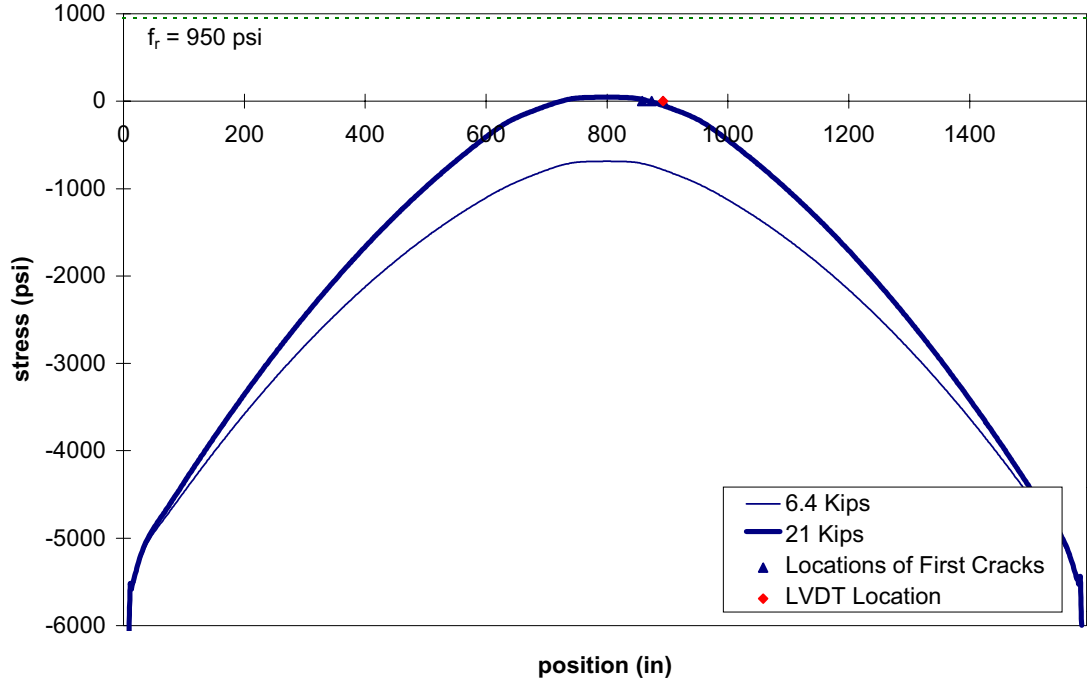

Figure D.1 Bottom Element Stress at Crack Testing for Girder I - 26.6% Prestress Loss

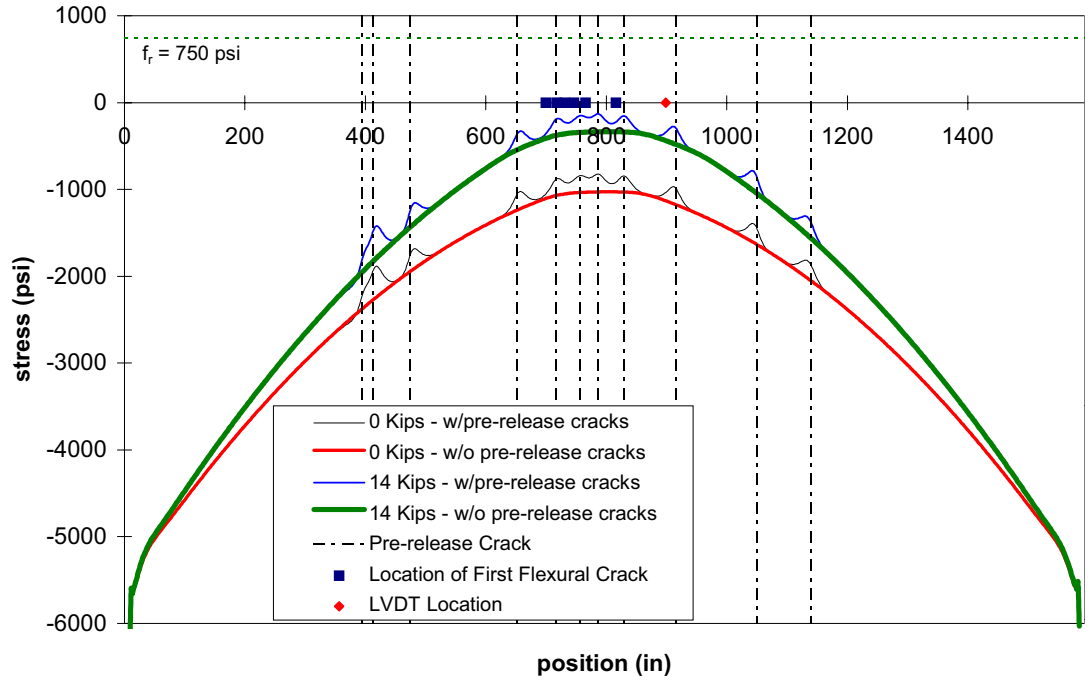

Figure D.2 Bottom Element Stress at Crack Testing for Girder II - 25.8% Prestress Loss